Novel simulation methods for Coulomb and hydrodynamic interactions

Dissertation

zur Erlangung des Grades

"Doktor der Naturwissenschaften"

am Fachbereich Physik

der Johannes Gutenberg-Universität

in Mainz

Igor Pasichnyk

geb. in Maksimovka (Ukraine)

Abstract

This thesis presents new methods to simulate systems with hydrodynamic and electrostatic interactions.

Part 1 is devoted to computer simulations of Brownian particles with hydrodynamic interactions. The main influence of the solvent on the dynamics of Brownian particles is that it mediates hydrodynamic interactions. In the method, this is simulated by numerical solution of the Navier–Stokes equation on a lattice. To this end, the Lattice–Boltzmann method is used, namely its D3Q19 version. This model is capable to simulate compressible flow. It gives us the advantage to treat dense systems, in particular away from thermal equilibrium. The Lattice–Boltzmann equation is coupled to the particles via a friction force. In addition to this force, acting on *point* particles, we construct another coupling force, which comes from the pressure tensor. The coupling is purely local, i. e. the algorithm scales linearly with the total number of particles. In order to be able to map the physical properties of the Lattice–Boltzmann fluid onto a Molecular Dynamics (MD) fluid, the case of an almost incompressible flow is considered. The Fluctuation–Dissipation theorem for the hybrid coupling is analyzed, and a geometric interpretation of the friction coefficient in terms of a Stokes radius is given.

Part 2 is devoted to the simulation of charged particles. We present a novel method for obtaining Coulomb interactions as the potential of mean force between charges which are dynamically coupled to a local electromagnetic field. This algorithm scales linearly, too. We focus on the Molecular Dynamics version of the method and show that it is intimately related to the Car–Parrinello approach, while being equivalent to solving Maxwell's equations with freely adjustable speed of light. The Lagrangian formulation of the coupled particles–fields system is derived. The quasi–Hamiltonian dynamics of the system is studied in great detail. For implementation on the computer, the equations of motion are discretized with respect to both space and time. The discretization of the electromagnetic fields on a lattice, as well as the interpolation of the particle charges on the lattice is given. The algorithm is as local as possible: Only nearest neighbors sites of the lattice are interacting with a charged particle. Unphysical self–energies arise as a result of the lattice interpolation of charges, and are corrected by a subtraction scheme based on the exact lattice Green's function. The method allows easy parallelization using standard domain decomposition. Some benchmarking results of the algorithm are presented and discussed.

Zusammenfassung

Die vorliegende Dissertation stellt neue Methoden zur Simulation von Systemen mit hydrodynamischer und elektrostatischer Wechselwirkung vor.

Teil 1 widmet sich der Computersimulation von Brown'schen Teilchen mit hydrodynamischer Wechselwirkung. Der wichtigste Einfluß des Lösungsmittels auf die Dynamik der Brown'schen Teilchen besteht darin, daß es hydrodynamische Wechselwirkungen vermittelt. In der vorgestellten Methode wird dies simuliert durch numerische Lösung der Navier–Stokes–Gleichung auf einem Gitter. Hierzu wird die "Lattice Boltzmann"–Methode benutzt, und zwar in ihrer sogenannten "D3Q19"–Version. Dieses Modell ist imstande, kompressible Strömungen zu simulieren. Dies hat den Vorteil, daß dichte Systeme studiert werden können, insbesondere auch unter Nichtgleichgewichtsbedingungen. Die "Lattice Boltzmann"– Gleichung wird mit den Teilchen über eine Reibungskraft gekoppelt. Zusätzlich zu dieser Kraft, die auf *Punktteilchen* wirkt, konstruieren wir eine weitere Kraft, die vom Drucktensor herrührt. Diese Kopplung ist streng lokal, d. h. der Algorithmus skaliert linear mit der Gesamtzahl der Teilchen. Um imstande zu sein, die physikalischen Eigenschaften der "Lattice Boltzmann"–Flüssigkeit auf diejenigen einer Molekulardynamik–Flüssigkeit abzubilden, wird der Fall einer fast inkompressiblen Strömung betrachtet. Die Analyse des Fluktuations–Dissipations– Theorems für die Hybridkopplung führt auf eine geometrische Interpretation des Reibungskoeffizienten im Sinne eines Stokes–Radius.

Teil 2 widmet sich der Simulation geladener Teilchen. Wir präsentieren eine neue Methode, um Coulomb–Wechselwirkungen als das "potential of mean force" zwischen Ladungen zu erhalten, die dynamisch an ein lokales elektromagnetisches Feld angekoppelt werden. Dieser Algorithmus skaliert ebenfalls linear. Wir konzentrieren uns auf die Molekulardynamik–Version der Methode, und zeigen, daß ein enger Zusammenhang zum Car–Parrinello–Verfahren besteht. Außerdem wird gezeigt, daß die Methode auf die Lösung der Maxwell–Gleichungen mit frei anpaßbarer Lichtgeschwindigkeit hinausläuft. Die Lagrange'sche Formulierung des gekoppelten Systems Teilchen–Felder wird hergeleitet. Die quasi–Hamilton'sche Dynamik des Systems wird im Detail studiert. Zur Implementation auf dem Computer werden die Bewegungsgleichungen sowohl räumlich als auch zeitlich diskretisiert. Die Diskretisierung der elektromagnetischen Felder auf dem Gitter sowie die Interpolation der Teilchenladungen auf das Gitter werden angegeben. Der Algorithmus ist so lokal wie nur möglich: Nur die nächsten Nachbarn des Gitters wechselwirken mit einem geladenen Teilchen. Die Gitter–Interpolation der Ladungen führt zu unphysikalischen Selbstenergien; diese werden durch ein Subtraktionsverfahren korrigiert, welches auf der exakten Gitter–Greensfunktion beruht. Die Methode läßt sich mit Standard–Gebietszerlegung leicht parallelisieren. Einige "Benchmark"– Testergebnisse des Algorithmus werden vorgestellt und diskutiert.

Contents

Acknowledgments

I would like to thank Dr. Burkhard Dünweg for suggesting the exciting field of local methods in hydrodynamics and electrostatics for my thesis and for his continuing interest in my progress. He encouraged me to pursue my scientific interests and always devoted time to clarifying discussion.

I am grateful to Tony Maggs (ESPCI, Paris) for inspiring ideas and judicious remarks. Without his useful discussions Part 2 would not have appeared in my thesis.

Very important were the contacts with Tony Ladd (University of Florida) and Mike Cates (University of Edinburgh).

I enjoyed playing table tennis with my officemate Dmytro Antypov.

Thank you to Bo Liu for introducing me to green tea pleasure.

Thank you to my parents for encouraging my intellectual pursuits.

And last but not least, I am indebted to my family – my wife Lena and daughter Nastasia – for their patience and great Love.

Thank you all.

Introduction

This thesis is divided into two main parts. The first part is devoted to the study of a system of slow Brownian particles (in our case: monomers which are connected to build polymer chains), immersed in a viscous fluid. The fast momentum transport through the solvent induces long-range correlations in the stochastic displacements. It is possible to explicitly simulate the solvent degrees of freedom together with the Brownian particles. Originally it was done by plain Molecular Dynamics [1], where the validity of the so-called Zimm model could be demonstrated in detail. However it turns out that it is much more efficient (roughly 20 times) to replace the solvent by a hydrodynamic Stokes background. P. Ahlrichs in his PhD thesis [2] has applied a simple dissipative point particle coupling of the solvent to the polymer system. The coupling is manifestly local. This was done in the framework of the stochastic Lattice Boltzmann (LB) method developed by Ladd [3, 4]. With such a hybrid method the problem of "hydrodynamic screening" could be solved [5].

In Part 1 we are trying to extend the above mentioned method to the study of dense systems in solvent.

A completely different matter is considered in Part 2. The problem of long-range electrostatic interactions in the simulation of complex systems is very challenging. Accurate evaluation of the electrostatic force is the computationally most expensive aspect of Molecular–Dynamics simulations. Though at first glance the systems studied in Part 1 and Part 2 are different, the methods which can be applied to this class of problems are similar. The Coulomb interaction $1/r$ between two charged particles can be considered as a static limit of the retarded interaction field. Just as in the hydrodynamic case, one can try to build a local method, which leads to linear scaling. Both the theoretical treatment and the practical implementation will be considered in the part "Simulation of Electrostatics".

Part I.

Simulation of hydrodynamics

1. Local hybrid method for hydrodynamic interactions

1.1. Introduction

The present part is devoted to a methodological problem that occurs in the computer simulation of Brownian particles with hydrodynamic interactions (HI). Essentially, HI is highly correlated motion of the particles due to fast diffusive momentum transport through the solvent. This is efficiently simulated by explicitly taking this momentum transport into account. This results in a local algorithm which scales linearly with the number of Brownian particles. The alternative approach (Brownian Dynamics), which considers the solvent degrees of freedom as completely integrated out, and puts the correlations directly onto the stochastic motion of the particles, works only for very small particle numbers, since the correlations are long-ranged. While straightforward Molecular Dynamics (MD) can in principle model the momentum transport, it has turned out to be advantageous to consider the solvent on a somewhat coarse-grained scale. Possible ways to describe the solvent are:

- solution of the Navier-Stokes equation on a grid via a finite-difference method;

- the Lattice Boltzmann (LB) equation [3, 4];

- Dissipative Particle Dynamics (essentially MD of soft particles with a momentum-conserving Langevin thermostat) [6];

- Multi-Particle Collision Dynamics [7].

Describing the solvent by such a mesoscopic method does not necessarily mean that the Brownian particles are modeled in the same way. On the contrary, such simulations are usually geared at taking the "microscopic" particle character into account. In particular, in polymer simulations one needs to take into account chain structure, excluded volume, plus (perhaps) solvent quality, chain stiffness, and further interactions like electrostatics. Therefore, the macromolecules need to be modeled in terms of a bead-spring model or similar. The question which then arises is how to couple the Brownian particles to the mesoscopic solvent. This is not immediately obvious; one only knows that the coupling should not violate

the essential ingredients of hydrodynamics, i.e. locality, mass conservation, and momentum conservation.

One possible hybrid approach for polymer-solvent systems was proposed by Ahlrichs and Duenweg [8]: The solvent is modeled by the LBE, while the monomers are MD point particles with a phenomenological friction coefficient, which are coupled dissipatively to the surrounding flow field in terms of a friction force proportional to the velocity difference. The solvent velocity at the position of a particle is obtained via simple linear interpolation from the surrounding lattice sites, and momentum conservation is enforced by removing from the lattice that amount of momentum which was transferred from the solvent to the particle. This has worked rather well for dilute and semidilute polymer solutions [8] where the solvent density is essentially constant (except for minor thermal fluctuations). However, the approach has the disadvantage that dense systems, in particular away from thermal equilibrium, cannot be properly treated. Consider, for instance, a dense polymer network which at time $t = 0$ is exposed to solvent which starts to penetrate and swell it. One would like to be able to explicitly simulate the flow of LB solvent into the matrix (or out of it). Firstly, this requires the replacement of the original D3Q18 LB model (18 velocities corresponding to the nearest and next-nearest neighbors of a 3-dimensional simple cubic lattice) [2], which can only simulate incompressible flow correctly, by the more general D3Q19 model, which adds a zero velocity and is capable of simulating compressible flow. Secondly, the coupling needs to be modified. This is again easily seen from our toy system: At time $t = 0$, the system is at rest and hence the unmodified coupling results in vanishing particle-solvent forces. The consequence is that the internal pressure of the particles forces them to "burst" into the solvent without any counter-force. The same happens to the solvent in the other direction. This unphysical behavior will be explicitly demonstrated in Sec. 1.7. The goal was therefore to find a coupling which would cure this "sickness", and to construct a hybrid model consisting of a mixture of LB fluid and MD fluid, where the LB fluid should be just a coarse-grained description of the MD fluid. In particular, we would require that model to describe the collective interdiffusion of the two "species" correctly.

This goal has not been achieved. The original idea was to assign some surface area to the particles, and to calculate the force on the particles by (essentially) integrating the pressure over the surface (note that the pressure tensor appears as a natural variable in the LB algorithm). As before, the overall momentum balance is enforced. This is indeed expected to introduce a suitable counter-force against the abovementioned "bursts". Nevertheless, it does not model the interactions between solvent and particles correctly in all cases. Consider, for instance, a system of MD particles with purely repulsive interactions immersed homogeneously in LB fluid (thermal equilibrium). Now, at time $t = 0$ we introduce a "quench" such that suddenly a sufficiently strong attractive interaction between the MD particles is turned on. Physically, this system should unmix into a MD-particle rich domain, and a LB-fluid rich domain. However, what our system will actually do is to form an aggregate of MD particles, while the LB fluid remains a homogeneous background.

This is the equilibrium configuration because it minimizes the internal pressure of the LB fluid, and there are no forces between LB fluid and the particles, since the LB pressure profile is constant, such that the surface integrals sum up to zero. Actually, it turns out that in thermal equilibrium the surface integral method is essentially *equivalent* to the original dissipative coupling. The main difference is that there is no longer any Langevin noise needed for the particles. Rather there is only one common source of noise, which is the fluctuating stress tensor of the LB method. This will be worked out in detail in Sec. 1.8.

In hindsight, it is now clear that most probably the solution to the problem is to just introduce a potential which acts from the particle on the surrounding lattice sites, giving rise to a local volume force. Nevertheless, the investigations on coupling MD and LB were not further continued after the somewhat sobering result on the surface integral method. There were several reasons to do so:

1. The abovementioned solution, though rather easy and straightforward, did not immediately occur to us at the time.

2. Originally, the project's plan had been to apply the improved coupling to the long-standing problem of the dynamics of the Theta collapse [9, 10, 11, 12, 13]: Upon sudden decrease of the solvent quality, a single chain undergoes a transition from a swollen coil to a collapsed globule. HI is expected to play an important role in that process. We had expected that the process would be simulated more faithfully with the modified coupling. In particular, the globular state is very dense. In the meantime, however, substantial progress had been made on the problem, by the simulations of Yethiraj et al. [14], Yeomans et al. [15], and, in particular, by the work of Abrams, Lee, and Obukhov [16].

3. We became very interested in the investigations of Part 2 at the time. The investigation and implementation of the potential coupling is thus left for future work.

The remainder of this part is organized as follows. At first we will describe the LB method, focusing on the D3Q19 model. Further we consider the case of an almost incompressible fluid in order to be able to map the physical properties of the LB fluid onto the MD fluid. We then demonstrate the failure of the original coupling in the interdiffusion problem, as sketched above. After that we introduce the surface integral coupling and analyze the Fluctuation-Dissipation theorem for that coupling. This allows us to show the (near) equivalence to the original dissipative coupling, and to assign some geometric interpretation to the friction coefficient in terms of (essentially) a Stokes radius.

1.2. Lattice-Boltzmann method

Lattice-Boltzmann methods were originally introduced [17] to simplify the macroscopic dynamics of the lattice-gas model, by removing the effects of thermal fluctuations. The averaging inherent in the Boltzmann equation leads to Navier-Stokes dynamics. Lattice-Boltzmann simulations of three-dimensional flow typically use a linearized collision operator [18] to simplify the complex collision rules of three-dimensional lattice gases [19]. Although a linearized collision operator loses the unconditional stability of the original lattice-gas [20] and Lattice-Boltzmann [17] models, this is compensated by the speed and simplicity of the code. A further advantage of the linearized collision operator is that equilibrium distributions can be constructed that lead to Galilean invariant forms of the hydrodynamic equations [21, 22, 23]. Further developments in lattice-Boltzmann simulation techniques are summarized in a recent review article [24].

The fundamental quantity in the lattice-Boltzmann model is the discretized one-particle velocity distribution function $n_i(\mathbf{r}, t)$, which describes the mass density of particles with velocity $\mathbf{c}_i$, at a particular node of the lattice $\mathbf{r}$, at a time t; $\mathbf{r}, t$ and $\mathbf{c}_i$ are discrete, whereas n_i is continuous. The hydrodynamics fields, mass density ρ, momentum density $\mathbf{j} = \rho\mathbf{u}$, and momentum flux $\mathbf{\Pi}$, are moments of this velocity distribution:

$$\rho = \sum_i n_i, \quad \mathbf{j} = \rho\mathbf{u} = \sum_i n_i\mathbf{c}_i, \quad \mathbf{\Pi} = \sum_i n_i\mathbf{c}_i\mathbf{c}_i. \tag{1.1}$$

For simulations of particulate suspensions, the lattice-Boltzmann model has two particularly useful properties. First, the connection to molecular mechanics makes it possible to derive simple local rules for the interactions between the fluid and the suspended solid particles [4]. Second, the discrete one-particle distribution function, n_i, contains additional information about the dynamics of the fluid beyond that contained in the Navier-Stokes equations; in particular, the fluid stress tensor, although dynamically coupled to the velocity gradient [25], has an independent significance at short times. This approach is quite different from Brownian dynamics [26] or Stokesian dynamics [27], where correlated fluctuations are applied directly to the particles.

1.3. A 3D Lattice-Boltzmann model

The time evolution of the velocity distribution function, $n_i(\mathbf{r}, t)$, is described by a discrete analogue of the Boltzmann equation [25],

$$n_i(\mathbf{r} + \mathbf{c}_i\Delta t, t + \Delta t) = n_i(\mathbf{r}, t) + \Delta_i\left[\mathbf{n}(\mathbf{r}, t)\right], \tag{1.2}$$

where Δ_i is the change in n_i due to instantaneous molecular collisions at the lattice nodes and Δt is the time step. The time evolution of a lattice-gas is described by a similar equation, except that the continuous population densities are replaced by discrete bit fields. The collision operator $\Delta_i(\mathbf{n})$ depends on all the n_i's at the node,

denoted collectively by $\mathbf{n}(\mathbf{r}, t)$. It can take any form, subject to the constraints of mass and momentum conservation. A computationally useful form for the collision operator can be constructed by linearizing about the local equilibrium $\mathbf{n}^{eq}$ [18], i.e.

$$\Delta_i(\mathbf{n}) = \Delta_i(\mathbf{n}^{eq}) + \sum_j \mathcal{L}_{ij} n_j^{neq}, \tag{1.3}$$

where $\mathcal{L}_{ij}$ are the matrix elements of the linearized collision operator, $n_j^{neq} = n_j - n_j^{eq}$, and $\Delta_i(\mathbf{n}^{eq}) = 0$. The computational utility of lattice-gas and lattice-Boltzmann models depends on the fact that only a small set of velocities are necessary to simulate the Navier-Stokes equations [20].

A particular lattice-Boltzmann model is defined by a set of velocities $\mathbf{c}_i$, an equilibrium distribution n_i^{eq}, and the eigenvalues of the collision operator. The population density associated with each velocity has a weight a^{c_i} that describes the fraction of particles with velocity $\mathbf{c}_i$, in a system at rest; these weights depend only on the speed c_i and are normalized so that $\sum_i a^{c_i} = 1$. Note that the velocities $\mathbf{c}_i$ are chosen such that all particles move from node to node simultaneously. For any cubic lattice,

$$\sum_i a^{c_i} \mathbf{c}_i \mathbf{c}_i = C_2 c^2 \mathbf{1}, \tag{1.4}$$

where $c = \frac{\Delta x}{\Delta t}$, Δx is the grid spacing, and C_2 is a numerical coefficient that depends on the choice of weights. However, in order for the viscous stresses to be independent of direction, the velocities must also satisfy the isotropy condition;

$$\sum_i a^{c_i} c_{i\alpha} c_{i\beta} c_{i\gamma} c_{i\delta} = C_4 c^4 \left\{ \delta_{\alpha\beta} \delta_{\gamma\delta} + \delta_{\alpha\gamma} \delta_{\beta\delta} + \delta_{\alpha\delta} \delta_{\beta\gamma} \right\}. \tag{1.5}$$

In three dimensions, isotropy requires a multi-speed model, for example the 18-velocity model described in reference [4]. This model uses the [100] and [110] directions of a simple cubic lattice, with twice the density of particles moving in [100] directions as in [110] directions; alternatively a 14-velocity model can be constructed from the [100] and [111] directions with the density ratio of 7:1. Although the 14-velocity model requires less computation and less memory than the 18-velocity model, it suffers from "checkerboard" invariants [28] and is less accurate. The 18-velocity model can be augmented by stationary particles, which then enables it to account for small deviations from the incompressible limit. Also the extension to 19 velocities should lead to substantial improvements in the equipartition of energy between particles and fluid in simulations of Brownian particles.

1.3.1. Equilibrium distribution

The form of the equilibrium distribution is constrained by the moment conditions required to reproduce the inviscid (Euler) equations on large length scales and time

Figure 1.1.: 19 velocity lattice-Boltzmann model with rest particles at each lattice site (D3Q19 model).
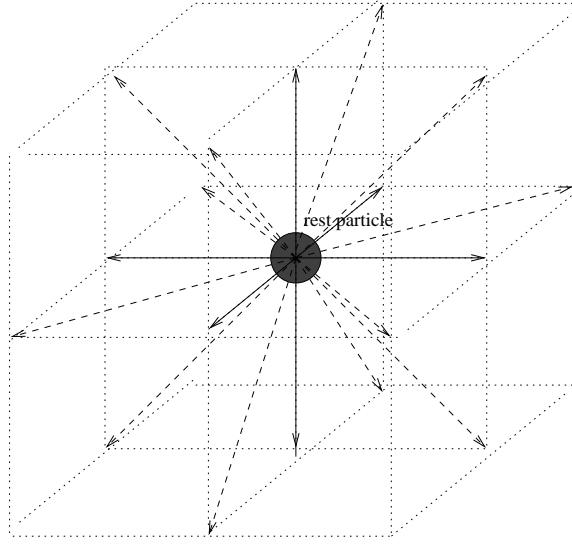
scales. In particular, the second moment of the equilibrium distribution should be equal to the inviscid momentum flux $p\mathbf{1} + \rho\mathbf{uu}$:

$$\rho \;=\; \sum_i n_i^{eq} \tag{1.6}$$

$$\mathbf{j} \;=\; \sum_i n_i^{eq}\mathbf{c}_i = \rho\mathbf{u} \tag{1.7}$$

$$\mathbf{\Pi}^{eq} \;=\; \sum_i n_i^{eq}\mathbf{c}_i\mathbf{c}_i = \rho c_s^2\mathbf{1} + \rho\mathbf{uu} \tag{1.8}$$

The equilibrium distribution can be used in Eqs. 1.6 and 1.7 because mass and momentum are conserved during the collision process; in other words

$$\sum_i n_i^{neq} = \sum_i n_i^{neq}\mathbf{c}_i = 0. \tag{1.9}$$

The pressure in Eq. 1.8, $p = \rho c_s^2$, takes the form of an ideal gas equation of state with adiabatic sound speed c_s. It is also adequate for the liquid phase if the density fluctuations are small (i.e. the Mach number $M = u/c_s \ll 1$), so that $\nabla p = c_s^2\nabla\rho$.

For small Mach numbers, the equilibrium distribution of the 19-velocity model that satisfies Eqs. 1.6- 1.8, as well as the isotropy condition (Eq. 1.5), is [23]

$$n_i^{eq} = a^{c_i}\left[\rho + \frac{\mathbf{jc}_i}{c_s^2} + \frac{\rho\mathbf{uu} : (\mathbf{c}_i\mathbf{c}_i - c_s^2\mathbf{1})}{2c_s^4}\right]\,, \tag{1.10}$$

where $c_s = \sqrt{c^2/3}$ and the coefficients of the three speeds are

$$a^0 = \frac{1}{3},\;\; a^1 = \frac{1}{18},\;\; a^{\sqrt{2}} = \frac{1}{36}. \tag{1.11}$$

In this the coefficient in Eq. 1.5 is $C_4 = (c_s/c)^4$.

In contrast to the equilibrium distributions of lattice-gas models [20], Eqs 1.10 and 1.11 ensure that the inviscid hydrodynamic equations are correctly reproduced. The viscous stresses come from moments of the non-equilibrium distribution, as in the Chapman-Enskog solution of the Boltzmann equation. The fundamental limitation of this class of lattice-Boltzmann models is that the Mach number be small, less than 0.3.

1.3.2. Collision operator

The linearized collision operator must satisfy the following eigenvalue equations:

$$\sum_i \mathcal{L}_{ij} = 0, \quad \sum_i \mathbf{c}_i \mathcal{L}_{ij} = 0, \quad \sum_i \overline{\mathbf{c}_i \mathbf{c}_i} \mathcal{L}_{ij} = \lambda \overline{\mathbf{c}_j \mathbf{c}_j}, \quad \sum_i c_i^2 \mathcal{L}_{ij} = \lambda_v c_j^2 \qquad (1.12)$$

where $\overline{\mathbf{c}_j \mathbf{c}_j}$ indicates the traceless part of $\mathbf{c}_j \mathbf{c}_j$. The first two equations follow from conservation of mass and momentum, and the last two equations describe the isotropic relaxation of the stress tensor; the eigenvalues λ and λ_v are related to the shear and bulk viscosities and lie in the range $-2 < \lambda < 0$. Equation 1.12 accounts for only 10 of the eigenvectors of $\mathcal{L}$. The remaining 9 modes are higher-order eigenvectors of $\mathcal{L}$ that are not relevant to the Navier-Stokes equations. In general the eigenvalues of these kinetic modes are set to -1, which both simplifies the simulation and ensures a rapid relaxation of the non-hydrodynamic modes [4].

The bulk viscous mode is free to relax, so as to account for all the viscous stresses present in a dense fluid.

The collision operator can be further simplified by taking a single eigenvalue for both the viscous and kinetic modes [29, 23]. This exponential relaxation time (ERT) approximation, $\Delta_i = -n_i^{neq}/\tau$, has become the most popular form for the collision operator because of its simplicity and computational efficiency. However, this results in an absence of a clear time scale separation between the kinetic and hydrodynamic modes, and thus we prefer the more flexible collision operator described by Eq. 1.12.

In our simulations we use a 3-parameter collision operator, allowing for separate relaxation of the 5 shear modes, 1 bulk mode, and 9 kinetic modes. The post-collision distribution $n_i^* = n_i + \Delta_i$ is written as a series of moments (Eq. 1.1), as for the equilibrium distribution (Eq. 1.10),

$$n_i^* = a^{c_i} \left[\rho + \frac{\mathbf{j} \mathbf{c}_i}{c_s^2} + \frac{(\rho \mathbf{u} \mathbf{u} + \mathbf{\Pi}^{neq,*}) : (\mathbf{c}_i \mathbf{c}_i - c_s^2 \mathbf{1})}{2 c_s^4} \right] . \qquad (1.13)$$

The zeroth (ρ) and first ($\mathbf{j} = \rho \mathbf{u}$) moments are the same as in the equilibrium distribution (Eq. 1.10), but the non-equilibrium second moment $\mathbf{\Pi}^{neq}$ is modified by the collision process, according to Eq. 1.12:

$$\mathbf{\Pi}^{neq,*} = (1 + \lambda) \overline{\mathbf{\Pi}}^{neq} + \frac{1}{3}(1 + \lambda_v)(\mathbf{\Pi}^{neq} : \mathbf{1})\mathbf{1}, \qquad (1.14)$$

where $\mathbf{\Pi}^{neq} = \mathbf{\Pi} - \mathbf{\Pi}^{eq}$. The kinetic modes can also contribute to the post-collision distribution, but we choose the eigenvalues of these modes to be -1, so that they have no effect on n_i^*. Equation 1.14 with $\lambda = \lambda_v = -1$ is equivalent to the ERT model with $\tau = 1$.

1.3.3.   External forces

In the presence of an externally imposed force density $\mathbf{f}$, for example a pressure gradient or a gravitational field, the time evolution of the lattice-Boltzmann model includes an additional contribution $f_i(\mathbf{r}, t)$,

$$n_i(\mathbf{r} + \mathbf{c}_i\Delta t, t + \Delta t) = n_i(\mathbf{r}, t) + \Delta_i\left[\mathbf{n}(\mathbf{r}, t)\right] + f_i(\mathbf{r}, t). \tag{1.15}$$

The forcing term can be expanded in a power series in the particle velocity; i.e.

$$f_i = a^{c_i}\ \left[A + \frac{\mathbf{B} \cdot \mathbf{c}_i}{c_s^2} + \frac{\mathbf{C} : (\mathbf{c}_i\mathbf{c}_i - c_s^2\mathbf{1})}{2c_s^4}\right]\ \Delta t, \tag{1.16}$$

where A, $\mathbf{B}$, and $\mathbf{C}$ are determined by requiring that the moments of f_i are consistent with the hydrodynamic equations. Then the zeroth and first moments are given by $\sum_i f_i = A = 0$ and $\sum_i f_i\mathbf{c}_i = \mathbf{B} = \mathbf{f}$. The second moment, $\mathbf{C}$, is usually neglected,because numerical simulations show the variations in $\mathbf{C}$ have negligible effect on the flow. A systematic introduction of external forces in the lattice-Boltzmann scheme can be found in reference [30].

1.3.4.   Fluctuations

The lattice-Boltzmann model can be extended to simulate thermal fluctuations, which lead to Brownian motion of the particles. The fluctuating lattice-Boltzmann model [3] incorporates a random component into the momentum flux during the collision process (c.f. Eq. 1.14):

$$\begin{aligned}
\mathbf{\Pi}^{neq,*} &= (1+\lambda)\overline{\overline{\mathbf{\Pi}}}^{neq} + \frac{1}{3}(1+\lambda_v)(\mathbf{\Pi}^{neq} : \mathbf{1})\mathbf{1} + \mathbf{\Pi}^f \\
\mathbf{\Pi}^f &= \zeta\overline{\mathbf{R}} + \zeta_v R_v\mathbf{1},
\end{aligned} \tag{1.17}$$

where R_v is a Gaussian random variable with zero mean and unit variance, and $\mathbf{R}$ is a symmetric matrix of Gaussian random variables of zero mean. The off-diagonal elements of $\mathbf{R}$ have a variance of 1, while the diagonal elements have a variance 2. In this particular implementation, 6 random numbers are required to generate the components of the symmetric matrix $\mathbf{R}$, together with the constraint that $\overline{\mathbf{R}}$ is traceless. The average stress fluctuations are local in space and time, as in Eq. 1.50, with a variance given by

$$\left\langle \Pi^f_{\alpha\beta}\Pi^f_{\gamma\delta} \right\rangle = \zeta^2\ \left[\overline{\delta_{\alpha\gamma}\delta_{\beta\delta}} + \overline{\delta_{\alpha\delta}\delta_{\beta\gamma}}\right]\ + \zeta_v^2\delta_{\alpha\beta}\delta_{\gamma\delta}. \tag{1.18}$$

The lattice modifies the result for continuous fluids and the amplitudes of the random fluctuations are given by these formulas

$$\zeta = \left(\frac{2k_bT\eta\lambda^2}{\Delta x^3\Delta t}\right)^{1/2}, \quad \zeta_v = \left(\frac{2k_bT\eta_v\lambda_v^2}{\Delta x^3\Delta t}\right)^{1/2}, \tag{1.19}$$

where η and η_v are shear and bulk viscosities in the continuum, respectively; Δx is the lattice spacing and Δt is the time step. The additional factor of $\sqrt{\lambda^2}$ is a consequence of discrete lattice artifacts. For the choice of eigenvalues $\lambda = \lambda_v = -1$, an exact correspondence with the fluctuation-dissipation relation for continuous systems is obtained. However the discrete version (Eq. 1.19) can also be applied to systems where the viscous eigenvalues are not equal to -1 [4].

1.4.   Decay rate of longitudinal waves

We turn now to the problem of describing the decay of long-wavelength fluctuations in the collective dynamical variables. The macroscopic local densities associated with the conserved variables are the mass density $\rho(\mathbf{r}, t)$, the momentum density $\mathbf{j}(\mathbf{r}, t)$ and the energy density $e(\mathbf{r}, t)$. Because lattice-Boltzmann has a very nice properties in the isothermal case, in the future we will use only isothermal equations. It means we will not consider the energy equations which in our case is trivial. The local velocity field $\mathbf{u}(\mathbf{r}, t)$ is defined via the relation

$$\mathbf{j}(\mathbf{r}, t) = \rho(\mathbf{r}, t)\mathbf{u}(\mathbf{r}, t) \tag{1.20}$$

The conservation laws for the local densities are of the form

$$\frac{\partial\rho(\mathbf{r}, t)}{\partial t} + \nabla\mathbf{j}(\mathbf{r}, t) = 0 \tag{1.21}$$

$$\frac{\partial\mathbf{j}(\mathbf{r}, t)}{\partial t} + \nabla\mathbf{\Pi}(\mathbf{r}, t) = 0. \tag{1.22}$$

where $\mathbf{\Pi}(\mathbf{r}, t)$ is the momentum current or stress tensor. These equations are supplemented by constitutive relation in which $\mathbf{\Pi}$ is expressed in terms of the dissipative processes in the fluid. The stress tensor is given macroscopically (Ref. [31])

$$\Pi_{\alpha\beta}(\mathbf{r}, t) = \delta_{\alpha\beta}p(\mathbf{r}, t) - \eta\left(\frac{\partial u_\alpha(\mathbf{r}, t)}{\partial r_\beta} + \frac{\partial u_\beta(\mathbf{r}, t)}{\partial r_\alpha}\right) + \delta_{\alpha\beta}\left(\frac{2}{3}\eta - \eta_v\right)\nabla\mathbf{u}(\mathbf{r}, t) \tag{1.23}$$

where $p(\mathbf{r}, t)$ is the local pressure, η is the shear viscosity and η_v is the bulk viscosity. We now choose a frame of reference in which the mean velocity of the fluid is zero, and assume that the local deviations of the hydrodynamic variables from their average values are small. The equations above may then be linearized with respect to the deviations. In particular, the momentum density may be expressed as

$$\mathbf{j}(\mathbf{r}, t) = [\rho + \delta\rho]\,\mathbf{u}(\mathbf{r}, t) \simeq \rho\mathbf{u}(\mathbf{r}, t) \tag{1.24}$$

Substitution of Eq. 1.23 and Eq. 1.24 in Eq. 1.22 gives the Navier-Stokes equation in linearized form

$$\rho\frac{\partial \mathbf{u}(\mathbf{r},t)}{\partial t} + \nabla p(\mathbf{r},t) - \eta\nabla^2\mathbf{u}(\mathbf{r},t) - \left[\frac{1}{3}\eta + \eta_v\right]\nabla\nabla\mathbf{u}(\mathbf{r},t) = 0 \tag{1.25}$$

If we invoke the hypothesis of thermodynamic equilibrium, the deviations of the local thermodynamic variables from their average values can be expressed in terms of a set of statistically independent quantities. Choosing as independent variable the density, for the pressure we obtain

$$\delta\rho(\mathbf{r},t) = \rho(\mathbf{r},t) - \rho_e \tag{1.26}$$

$$\delta p(\mathbf{r},t) = \left(\frac{\partial p}{\partial \rho}\right)_T \delta\rho(\mathbf{r},t) \tag{1.27}$$

We consider also the isothermal case $\delta T(\mathbf{r},t) = 0$. The continuity equation may be rewritten as

$$\frac{\partial \delta\rho(\mathbf{r},t)}{\partial t} + \nabla\mathbf{j}(\mathbf{r},t) = 0 \tag{1.28}$$

and the Navier-Stokes equation as

$$\left[\frac{\partial}{\partial t} - \frac{\eta}{\rho}\nabla^2 - \frac{\frac{1}{3}\eta + \eta_v}{\rho}\nabla\nabla\right]\mathbf{j}(\mathbf{r},t) + \left(\frac{\partial p}{\partial \rho}\right)_T\nabla\delta\rho(\mathbf{r},t) = 0 \tag{1.29}$$

Equations 1.28 and 1.29 are readily solved by taking the double transforms with respect to space (Fourier) and time (Laplace) to give

$$-iz\tilde{\rho}_{\mathbf{k}}(z) + i\mathbf{k}\tilde{\mathbf{j}}_{\mathbf{k}}(z) = \rho_{\mathbf{k}} \tag{1.30}$$

$$\left[-iz + \frac{\eta}{\rho}k^2 + \frac{\frac{1}{3}\eta + \eta_v}{\rho}\mathbf{k}\mathbf{k}\right]\tilde{\mathbf{j}}_{\mathbf{k}}(z) + i\mathbf{k}\left(\frac{\partial p}{\partial \rho}\right)_T\tilde{\rho}_{\mathbf{k}}(z) = \mathbf{j}_{\mathbf{k}} \tag{1.31}$$

where the transformations are given by these formulas:

$$\tilde{\rho}_{\mathbf{k}} = \int_0^\infty dt\, exp(izt)\int \delta\rho(\mathbf{r},t)exp(-i\mathbf{k}\mathbf{r})d\mathbf{r} \tag{1.32}$$

$$\rho_{\mathbf{k}} = \tilde{\rho}_{\mathbf{k}}(t=0) \tag{1.33}$$

Choosing $\mathbf{k}$ along the z-axis we obtain:

$$\left[-iz + bk^2\right]\tilde{j}_{\mathbf{k}}^z(z) + ik\left(\frac{\partial p}{\partial \rho}\right)_T\tilde{\rho}_{\mathbf{k}}(z) = j_{\mathbf{k}}^z \tag{1.34}$$

$$\left[-iz + \nu k^2\right]\tilde{j}_{\mathbf{k}}^\alpha = j_{\mathbf{k}}^\alpha, \alpha = x,y \tag{1.35}$$

where $b = \frac{\frac{4}{3}\eta + \eta_v}{\rho}$ is the kinematic longitudinal viscosity, and $\nu = \frac{\eta}{\rho}$ is the kinematic shear viscosity.

In matrix form our system of linear equations can be written

$$
\begin{pmatrix}
-iz & ik & 0 & 0 \\
ik \left. \frac{\partial p}{\partial \rho} \right|_T & -iz + bk^2 & 0 & 0 \\
0 & 0 & -iz + \nu k^2 & 0 \\
0 & 0 & 0 & -iz + \nu k^2
\end{pmatrix}
\begin{pmatrix}
\tilde{\rho}_{\mathbf{k}}(z) \\
\tilde{j}^z_{\mathbf{k}}(z) \\
\tilde{j}^x_{\mathbf{k}}(z) \\
\tilde{j}^y_{\mathbf{k}}(z)
\end{pmatrix}
=
\begin{pmatrix}
\rho_{\mathbf{k}}(z) \\
j^z_{\mathbf{k}}(z) \\
j^x_{\mathbf{k}}(z) \\
j^y_{\mathbf{k}}(z)
\end{pmatrix}
$$

The matrix of coefficients is called the hydrodynamic matrix. Its block-diagonal structure shows that the transverse-current fluctuations are completely decoupled from the fluctuations in the other (longitudinal) variables. The determinant of the hydrodynamic matrix therefore factorizes into the product of purely longitudinal (l) and transverse (t) parts, i.e.

$$ D(k, z) = D_l(k, z) D_t(k, z) \tag{1.36} $$

with

$$ D_l(k, z) = -z^2 - izbk^2 + k^2 \left. \frac{\partial p}{\partial \rho} \right|_T \tag{1.37} $$

The dispersion relation for the longitudinal collective modes is given by the complex roots of the equation $D_l(k, z) = 0$, i.e.

$$ z^2 + ibk^2 z - k^2 \left. \frac{\partial p}{\partial \rho} \right|_T = 0. \tag{1.38} $$

Defining the adiabatic sound velocity

$$ c_s^2 = \gamma \left. \frac{\partial p}{\partial \rho} \right|_T = \frac{c_p}{c_v} \left. \frac{\partial p}{\partial \rho} \right|_T, $$

where c_p and c_v are the specific heat at constant pressure and constant volume, respectively, we obtain the solution for z:

$$ z = -\frac{ib}{2} k^2 \pm \sqrt{\frac{c_s^2}{\gamma} - \frac{b^2 k^2}{4}} \; k \tag{1.39} $$

Since the hydrodynamic calculation is valid only in the long-wavelength limit, it is sufficient to calculate complex frequencies to order k^2. For small k we obtain the decay rate, or sound-attenuation coefficient as:

$$ \Gamma = \frac{b}{2} k^2 \tag{1.40} $$

1.5.   Simulations of sound modes

Equation 1.40 shows that sound modes in our LB model are characterized by

- the isothermal sound velocity

$$c_s \gamma^{-1/2} = \left. \frac{\partial p}{\partial \rho} \right|_T,$$

  which follows trivially from the model's ideal gas equation of state, and

- the shear and bulk viscosities η and η_v, which are input parameters directly related to the eigenvalues λ and λ_v.

Figure 1.2 shows the expected behavior of a damped harmonic oscillator for the longitudinal component of the current density. These data were obtained by a simple computer experiment, where at $t = 0$ a small sine wave was superimposed over the constant density profile, such that it was compatible with the periodic boundary conditions of the overall simulation box. The parameter η_v was first set to zero, and then varied over two orders of magnitude. One sees that even for $\eta_v = 0$ there is a substantial damping of the sound, as a consequence of the nonzero value of η, whereas a really large value of η_v results in completely overdamped motion.

Such computer experiments are, on the contrary, very useful to determine the material parameters, by fitting the curves to the expected behavior. This is of course not needed for the LB model (there the macroscopic transport coefficients are anyways known beforehand), but for an MD fluid it clearly is: Recall that the goal is to map an MD fluid as faithfully as possible onto the LB fluid. This requires that all three parameters (speed of sound, plus viscosities) are measured via MD. The older work by Ahlrichs and Dünweg [8] needed to worry only about the shear viscosity, but in the present case, where we are interested in longitudinal fluctuations, too, we need the other two parameters as well. Figure 1.2 then suggests a rather straightforward way how to obtain them: Set up a long-wavelength density wave and study its decay. This allows to simultaneously determine the sound velocity and the attenuation coefficient. Furthermore, the shear viscosity can be determined by setting up an analogous transversal velocity mode, and studying its (purely exponential) decay. A little caveat must be taken into account. Since the MD should be run with realistic dynamics, one should do nothing but solve Newton's equations of motion. This implies that in the MD system the energy is conserved, and thermal conduction must be taken into account in the hydrodynamics. In this case the sound attenuation coefficient is not given by Eq. 1.40, but rather by [32]

$$\Gamma = \frac{k^2}{2} \left[\frac{a(\gamma - 1)}{\gamma} + b \right] \tag{1.41}$$

where $a = \lambda_T / (\rho c_v)$, and λ_T the thermal conductivity. Therefore, one also needs to determine λ_T (this can be done, for instance, by the algorithm developed by Müller-Plathe [33]), and the specific heat (this can be done via a fluctuation relation [32]).
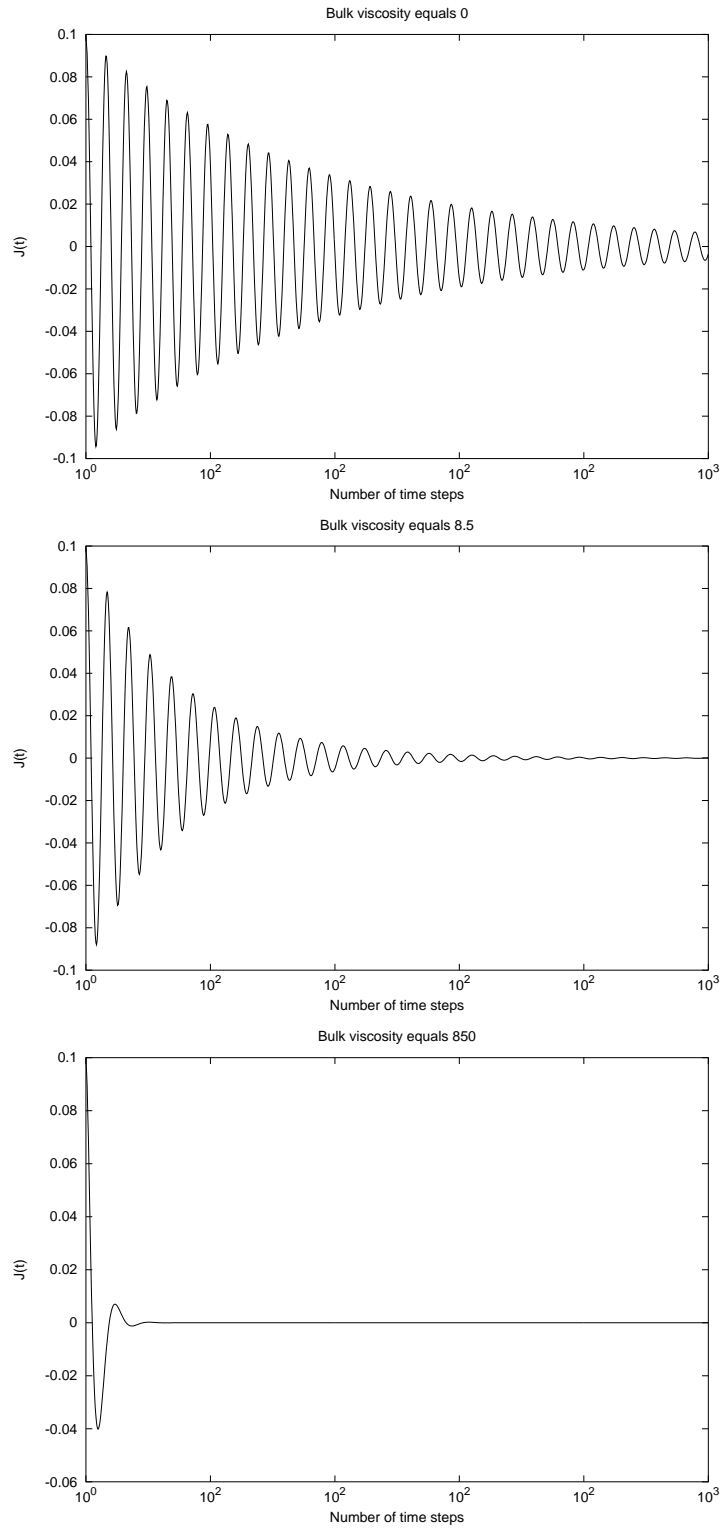
Figure 1.2.: The damping of longitudinal modes for the fluid with different values of bulk viscosity.

1.6.   Realization of the coupling

Let us recapitulate the original coupling term, presented in the work [8].

The coupling force can be divided in 2 terms - the pure friction term, the fluctuating force term. The first term is an analogy of the Stokes Law for a sphere in a viscous fluid, i.e. the force which acts on the fluid from the monomer is proportional to the difference of monomer velocity $\mathbf{v}$ and the fluid velocity $\mathbf{u}(\mathbf{R})$ at the position of the monomer

$$\mathbf{F}_{fl}^{(fric)} = -\xi_{bare} \left[\mathbf{v} - \mathbf{u}(\mathbf{R}, t) \right]. \tag{1.42}$$

Here the ξ_{bare} is the coefficient of proportionality, which will be referred to as the "bare" friction coefficient. Due to the dissipative character of the coupling, it is necessary to incorporate fluctuations in the particle equations by extending Eq. 1.42 to

$$\mathbf{F}_{fl}^{(fric)} = -\xi_{bare} \left[\mathbf{v} - \mathbf{u}(\mathbf{R}, t) \right] + \mathbf{f}. \tag{1.43}$$

Here $\mathbf{f}$ is a stochastic force of zero mean and variance

$$\langle f_\alpha(t_1) f_\beta(t_2) \rangle = 2k_B T \xi_{bare} \delta_{\alpha\beta} \delta(t_1 - t_2) \tag{1.44}$$

Because the fluid velocity is only calculated at the discrete lattice sites in the simulation, one has to interpolate to get $\mathbf{u}(\mathbf{R}, t)$ at the monomer's position. One can use a simple linear interpolation using the grid points on the elementary lattice cell containing the monomer. This scheme can be interpreted also as flow field which acts on a particle of finite extent. For example, using a particle of the same size as a grid cell and of rectangular form, as shown on Fig. 1.3, the flow velocity from the grid point (i,j) comes with the weight which is the closest shaded area to this point. This area weighting procedure is easily seen to be a bilinear interpolation and is readily generalized to three dimensions by using 8 nearest cell centers [34]. This approach is particularly useful when we will consider the electrodynamic problems.

From the above mentioned considerations, the flow velocity is averaged over the size of the particle. Denoting the relative position of the particle in this cell as (x, y, z), with the origin being at the lower left front edge (see Fig. 1.3), we can write

$$\mathbf{u}(\mathbf{R}, t) = \sum_{\mathbf{r} \in ng} w_\mathbf{r} \mathbf{u}(\mathbf{r}, t) \tag{1.45}$$

where ng denotes the grid points on the considered elementary lattice cell and weights are given by the formulas

$$\begin{align} w_{(i,j,k)} &= (1 - x/\Delta x)(1 - y/\Delta x)(1 - z/\Delta x) \tag{1.46} \\ w_{(i+1,j,k)} &= x/\Delta x (1 - y/\Delta x)(1 - z/\Delta x). \end{align}$$

In order to conserve the total momentum of fluid and monomer we have to assign the opposite force to the fluid in that cell. Then the interaction is purely
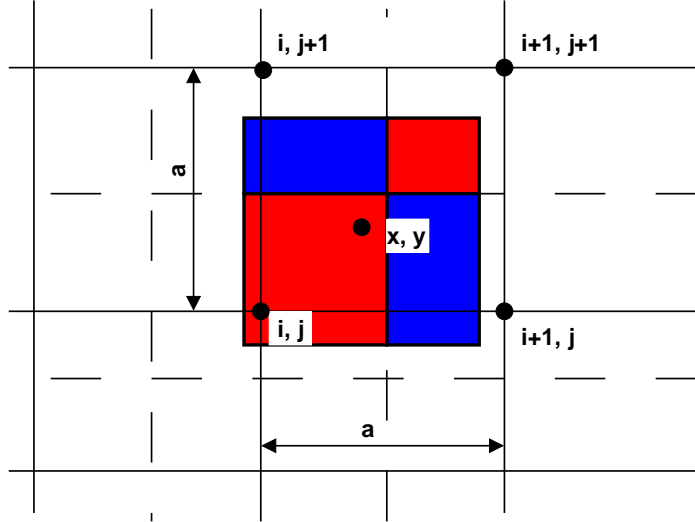
Figure 1.3.: An interpolation scheme for the coupling of the monomer with fluid.

local, the force density $-\mathbf{F}_{fl}/(\Delta x)^3$ which is to be given to the fluid leads to a momentum density transfer per MD time step Δt of

$$-\mathbf{F}_{fl}/(\Delta x)^3 = \frac{\Delta \mathbf{j}}{\Delta t} = \sum_{i,\mathbf{r}\in ng} \Delta n_i(\mathbf{r}, t)\mathbf{c}_i \frac{1}{\Delta t} \qquad (1.47)$$

The way how to calculate the corresponding Δn_i is described in [8].

1.7. Diffusion properties of Lennard–Jones and Lattice–Boltzmann mixture

Diffusion phenomena in fluids and fluid mixtures are of immense importance [35] and have been investigated from time to time using the latest tools available at each stage. In order to be able to freely interchange between Lennard-Jones particles and Lattice–Boltzmann particles we have to adjust the collective properties of these two different fluids. The first transport coefficient on our agenda is the diffusion coefficient.

Even the simple one-component Lennard–Jones fluid can be considered as a mixture of several components. This can be achieved by labeling the atoms of the fluid. Further we will call it coloring and consider only binary mixtures. This allows us to study the collective interdiffusion coefficient, whose value is similar to the single-particle single–diffusion coeffcient.

For this problem we perform simple test simulations, studying a dense repulsive Lennard–Jones fluid whose parameters are given in Ref. [8]. Let us prepare a system in which red particles are contained in the slab directly at the center of the simulation box. The rest part of the box is occupied by the blue one. In Fig. 1.4

we present the changing of the shape of the density profile with respect to time of simulation. One can easily see that we observe diffusive behavior. Next we
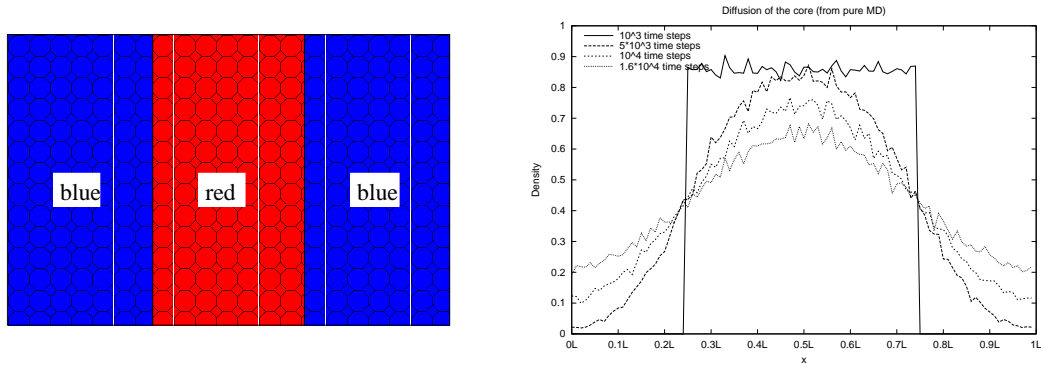
Figure 1.4.: Evolution of the density profile for the Lennard-Jones fluid mixture of "red" and "blue" particles.

want to perform the same experiment for a mixture of Lennard–Jones particles and Lattice–Boltzmann particles. From Fig. 1.5 one can directly see that in the case of
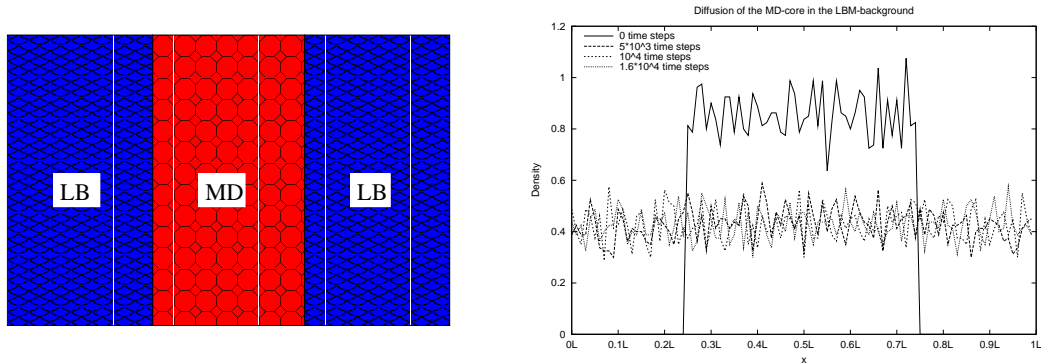
Figure 1.5.: Evolution of the density profile for the mixture of Lennard-Jones fluid (middle core) and lattice-Boltzmann fluid (background fluid).

this mixture there is no diffusive behavior of the MD-particles. After a short time the MD-particles are simply smeared out through the whole simulation box. There must be a driving force and this force is pressure (see Fig. 1.6). At the beginning the pressure must relax and only after that one can observe diffusive behavior.

It means our coupling force between lattice-Boltzmann fluid and MD-particles can not catch the changes in the pressure. We have to modify this term and we do it directly by adding pressure and counter pressure terms in our equations.
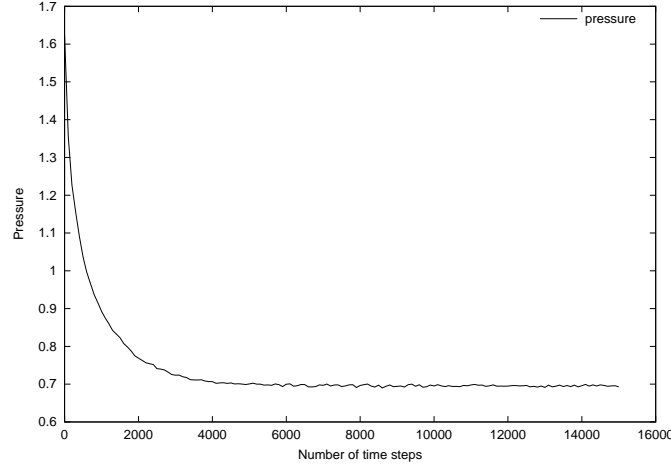
Figure 1.6.: Pressure drop in the system of lattice-Boltzmann and Lennard-Jones particles.

1.8.   Modification of the coupling

1.8.1.   Pressure and counter pressure

In this work we propose to modify the coupling force between monomers and the fluid, which was introduced in the work [8] and is given by Eq. 1.43. In addition to using the friction force, acting on the point particle, we construct another coupling force, which comes from the pressure tensor. This method can catch the differences in the density of the fluid. Because pressure always acts on a surface, we need to assign to our particles some artificial surface. The simplest approach would be to consider our particles as spheres of radius R. The value of this radius will be defined from the Fluctuation–Dissipation theorem.

   The coupling force can be divided into three terms - the pure friction term, the pressure term and the fluctuating stress tensor term. The first term is an analogy of the Stokes Law for a sphere in a viscous fluid, i.e. the force which acts on the fluid from the monomer is proportional to the difference of monomer velocity $\mathbf{v}$ and the fluid velocity $\mathbf{u}(\mathbf{R})$ at the position of the monomer

$$\mathbf{F}_{fl}^{(fric)} = -\xi_{bare} \left[\mathbf{v} - \mathbf{u}(\mathbf{R}, t) \right]. \tag{1.48}$$

Here the ξ_{bare} is the coefficient of proportionality, which will be referred to as the "bare" friction coefficient. This term is needed as a symplistic replacement of the hydrodynamic "stick" boundary condition. The second term incorporates the response of the force to the local changes of the density and therefore pressure (see Fig. 1.7):

$$\mathbf{F}_{fl}^{(pressure)} = -\sum_i \mathbf{\Pi}_i \mathbf{A}_i \tag{1.49}$$

where the summation goes over the surrounding lattice sites i, and $\mathbf{\Pi}_i$ is the pressure tensor on site i. The area vectors $\mathbf{A}_i$ point in [111] direction; the precise direction

is given by the octant in which site i is found. The underlying picture of the sphere of radius R, whose surface is divided into eight sub-surfaces of equal size,

$$|\mathbf{A}_i| = \frac{1}{8} 4\pi R^2.$$

The momentum transfer to the fluid and the interpolation scheme for the new coupling are the same as for the case of the original coupling.

1.8.2. Modification of the stochastic force

One has to take care when adding stochastic terms to the system. Due to the dissipative nature of the coupling, it is necessary to incorporate fluctuations to both the fluid and the monomers. In order to be able to consider the fluctuational hydrodynamic one can add fluctuations directly to the stress tensor. The amplitude of these fluctuations can be calculated from statistical thermodynamics [36], and their time evolution is described by the laws of linear hydrodynamics [31]. The components of the stress tensor $\mathbf{\Pi}^f$ behave as Gaussian random variables with zero mean and variance [31]:

$$\langle \delta\Pi_{ik}(\mathbf{r}_1, t_1)\delta\Pi_{lm}(\mathbf{r}_2, t_2)\rangle =$$
$$2k_BT \quad \eta\left(\delta_{il}\delta_{km} + \delta_{im}\delta_{kl}\right) + \quad \eta_v - \frac{2}{3}\eta \quad \delta_{ik}\delta_{lm} \quad \delta(\mathbf{r}_1 - \mathbf{r}_2)\delta(t_1 - t_2) \tag{1.50}$$

It should be noted that Eq. 1.50 does not describe the instantaneous fluctuations in stress on a molecular time scale. Rather it expresses the time-dependent relaxation of stress fluctuations in a form that is local in space and time, yet consistent with the Green-Kubo expressions for the shear and bulk viscosities. Such expressions are valid on length and time scales that are large compared with molecular scales; our simulations satisfy both these requirements.

Let us now discuss the coupling term $-\sum_i \mathbf{\Pi}_i\mathbf{A}_i$, which can be viewed as a surface integral, in some more detail. We are particularly interested in this coupling in the case of thermal equilibrium. In the continuum limit, the pressure tensor has the form

$$\mathbf{\Pi} = p\mathbf{1} - \eta \quad \nabla\mathbf{u} + (\nabla\mathbf{u})^\dagger \quad + \quad \frac{2}{3}\eta - \eta_v \quad \nabla \cdot \mathbf{u} + \delta\mathbf{\Pi} \tag{1.51}$$

where $(\nabla\mathbf{u})^\dagger$ is the matrix transpose of $(\nabla\mathbf{u})$ and the $\delta\mathbf{\Pi}$ is a fluctuating part of the stress.

However, in the coupling term in thermal equilibrium we can neglect all terms of $\mathbf{\Pi}$ except the fluctuating stress. The reason is that neither p nor $\mathbf{u}$ vary much in thermal equilibrium. Hence the contributions of the neglected terms to the surface integral are small. In particular, these contributions are proportional to the lattice spacing, and become vanishingly small in the limit of small lattice spacing. Conversely, the fluctuating stress at a lattice site scales as $(\Delta x)^{-3/2}$, where Δx is the lattice spacing. The particle radius will later on turn out to scale as $(\Delta x)^{3/4}$, i. e.

the areas $\mathbf{A}_i$ scale as $(\Delta x)^{3/2}$. In other words, the fluctuating part is independent of the lattice spacing. The omitted parts are hence safe to neglect in the limit of vanishing lattice spacing. We thus arrive at

$$\mathbf{F}_{fl} = -\xi_{bare} \left[\mathbf{v} - \mathbf{u}(\mathbf{R}, t) \right] + \mathbf{f}_p. \qquad (1.52)$$

where $\mathbf{f}_p$ is a stochastic force of the form

$$\mathbf{f}_p = -\sum_i \delta \mathbf{\Pi}_i \mathbf{A}_i$$

We now wish to make sure that this stochastic force satisfies the usual fluctuation–dissipation theorem, i. e.

$$\langle f_\alpha(t_1) f_\beta(t_2) \rangle = 2 k_B T \xi_{bare} \delta_{\alpha\beta} \delta(t_1 - t_2).$$
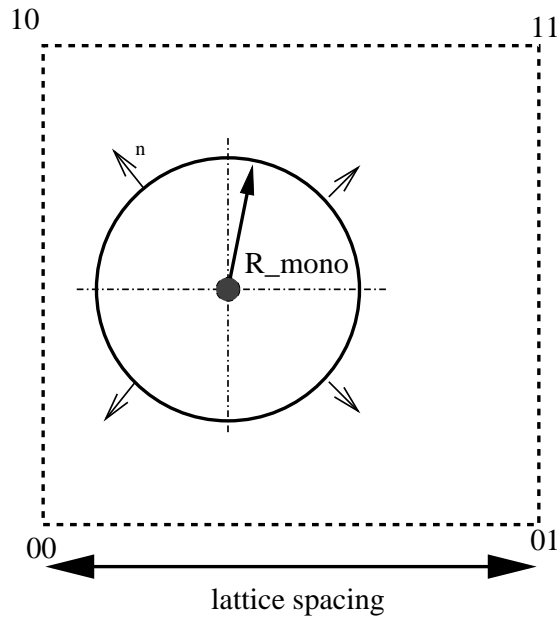
Figure 1.7.: The stochastic force in the coupling of the monomer with fluid.

The left-hand side is straightforward to calculate:

$$\langle f_\alpha(t_1) f_\beta(t_2) \rangle = \sum_{\mathbf{r}_i} \sum_{\mathbf{r}_j} A_\gamma(\mathbf{r}_i) A_\delta(\mathbf{r}_j) \left\langle \Pi_{\alpha\gamma}^f(\mathbf{r}_i, t) \Pi_{\beta\delta}^f(\mathbf{r}_j, t) \right\rangle \qquad (1.53)$$

where the repeated index means summation over. Using the explicit form of the variance of stress tensor (Eq. 1.50) we get

$$\langle f_\alpha(t_1) f_\beta(t_2) \rangle = 2 k_B T \frac{\delta(t_1 - t_2)}{(\Delta x)^3}$$

$$\sum_{\mathbf{r}_i} \sum_{\mathbf{r}_j} A_\gamma(\mathbf{r}_i) A_\delta(\mathbf{r}_j) \delta_{\mathbf{r}_i, \mathbf{r}_j} \quad \eta \left(\delta_{\alpha\beta} \delta_{\gamma\delta} + \delta_{\alpha\delta} \delta_{\gamma\beta} \right) + \quad \eta_v - \frac{2}{3} \eta \quad \delta_{\alpha\gamma} \delta_{\beta\delta} \quad (1.54)$$

In the three dimensional space the value of surface area is given by the area of sphere, noting the fact, that we have 8 neighbor sites, for the area per one neighbor site we have

$$\mathbf{A}(\mathbf{r}_i) = \frac{4\pi R^2}{8}\mathbf{n}_i = \frac{\pi R^2}{2}\mathbf{n}_i \tag{1.55}$$

After inserting the expression for the area surface to Eq. 1.54 the equation for the variance of the stochastic force obtains the form

$$\langle f_\alpha(t_1)f_\beta(t_2)\rangle = k_B T \frac{\pi^2 R^4}{2}\frac{\delta(t_1-t_2)}{(\Delta x)^3}\times$$

$$\sum_{\mathbf{r}_i} n_\gamma(\mathbf{r}_i)n_\delta(\mathbf{r}_i)\ \left[\eta\left(\delta_{\alpha\beta}\delta_{\gamma\delta}+\delta_{\alpha\delta}\delta_{\gamma\beta}\right)+\left(\eta_v-\frac{2}{3}\eta\right)\delta_{\alpha\gamma}\delta_{\beta\delta}\right]=$$

$$= k_B T \frac{\pi^2 R^4}{2}\frac{\delta(t_1-t_2)}{(\Delta x)^3}\times$$

$$\sum_{\mathbf{r}_i}\left[\eta\left(\delta_{\alpha\beta}n^2(\mathbf{r}_i)+n_\alpha(\mathbf{r}_i)n_\beta(\mathbf{r}_i)\right)+\left(\eta_v-\frac{2}{3}\eta\right)n_\alpha(\mathbf{r}_i)n_\beta(\mathbf{r}_i)\right] \tag{1.56}$$

For the normal vector $\mathbf{n}(\mathbf{r}_i)$ we can use the elementary properties such as the unity of the absolute value and orthogonality:

$$\sum_{\mathbf{r}_i} n_\alpha(\mathbf{r}_i)n_\beta(\mathbf{r}_i) = \frac{8}{3}\delta_{\alpha\beta}, \quad \sum_{\mathbf{r}_i} n^2(\mathbf{r}_i) = 8 \tag{1.57}$$

Finally we have the following expression for the variance of the stochastic force

$$\langle f_\alpha(t_1)f_\beta(t_2)\rangle =$$

$$k_B T \pi^2 R^4 \frac{\delta(t_1-t_2)}{2(\Delta x)^3}\left[\eta\left(8\delta_{\alpha\beta}+\frac{8}{3}\delta_{\alpha\beta}\right)+\left(\eta_v-\frac{2}{3}\eta\right)\frac{8}{3}\delta_{\alpha\beta}\right]=$$

$$= \frac{4k_B T \pi^2 R^4}{3}\frac{\delta(t_1-t_2)}{(\Delta x)^3}\delta_{\alpha\beta}\left(\frac{10}{3}\eta+\eta_v\right) \tag{1.58}$$

Therefore the value of the radius R of our artificial sphere is determined by relating the last equation to the usual Langevin equation with the friction term

$$\xi_{bare} = \frac{2}{3}\pi^2\frac{R^4}{(\Delta x)^3}\left(\frac{10}{3}\eta+\eta_v\right) \tag{1.59}$$

1.9.   Fluctuation–Dissipation theorem

The main requirement for our model is the fulfillment of Fluctuation–Dissipation theorem. Only in this case we can be sure in the reliability of the obtained data. In this section we want to prove the Fluctuation-Dissipation Theorem for our model in the continuum case. As a consequence it means the equivalence of the two formulations of the coupling term (original and modified).

The starting point is the compressible Navier–Stokes equation with fluctuations.

Our system consists of the coupled equations of the monomer movement and the compressible Navier–Stokes equations. Defining as m the mass of the particle, $\mathbf{R}$ - position of the particle, $\mathbf{v}$ - the velocity and by $\mathbf{F}^{ext}$ the external force, we obtain:

$$\frac{d\mathbf{R}}{dt} = \mathbf{v} \tag{1.60}$$

$$\frac{d\mathbf{v}}{dt} = \frac{1}{m}\mathbf{F}^{ext} - \xi_{bare}\left(\mathbf{v} - \mathbf{u}\right) + \frac{1}{m}\mathbf{F}^f \tag{1.61}$$

$$\frac{\partial\rho}{\partial t} + \nabla\mathbf{j} = 0 \tag{1.62}$$

$$\frac{d\mathbf{j}}{dt} = -\nabla\mathbf{\Pi} + \xi_{bare}\left(\mathbf{v} - \mathbf{u}\right) - \frac{1}{m}\mathbf{F}^f\delta(\mathbf{r} - \mathbf{R}) \tag{1.63}$$

where $\mathbf{F}^f$ is the stochastic force discussed in the previous section.

The longitudinal $\mathbf{j}_\parallel = \hat{k}\cdot\mathbf{j}$ and transverse $\mathbf{j}_\perp = (1 - \hat{k}\hat{k})\mathbf{j}$ components can be calculated separately.

Our transformed system of equations have the following form

$$\frac{d\mathbf{R}}{dt} = \mathbf{v} \tag{1.64}$$

$$\frac{d\mathbf{v}}{dt} = \frac{1}{m}\mathbf{F}^{ext} - \frac{\xi_{bare}}{m}\left(\mathbf{v} - \frac{\mathbf{j}}{\rho}\right) + \frac{1}{m}\mathbf{F}^f \tag{1.65}$$

$$\frac{\partial\rho}{\partial t} = i\mathbf{k}\mathbf{j} \tag{1.66}$$

$$\frac{d\mathbf{j}_\parallel}{dt} = -\nu_l k^2\mathbf{j}_\parallel + \frac{1}{V}\xi_{bare}\left(\mathbf{v}_\parallel - \frac{1}{\rho}\mathbf{j}_\parallel\right) - \mathbf{F}_\parallel^f e^{-i\mathbf{k}\mathbf{R}} + ik\delta\mathbf{\Pi}_\parallel(\mathbf{k}, t) \tag{1.67}$$

$$\frac{d\mathbf{j}_\perp}{dt} = -\nu k^2\mathbf{j}_\perp + \frac{1}{V}\xi_{bare}\left(\mathbf{v}_\perp - \frac{1}{\rho}\mathbf{j}_\perp\right) - \mathbf{F}_\perp^f e^{-i\mathbf{k}\mathbf{R}} + ik\delta\mathbf{\Pi}_\perp(\mathbf{k}, t) \tag{1.68}$$

These equations are Langevin equations with random forces $\delta\mathbf{\Pi}_\parallel = \hat{k}\cdot\delta\mathbf{\Pi}\cdot\hat{k}$, $\delta\mathbf{\Pi}_\perp = \hat{k}\cdot\delta\mathbf{\Pi}\cdot(1 - \hat{k}\hat{k})$, $\mathbf{F}_\parallel = \hat{k}\cdot\mathbf{F}\cdot\hat{k}$ and $\mathbf{F}_\perp = \hat{k}\cdot\mathbf{F}\cdot(1 - \hat{k})$. Given the results of Ref. [2], it will be very surprising if the Fluctuation–Dissipation theorem does not hold for our system. We can convince ourselves by explicit calculations.

As shown in Ref. [2] one can restrict attention to the additional terms in the equations of motion, because separately both fluid and the particles satisfy the Fluctuation–Dissipation theorem. We have to calculate only the additional term $\mathcal{L}_{add}$ in the dynamical operator. The dynamic operator in general is the sum of drift and diffusional parts [37]

$$-i\mathcal{L} = -\frac{\partial}{\partial x_i}D_i\left(\{x\}, t\right) + \frac{\partial^2}{\partial x_i\partial x_j}D_{ij}\left(\{x\}, t\right), \tag{1.69}$$

where the $\{x\}$ are the phase space variables, $D_i\left(\{x\}, t\right)$ is the drift vector and $D_{ij}\left(\{x\}, t\right)$ is the diffusion matrix and Einstein summation is applied. They are

defined through these formulas:

$$D_i\left(\{x\},t\right) = \lim_{\tau\to 0}\frac{1}{\tau}\left\langle\xi_i(t+\tau)-\xi_i(t)\right\rangle|_{\xi_k(t)=x_k} \tag{1.70}$$

$$D_{ij}\left(\{x\},t\right) = \frac{1}{2}\lim_{\tau\to 0}\frac{1}{\tau}\left\langle\left[\xi_i(t+\tau)-\xi_i(t)\right]\left[\xi_j(t+\tau)-\xi_j(t)\right]\right\rangle|_{\xi_k(t)=x_k} \tag{1.71}$$

where $|_{\xi_k(t)=x_k}$ means that the stochastic variables ξ_k at time t have the values x_k. In our case the variables are $\{x\} = \left(\mathbf{R}, v_\parallel, v_\perp, \mathbf{j}_\parallel(\mathbf{k},t), \mathbf{j}_\perp(\mathbf{k},t), \rho\right)$. Further we use a shorthand notation $\Delta x_i = \left[\xi_i(t+\tau)-\xi_i(t)\right]$ and instead of $|\xi_k(t)=x_k$ write $|_\tau$.

Because the longitudinal and transverse components in the equations are fully decoupled, we can consider only one case, for example the longitudinal components. The additional term to the drift coefficient is caused by the coupling term:

$$-i\mathcal{L}_{add}^{(drift)} = -\frac{\xi_{bare}}{\rho m}\mathbf{j}_\parallel\cdot\frac{\partial}{\partial\mathbf{v}_\parallel} - \sum_\mathbf{k}\frac{\partial}{\partial\mathbf{j}_\parallel(\mathbf{k})}\frac{\xi_{bare}}{V}\left(\mathbf{v}_\parallel-\frac{\mathbf{j}_\parallel(\mathbf{R})}{\rho}\right)e^{-i\mathbf{kR}}. \tag{1.72}$$

The additional second order term comes from the additional stochastic force in the Navier-Stokes equation. There are 2 terms, the first:

$$\lim_{\tau\to 0}\frac{1}{\tau}\left\langle\Delta\mathbf{j}_\parallel(\mathbf{k},t)\Delta\mathbf{v}_\parallel\right\rangle|_\tau=$$
$$-\lim_{\tau\to 0}\frac{1}{\tau V m}e^{-i\mathbf{kR}}\int_0^\tau dt\int_0^\tau dt'\left\langle\mathbf{F}_\parallel(t)\mathbf{F}_\parallel(t')\right\rangle = -2\frac{\xi_{bare}k_B T}{V m}e^{-i\mathbf{kR}}. \tag{1.73}$$

The prefactor $1/2$ was omitted because the term occurs twice. The second term has a similar structure and we give only the result

$$\lim_{\tau\to 0}\frac{1}{2\tau}\left\langle\Delta j_\parallel^*(\mathbf{k},t)\Delta\mathbf{j}_\parallel(\mathbf{q},t)\right\rangle|_\tau=\frac{\xi_{bare}k_B T}{V^2}e^{i(\mathbf{k}-\mathbf{q})\mathbf{R}}. \tag{1.74}$$

Combining the additional terms we obtain this expression for the diffusional operator

$$-i\mathcal{L}_{add}^{(diff)} = \frac{\xi_{bare}k_B T}{V^2}\sum_{\mathbf{k},\mathbf{q}}e^{i(\mathbf{k}-\mathbf{q})\mathbf{R}}\frac{\partial^2}{\partial\mathbf{j}_\parallel(\mathbf{k})\partial\mathbf{j}_\parallel^*(\mathbf{q})}-$$
$$-\frac{2\xi_{bare}k_B T}{V m}\sum_\mathbf{k}e^{-i\mathbf{kR}}\frac{\partial^2}{\partial\mathbf{v}_\parallel\partial\mathbf{j}_\parallel(\mathbf{k})} \tag{1.75}$$

The equilibrium distribution for the longitudinal components in our case has the form

$$\mathcal{P}\propto exp\left(-\frac{m\mathbf{v}_\parallel^2}{2k_B T}-\frac{V}{2k_B T\rho}\sum_\mathbf{q}|\mathbf{j}_\parallel|^2\right). \tag{1.76}$$

The action of the additional terms in the dynamic operator on the distribution function is

$$-i\mathcal{L}_{add}\mathcal{P} = -\frac{\xi_{bare}}{\rho}\mathbf{j}_{\parallel} \quad -\frac{\mathbf{v}_{\parallel}}{k_B T} \quad \mathcal{P}-$$

$$-\frac{\xi_{bare}}{V} \quad \mathbf{v}_{\parallel} - \frac{\mathbf{j}_{\parallel}(\mathbf{R})}{\rho} \quad \sum_{\mathbf{k}} e^{-i\mathbf{k}\mathbf{R}} \quad -\frac{V}{k_B T\rho} \quad \mathbf{j}_{\parallel}^*(\mathbf{k})\mathcal{P} +$$

$$+\frac{\xi_{bare}}{\rho V} \quad \sum_{\mathbf{k}} 1 \Bigg) \mathcal{P} -$$

$$-\frac{2\xi_{bare}k_B T}{V} \sum_{\mathbf{k}} e^{-i\mathbf{k}\mathbf{R}} \quad -\frac{\mathbf{v}_{\parallel}}{k_B T} \quad -\frac{V}{k_B T\rho} \quad \mathbf{j}_{\parallel}^*(\mathbf{k})\mathcal{P} -$$

$$-\frac{V}{k_B T\rho}\frac{\xi_{bare}k_B T}{V^2} \sum_{\mathbf{k},\mathbf{q}} e^{i(\mathbf{k}-\mathbf{q})\mathbf{R}} \quad \delta_{\mathbf{k}\mathbf{q}} - \frac{V}{2k_B T\rho}\mathbf{j}_{\parallel}(\mathbf{k})\mathbf{j}_{\parallel}^*(\mathbf{q}) \quad \mathcal{P} \qquad (1.77)$$

Applying the Fourier transformation to the last equation finally we obtain

$$-i\mathcal{L}_{add}\mathcal{P} = \frac{\xi_{bare}}{\rho k_B T}\mathbf{v}_{\parallel}\mathbf{j}_{\parallel}\mathcal{P} + \frac{\xi_{bare}}{\rho k_B T} \quad \mathbf{v}_{\parallel} - \frac{\mathbf{j}_{\parallel}(\mathbf{R})}{\rho} \quad \mathbf{j}_{\parallel}(\mathbf{R})\mathcal{P}$$

$$+\frac{\xi_{bare}}{\rho V} \quad \sum_{\mathbf{k}} 1 \Bigg) \mathcal{P} - \frac{\xi_{bare}}{\rho V} \quad \sum_{\mathbf{k}} 1 \Bigg) \mathcal{P} + \frac{\xi_{bare}}{k_B T\rho^2}\mathbf{j}_{\parallel}(\mathbf{R})^2\mathcal{P} \qquad (1.78)$$

$$-2\frac{\xi_{bare}}{\rho k_B T}\mathbf{v}_{\parallel}\mathbf{j}_{\parallel}\mathcal{P} = 0.$$

From the obtained result we see that the Boltzmann distribution function satisfies the stationary Fokker-Planck equation. Therefore the Fluctuation-Dissipation theorem is also satisfied for our model.

1.10. Technical details and numerical tests

For the integration of the Molecular Dynamics (MD) part we apply the Velocity-Verlet integrator [38, 39, 40]. For the fluid update we apply a further scheme: the calculation of the force between fluid and particles at the current position of the particle. With this coupling we change n_i and also the fluid velocity $\mathbf{u}$. After that we apply collision and propagation steps for the fluid. In order to accelerate the force calculation between particles we use standard tricks of MD-simulation for short-ranged forces between particle pairs. The link–cell algorithm is applied in our case [38, 39]. In order to check the validity of our new model we can do a simple experiment of the relaxation of the initially kicked particle in the fluid. The particle at time $t = 0$ has the initial velocity v_x in x-direction and moves freely through the fluid which at the moment $t = 0$ has zero velocity. The expected behavior is an initial exponential decay $v_x \propto exp(-\xi t/m)$. The asypmtotic behavior for long times
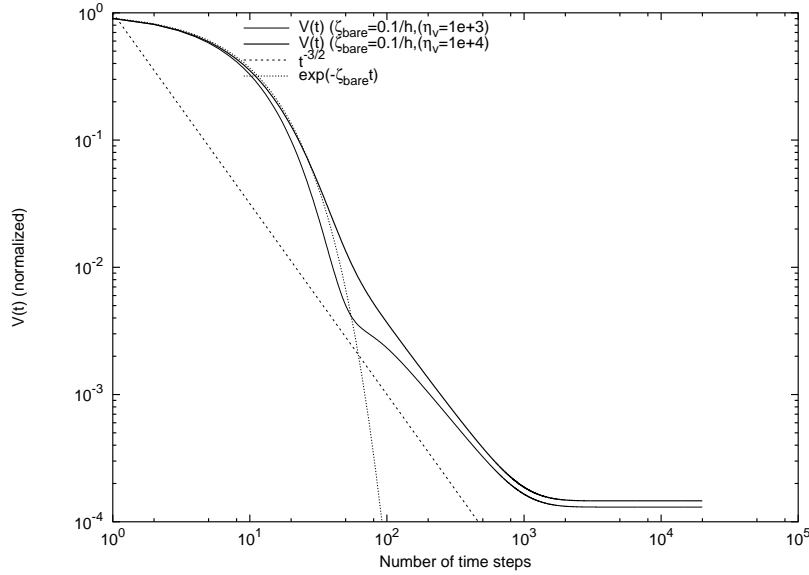
Figure 1.8.: Relaxation of the kicked at t=0 particle in the fluid for two different
bulk viscosities η_v.

is given by hydrodynamic interaction, "the long-time tail" regime is expected, i.e.
$v_x(t) \propto t^{-3/2}$ [41, 42]. These two regimes are actually observed in the experiment
(see Fig. 1.8). In two simulations we have chosen the same time step for the fluid
update and for the particle propagation $\delta t = h = 0.01$, the value for the mass of the
fluid particles and MD-particles $m_p = m_{fl} = 1.0$, $\rho = 0.85 m_{fl}/(\Delta x)^3$, $\lambda = -1.75$
and $\Delta x = 1.0$. It has to be noted that the function $v_x(t)$ does not go to zero,
because the simulation is performed in a simulation box of length L with periodic
boundary conditions: In the long–time regime , one observes the overall motion of
the particle–fluid system.

Furthermore, it is interesting to note that the "hump" in the relaxation function
is apparently an effect of longitudinal sound modes: For a large value of the bulk
viscosity (strong sound attenuation), this feature goes away.

Part II.

Simulation of electrostatics

2. Trying to understand the evolution of charged systems

2.1. Introduction

Simulations of charged systems face a big computational challenge due to the long–range nature of the electrostatic interaction. If N is the number of charges, then the computational cost of the most naive approach to evaluate the interaction energy would scale as N^2, since every charge interacts with every other charge. Very sophisticated algorithms have been developed to tackle this problem and to reduce the computational complexity. The most prominent ones are the so–called P^{3}M method ("particle–particle / particle–mesh"), which is based on Fast Fourier Transforms and scales as $N \log N$ [43], and the Fast Multipole method [44] which scales linearly with N.

A similar problem arises in the simulation of Brownian particles which interact hydrodynamically: Their stochastic displacements are highly correlated, due to fast diffusive momentum transport through the solvent. For sufficiently slow particles, a quasi–static approximation works excellently, and in this case the correlation function decays as $1/r$ (r interparticle distance) [45], just as in electrostatics. For these systems, it has turned out that it is both much simpler and also more efficient to explicitly simulate the momentum transfer through the surrounding solvent. This makes the simulation of several ten thousands of Brownian particles feasible [46, 5]. Although most of the computational effort goes into the flow field (for *two* reasons — one needs reasonable spatial resolution of the flow field, and it moves much faster than the Brownian particles), this approach ultimately wins, because it is inherently local, and therefore scales linearly with N.

This observation raises the question if something similar could be tried for Coulomb interactions. After all, electrostatics is just the quasi–static limit of full electrodynamics. The obvious approach would be to couple a system of charges to an electromagnetic field which propagates according to the Maxwell equations (ME), and then run Molecular Dynamics (MD). A suitable acronym for such a method might be MEMD ("Maxwell equations Molecular Dynamics"). Just as in the hydrodynamic case, this is an intrinsically local algorithm, and therefore scales linearly. The instantaneous $1/r$ interaction is thus replaced by some retarded interaction travelling with the speed of light c. Using the actual physical value of c

will of course not work, since then the separation of time scales between charges and fields will be prohibitive. However, there is no need to take such a large c value. It is sufficient to just make c large enough such that the quasi–static approximation still holds to sufficient accuracy. This is the lesson we have learned from Car–Parrinello (CP) simulations [47], where the electrons are assigned an unphysically large mass, precisely for the same reason. The analogy between MEMD and CP actually goes much further, as we will see in Chapter 3. This should not be too much of a surprise, since the universal applicability of the CP approach to a wide variety of problems in physics (e. g. classical field theories) has already been observed in the original publication [47], and exploited in the context of classical density–functional theory [48].

The MEMD idea has been pursued recently by A. C. Maggs and collaborators [49, 50, 51], and by us [52], in close contact with him.

In the current chapter we will give an outline of the Car–Parrinello method. Furthermore, present methods for the simulation of charged systems will be critically discussed. In order to understand the evolution of charged systems, the relations between Quantum Lattice Models and Classical Field Theory will be investigated. The naive approach of direct application of the Car–Parrinello method to Molecular Dynamics of charged systems will be presented, as well as its drawbacks. Although this approach has appeared to be unsuccessful, it will help us to construct the right method in the next chapter.

2.2.   Car–Parrinello method

2.2.1.   Kohn-Sham equations

We begin with considering possible methods of solving the Kohn-Sham equations.

Suppose we want to construct a Molecular Dynamics method for the electronic structure of solids. Particularly we consider such a system for which the Born-Oppenheimer (BO) approximation holds, i.e. we will assume that the electronic excitation spectrum has a gap between the ground state and the first excited state which is much larger than the energy associated with the ionic motion. If this condition is satisfied, the behavior of the coupled electron ion system can be regarded as adiabatic. It can also be assumed that the ions are described by classical mechanics, with interaction potential

$$\Phi\left(\{\mathbf{R}_I\}\right) = \langle\psi_0\,|H|\,\psi_0\rangle \tag{2.1}$$

where H is the Hamiltonian of the system at fixed ionic position $\mathbf{R}_I$ and ψ_0 is the corresponding instantaneous ground state. The use of this equation allows us to define the interaction potential from first principles (*ab-inito* simulation). In order to use Eq. 2.1 in a Molecular Dynamics (MD) run, calculations of ψ_0 for a number of configurations are needed. This is computationally very expensive. A viable alternative is offered by *Density functional theory (DFT)* [53] which provides

a practical and accurate method of calculating $\Phi\left(\{\mathbf{R}_I\}\right)$. According to DFT the total energy $E\left(\{\mathbf{R}_I\}\right)$ of a system of interacting electrons and nuclei, corresponding to the nuclear configuration $\{\mathbf{R}_I\}$, is a unique functional of the electronic density $\rho_e(\mathbf{r})$ [54]. Within a mean field framework $\rho_e(\mathbf{r})$ can be expressed in terms of N doubly occupied single-particle orbitals (ψ_i):

$$\rho_e(\mathbf{r}) = 2\sum_i^{occ} |\psi_i(\mathbf{r})|^2 \tag{2.2}$$

where the factor 2 accounts for double occupancy of each electronic state. If one assumes that all occupation numbers are equal (there is no incompletely filled state), then the ground-state energy Φ can be found by minimizing the functional $E\left[\{\psi_i\}, \{\mathbf{R}_I\}\right]$ with respect to the electronic degrees of freedom $\{\psi_i\}$, i.e.

$$\Phi\left(\{\mathbf{R}_I\}\right) = \min_{\{\psi_i\}} E\left[\{\psi_i\}, \{\mathbf{R}_I\}\right]. \tag{2.3}$$

The functional $E\left[\{\psi_i\}, \{\mathbf{R}_I\}\right]$ is given by (we use atomic units $e = \hbar = m_e = 1$)

$$E\left[\{\psi_i\}, \{\mathbf{R}_I\}\right] = 2\sum_i^{occ} \int d\mathbf{r}\psi_i^*(\mathbf{r}) \left[-\frac{1}{2}\nabla^2\right] \psi_i(\mathbf{r}) + \int d\mathbf{r}V^{ext}(\mathbf{r})\rho_e(\mathbf{r})$$
$$+ \frac{1}{2}\int d\mathbf{r}d\mathbf{r}'\frac{\rho_e(\mathbf{r})\rho_e(\mathbf{r}')}{|\mathbf{r}-\mathbf{r}'|} + E^{exch}\left[\rho_e\right] + \frac{1}{2}\sum_{I\neq J}\frac{Z_IZ_J}{|\mathbf{R}-\mathbf{R}'|}. \tag{2.4}$$

$V^{ext}(\mathbf{r})$ is the total external potential felt by electrons, i.e. the total electrostatic potential from the nuclei in an all-electron formulation, Z_I are the nuclear charges. $E^{exch}\left[\rho_e\right]$ is the exchange-correlation energy functional, in which all the intricacies of the many-body electronic problem are contained. The so–called local density approximation (LDA) [55, 53] assumes that $E^{exch}\left[\rho_e\right]$ is a function and not a functional of $\rho_e(\mathbf{r})$.

The single-particle orbitals ψ_i are subject to orthonormality constraints:

$$\int d\mathbf{r}\psi_i^*(\mathbf{r})\psi_j(\mathbf{r}) = \delta_{ij}. \tag{2.5}$$

The standard way of solving Eq. 2.3, subject to constraints given by Eq. 2.5, consists of solving the associated Euler-Lagrange equations, i.e.

$$H\psi_i(\mathbf{r}) = \epsilon_i\psi_i(\mathbf{r}), \tag{2.6}$$

where

$$H = -\frac{1}{2}\nabla^2 + V^{ext}(\mathbf{r}) + V^H(\mathbf{r}) + \mu^{exch}(\mathbf{r}). \tag{2.7}$$

Here $V^H(\mathbf{r}) = \int d\mathbf{r}'\frac{\rho_e(\mathbf{r}')}{|\mathbf{r}-\mathbf{r}'|}$ is the Hartree potential and

$$\mu^{exch}(\mathbf{r}) = \delta E^{exch}\left[\rho_e\right]/\delta\rho_e(\mathbf{r})$$

is the exchange-correlation potential. The Schrödinger-type equations 2.6 are called *Kohn-Sham (KS)* [55] equations and provide the theoretical framework of most self-consistent electronic structure calculations. In a conventional approach [56], one would proceed as follows:

1. An initial value for $\rho_e(\mathbf{r})$ is estimated.

2. The potential in Eq. 2.7 is then calculated accordingly and Eqs. 2.6 are solved by diagonalization of the Hamiltonian matrix.

3. From the eigenvectors a new $\rho_e(\mathbf{r})$ is calculated and the entire process is repeated till self-consistency is achieved.

Since the cost of a standard diagonalization grows as $O(M^3)$, where M is the number of functions in the basis set in terms of which the Kohn and Sham orbitals are expanded, this procedure becomes very costly for large systems.

2.2.2. Molecular Dynamics in the coupled electron–ion parameter space

It is therefore highly desirable to have an alternative approach in which the interatomic forces are generated in a consistent and accurate way as the simulation proceeds. Such an alternative scheme was devised by Car and Parinello (CP) [47].

Here we show how the Newtonian dynamics (second order differential equations) in the DF parameter space enhances our computational capabilities and allows us to implement a DF-based MD scheme. For this purpose we consider the parameters ψ_i and $\mathbf{R}_I$ in the E functional to be dependent on time and write the Lagrangian [47, 57]

$$
\begin{aligned}
\mathcal{L} =& \frac{1}{2} \sum_i^{occ} \int d\mathbf{r} \mu_i \ \dot{\psi}(\mathbf{r})^2 + \frac{1}{2} \sum_I M_I \dot{\mathbf{R}}_I^2 - E\left[\{\psi_i\}, \mathbf{R}_I\right] + \\
& \frac{1}{2} \sum_{ij} \Lambda_{ij} \ \int d\mathbf{r} \psi_i^*(\mathbf{r})\psi_j(\mathbf{r}) - \delta_{ij} \quad ,
\end{aligned}
\tag{2.8}
$$

where M_I are the physical ionic masses and μ_i are arbitrary mass–like parameters of appropriate units. We assume equality of all μ_i. In Eq. 2.8 we have two classical kinetic energy terms: $K_e = 1/2 \sum_i^{occ} \int d\mathbf{r} \mu_i \ \dot{\psi}(\mathbf{r})^2$, associated with the electronic parameters ψ_i, and $K_I = \frac{1}{2} \sum_I M_I \dot{\mathbf{R}}_I^2$, associated with the nuclear coordinates. K_e and K_I measure the rate of variation of the respective degrees of freedom in the coupled electron-ion parameter space. The Lagrangian multipliers Λ_{ij} are used to impose the orthonormality constraints (Eq. 2.5) that, in a language of classical mechanics, are simply *holonomic constraints* [58].

The Lagrangian in Eq. 2.8 generates a dynamics for the parameters ψ_i and $\mathbf{R}_I$ through the equations of motion:

$$\mu\ddot{\psi}_i(\mathbf{r}, t) = -\frac{\delta E}{\delta \psi_i^*(\mathbf{r}, t)} + \sum_j \Lambda_{ij} \psi_j(\mathbf{r}, t) \qquad (2.9)$$

$$M_I \ddot{\mathbf{R}}_I = -\frac{\partial E}{\partial \mathbf{R}_I(t)}. \qquad (2.10)$$

These equations allow the sampling of the complex parameter space of the ψ_i and $\mathbf{R}_I$ with the MD techniques used in statistical mechanics simulations [59]. In particular, the equilibrium value $\langle K \rangle$ of the classical kinetic energy $K = K_e + K_I$ can be calculated as the temporal average over the trajectories generated by the equations of motion (2.9) and (2.10), and related to the temperature of the system by suitable normalization. By variation of the velocities, i.e. the $\dot{\psi}_i$ and the $\dot{\mathbf{R}}_I$, one can vary the temperature of the system. In this way one can make the fictitious dynamical system undergo various thermal treatments, such as annealing and quenching. During such processes, all relevant degrees of freedom, both nuclear and electronic, are relaxed simultaneously. In particular, we can set up a dynamical process that brings the system to its equilibrium state at $T = 0$ by slowly reducing the temperature. This process is called *dynamical simulated annealing (DSA)*, which is a specific application of the concept of simulated annealing, introduced by Kirkpatrick, Gelatt and Vecchi [60] to solve complex optimization problems.

If one wants to compare the ionic dynamics generated with Eq. 2.10 and the correct classical dynamical equations for the nuclei given by

$$M_I \ddot{\mathbf{R}}_I = -\frac{\partial \Phi \left(\{\mathbf{R}_I\} \right)}{\partial \mathbf{R}_I} \qquad (2.11)$$

where $\Phi \left(\{\mathbf{R}_I\} \right)$ is the physical potential defined in Eq. 2.3, one finds nonequivalence of the two dynamics. Indeed, the nuclear trajectories generated by Eq. 2.10 and those obtained from Eq. 2.11 generally do not coincide, unless $E \left[\{\psi_i\}, \{\mathbf{R}_I\} \right]$ is at the instantaneous minimum. However, the parameter μ and the initial conditions $\{\psi_i\}_0, \{\dot{\psi}_i\}_0$ can be chosen such that the time scale for the electronic degrees of freedom is much shorter than that of the nuclei. In this case the nuclear trajectories, initially lying on the Born-Oppenheimer surface, will fluctuate around it, and deviate substantially only after rather long times. In other words, if μ and $\{\psi_i\}_0, \{\dot{\psi}_i\}_0$ are chosen such that the two sets of classical degrees of freedom, ions and electrons, are only weakly coupled, the transfer of energy between them is small enough to allow the electrons to follow adiabatically the ionic motion, remaining close to their instantaneous Born-Oppenheimer surface. In such a metastable situation meaningful temporal averages can be computed. This dynamics is meant to reproduce in a computationally effective way what indeed occurs in reality, that is electrons following adiabatically the motion of the ions.

2.3. Analysis of current simulation methods for Coulomb interaction

The electrostatic interaction between two point charges in a medium with uniform dielectric constant ϵ_0 varies as $q_1 q_2 / 4\pi\epsilon_0 r$. The large numerical value of this energy together with its long range are such that the accurate evaluation of this interaction is almost always the most costly component in the simulation of charged condensed matter systems [61]. Naive evaluation of the electrostatic energies in Molecular Dynamics and Monte-Carlo algorithms leads to inner loops where the summation over all particle pairs leads to a complexity of the order of $\mathcal{O}(N^2)$. Historically, the quadratic ($\mathcal{O}(N^2)$) computational complexity of the all-pairs N-body problem of electrostatics was reduced by using truncated Coulomb potentials, where all interactions past a certain distance were simply ignored. Though acceptable for some simulation experiments, this cutoff approximation leads to unphysical behavior in many situations [62]. An alternative "brute force" quadratic method tailored to specialized parallel hardware [63] increased the size of systems that could be simulated "exactly", but the quadratic complexity eventually overwhelmed such systems.

New algorithms and new implementations of old algorithms have dramatically reduced the cost of performing accurate evaluations of electrostatic interactions. These methods have linear ($\mathcal{O}(N)$) or $\mathcal{O}(N \log N)$ computational complexity for the N-body problem. This section describes the contemporary methods used in MD and Monte Carlo algorithms.

2.3.1. Optimized Ewald summation

Many simulations are best suited for periodic boundary conditions. Periodic boundary conditions are a standard way of imitating a bulk system with a finite set of particles. They also help to reduce surface effects. A primary box is taken as the unit cell (or "base") of a space-filling "crystal" of such boxes (actually, a Bravais lattice), and all particles in this infinite and periodic universe interact with each other [39, 38]. In an appropriate unit system, the potential on particle i in the original simulation cell of the size L due to all other particles j in the cell and all periodic images of all particles can be written as

$$\Phi_i = \sum_{j=1}^{N} \sum_{\mathbf{n}}' \frac{q_i q_j}{r_{i,j_{\mathbf{n}}}} \tag{2.12}$$

where $\mathbf{n}$ is an integer triple identifying a particular image cell; $\mathbf{n}$=(0,0,0) indicates the "real" simulation cell, and all other cells are identified by their displacement from the central cell; $r_{i,j_{\mathbf{n}}} = |\mathbf{r}_i - \mathbf{r}_j + \mathbf{n}L|$. The prime on the second sum indicates that for $i = j$ the lattice vector $\mathbf{n} = \mathbf{0}$ must be omitted.

The Ewald summation was invented in 1921 [64] to permit the efficient computation of lattice sums arising in solid state physics. These sums are not absolutely,

but only conditionally convergent. Ewald recognized that the slowly convergent sum can be recast as two rapidly converging sums, one in real space and one in reciprocal (or Fourier) space. One physical explanation of Ewald's observation is that an auxiliary Gaussian charge distribution can be both added to and subtracted from the original charge distribution (see Fig. 2.1). From the mathematical point of view this transformation can be regarded as a special case of the Jacobi imaginary transformation for the theta functions [65]. The real space sum is now in terms of
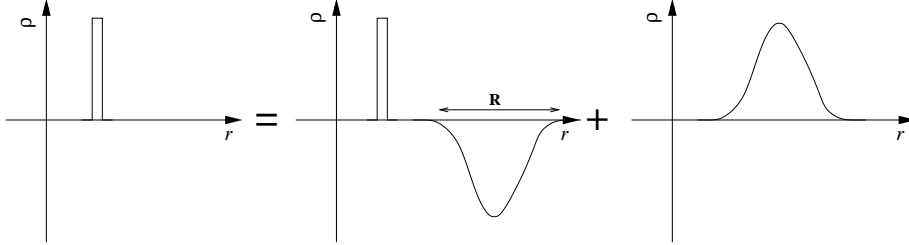

Figure 2.1.: Motivation for the Ewald formulae. A point charge distribution is split into a screened point charge distribution (in the real space) and the corresponding screening distribution.

the rapidly converging complementary error function $erfc(r)$ rather than the slowly converging $1/r$ thanks to the Gaussian screening of the charges; the other sum of Gaussian countercharges can be Fourier transformed into a rapidly converging form as well.

Ewald's formalism reduces the infinite lattice sum to a serial complexity of $\mathcal{O}(N^2)$ in naive implementation. The Fourier transformations involved in the calculation of the Ewald sum are the most time consuming part of the method. A more efficient method can be constructed if one combines the existing Ewald method with a "Link–Cell" method of Hockney and Eastwood [43]. This method has been known for some time [66] and the idea is the following. The Fourier transform can be represented by the finite amount of reciprocal lattice vectors **k**. It means the k-values have an upper bound, say k_{max}. This k_{max} is independent of the number of particles, hence we would expect the overhead from the Fourier space contribution to become relatively less important as the number of particles N increases. For the real space part we can use the property of "short-ranged" interactions, i.e. contributions to the real space forces on a particular particle could be neglected for all but particles in the immediate vicinity. More precisely, suppose that we divide each side of the cubic simulation box into m equal segments, each of length L/m. This leads to a tesselation of the original cubic box into $M = m^3$ identical cubic sub-boxes, each containing on average N/M particles. If we insist that all interactions between particles separated by more than this distance L/m can be neglected, then we need only to evaluate the real space contribution to the force on a particle from particles in the same small box and from those in half of the (3^3-1) neighboring boxes. If the boxing algorithm is implemented with the optimum value of the number of boxes, then the computer time increases as $N^{3/2}$, a considerable

improvement over the rate N^2 for traditional methods.

2.3.2. Fast multipole method

Multipole-accelerated algorithms first appeared in the astrophysical literature for solving gravitational N-body problem [67, 68]; Greengard and Rokhlin [44] have placed this class of algorithms on a more rigorous theoretical footing. The multipole-accelerated algorithms overcome the $\mathcal{O}(N^2)$ complexity of the N-body problem by using a hierarchy of approximations to represent the effect of increasingly distant groups of charged particles on a particle of interest (Fig. 2.2). The central strategy
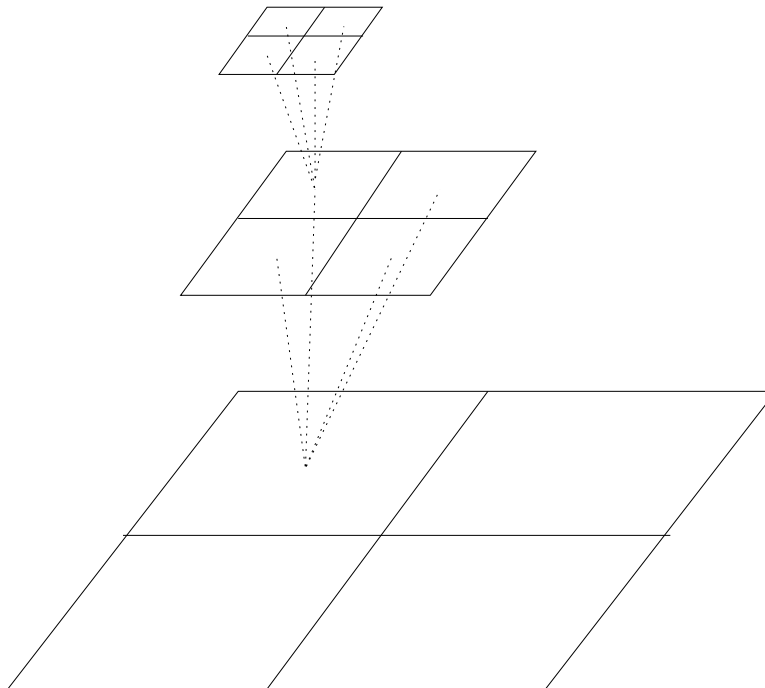
Figure 2.2.: The fast–mutipole algorithm exploit an approximate representation of the effect of groups of distant particles. A hierarchy of this approximations allows increasingly larger groups of particles to be represented by a single power series as the distance from the particles of interest increases.

of the method is clustering particles at various spatial lengths and computing interactions with other clusters which are sufficiently far away by means of multipole expansions. Interactions with particles which are nearby are handled directly.

To be more specific, let us at first define the multipole expansion. In the two–dimensional case the potential at point z with $|z| > r$ from m charges $\{q_i, i = 1, \ldots, m\}$, located at points $\{z_i, i = 1, \ldots, m\}$, with $|z_i| < r$ is given by

$$\phi(z) = Q \ln(z) + \sum_{k=1}^{m} \frac{a_k}{z^k}, \qquad (2.13)$$

where

$$Q = \sum_{i=1}^{m} q_i, \quad a_k = \sum_{i=1}^{m} \frac{-q_i z_i^k}{k} \tag{2.14}$$

Furthermore, the error of the truncation approximation is bounded

$$\left| \phi(z) - Q \ln(z) - \sum_{k=1}^{p} \frac{a_k}{z_k} \right| \le \sum_{i=1}^{m} |q_i| \left| \frac{1}{2} \right|^p \tag{2.15}$$

where $p \ge 1$ is. This means that in order to obtain a relative precision ϵ (with respect to the total charge), p must be of the order $-\log_2(\epsilon)$. Therefore the multipole expansion is one suitable power series representation which converges quite rapidly when groups of particles are "well separated". This rapid convergence permits the series to be truncated at a relatively small number of terms and still provide an accurate representation of the exact potential. For close interparticle separations, the power series representation typically converges very slowly or not at all (logarithm in our formulas for the two-dimensional case); thus, Coulomb interactions involving nearby particles must be computed directly via the $1/r$ law.

2.3.3. Lattice methods

The Fourier transformations involved in the calculation of the Ewald sum are the most time-consuming part of the algorithm. The essential idea of lattice methods is to modify the problem in such a way that it permits the application of the Fast Fourier Transformation (FFT, see [69]). This reduces the complexity of the reciprocal part of the Ewald sum to $N \log N$. If the real space cutoff is chosen to be small enough, this scaling applies to the complete Ewald sum. Since FFT is a grid transformation there are discretization problems to be solved and corresponding discretization errors to be minimized.

The algorithm, called the particle mesh Ewald (PME) method [70], was inspired by Hockney and Eastwood's [43] particle-particle particle-mesh method of splitting the total electrostatic energy into local interactions which are computed explicitly and long-range interactions which are approximated by a discrete convolution on an interpolating grid, using the three-dimensional fast Fourier transform (3DFFT) to efficiently perform the convolution.

The first thing that one has to do in order to use the PME algorithm is to interpolate charges on some grid (See Fig. 2.3). The accuracy of charge assignment scheme depends on the number of grid points used in the interpolation. Of course, the complexity of such an algorithm is increased. PME originally employed Lagrange interpolation, but later a revised PME formulation which uses B-spline interpolation functions was developed [71].

After the interpolation one has to solve the Poisson equation on the lattice, and finally to calculate electrostatic forces.
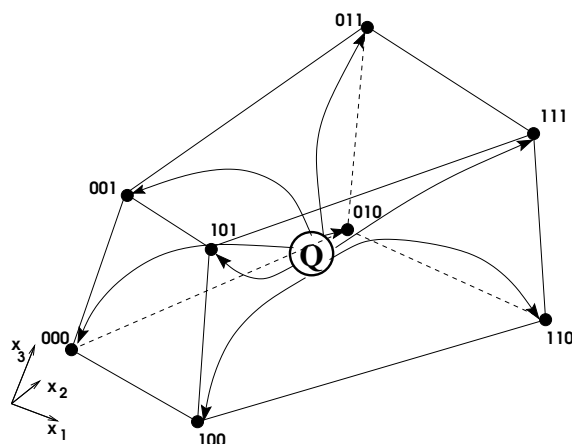
Figure 2.3.: Charge assignment from a single particle in a curvilinear coordinate system (general case). The interpolation is done only for the neighboring grid points.

2.3.4. Various drawbacks of the present day simulation schemes for Coulomb interactions

It is impressive to look back and appreciate how far the field of electrostatic modeling has progressed from the first attempts of simulation. Developments in theory, experiment, and computer technology have made simulations of larger systems over longer times with greater accuracy possible. But the asymptotic improvement in efficiency comes with great increases in the complexity of the coding, especially when distributed on multiprocessor computers. The numerical prefactors in these scaling laws are uncomfortably large: Despite the great effort put into optimizing the electrostatic loop, it is found that in simulations of large systems the great majority of the CPU time is still used there.

The classical methods for treating charged systems have another disadvantage, their inability to treat systems with inhomogeneous dielectric constants. In standard accelerated Coulomb methods dielectric effects must be included by adding supplementary charge degrees of freedom to mimic, for instance, electronic polarizability. It would be of a great interest if a simpler method were available to simulate inhomogeneous systems.

2.4. Monte Carlo method for constrained electrostatics

Help comes from a completely different point of view. All present day methods are based on the construction of a fast "Poisson solver". The Poisson equation is an elliptic equation, the solution of which is completely defined by the boundary conditions. It means that in order to solve the electrostatic problem in a given region

one has to propagate an iterative method through all of the system. Therefore Poisson solver methods are global methods.

But one can find interesting properties of electrostatics by investigating the corresponding quantum field theory. The classical quantization of the electromagnetic field is the substitution of the continuum field theory by discretized quantities. Could it be that by observing the analogies between Quantum Electrodynamics and the discretized equations of the electrodynamics we can find something special and helpful?

2.4.1. Lattice Gauge theory

An important topic in the physics of the 20th century is local gauge invariance. The notion of gauge invariance was first introduced by Weyl [72] in his attempt to describe the gravitational and electromagnetic interaction of an electron on equal footing. In order to understand the meaning of this notion we will consider the famous "toy" of the physicist - the Ising model.

Consider a square lattice in two dimensions with sites labeled by a vector of integers, $\mathbf{n} = (n_1, n_2)$. Place a "spin" variable $\sigma(\mathbf{n})$ at each site and suppose that σ can only be "up" ($\sigma = +1$) or "down" ($\sigma = -1$. Then the energy or "action" of the model is

$$S = -J \sum_{\mathbf{n}, \hat{\mu}} \sigma(\mathbf{n}) \sigma(\mathbf{n} + \hat{\mu}) \tag{2.16}$$

where $\hat{\mu}$ denotes one of the two unit vectors of the lattice as depicted in Fig. 2.4. J is the coupling constant and positive, so the action favors aligned spins. It is
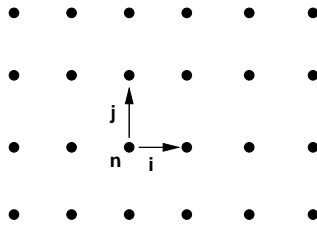
Figure 2.4.: The unit vectors of the square lattice in two dimensions.

necessary to note two important properties of the model:

1. Only nearest-neighbor spins are coupled. The action is as local as possible.

2. The model has a global symmetry. If all spins are flipped, S is left unchanged.

Now we want to take the degrees of freedom of the Ising model and couple them together in such a way that the global symmetry of the old model is changed to a *local* symmetry. The notion "local symmetry" reflects the idea of invariance with respect to local reference frame transformations. Suppose there is a "frame of reference" at each site of our lattice. Suppose that these frames can be oriented

arbitrarily from site to site. We want to construct the action of the theory so that it is invariant to changes in the orientation of the local frames of reference.

F. Wegner invented such an "Ising lattice gauge theory" in 1971 [73]. His motivation was to obtain models which could not magnetize but would have non trivial phase diagrams.

Consider again a cubic lattice in a three-dimensional Euclidean space. Label the links which connect the adjacent points of the lattice by a site $\mathbf{n}$ and a unit lattice vector $\hat{\mu}$. The same link can be labeled as $(n, \hat{\mu})$ or $(\mathbf{n} + \hat{\mu}, -\hat{\mu})$ where site $(\mathbf{n} + \hat{\mu})$ means the site adjacent to n in the direction $\hat{\mu}$. At this time we place Ising spins σ on the links. Again we consider only "up" and "down" spins. Define a local gauge transformation at the site $\mathbf{n}$ as the operation $G(\mathbf{n})$ of flipping all the spins on links connected to that site. An example is shown in Fig. 2.5. An action has a
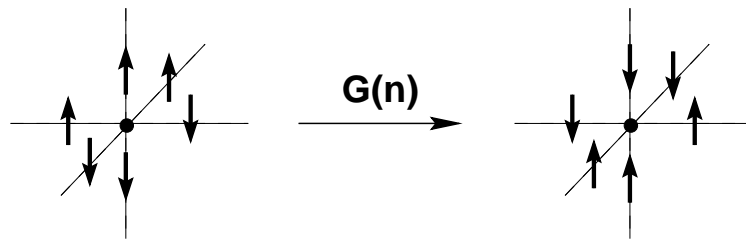

Figure 2.5.: A local symmetry operation in Ising lattice gauge theory in three dimensions.

huge invariance group because $G(n)$ can be applied everywhere. A nontrivial action having this symmetry consists of the product of spins around primitive squares, or "plaquettes", of the lattice,

$$S = -J \sum_{\mathbf{n},\hat{\mu},\hat{\nu}} \sigma(\mathbf{n}, \hat{\mu})\sigma(\mathbf{n} + \hat{\mu}, \hat{\nu})\sigma(\mathbf{n} + \hat{\mu} + \hat{\nu}, -\hat{\mu})\sigma(\mathbf{n} + \hat{\nu}, -\hat{\nu}) \qquad (2.17)$$

where the arguments of the spin variables label the links. We must check that S is invariant under arbitrary local gauge transformations. If the operation $G(\mathbf{n})$ is applied at the site $\mathbf{n}$, then both spins $\sigma(\mathbf{n}, \hat{\mu})$ and $\sigma(\mathbf{n} + \hat{\nu}, -\hat{\nu}) = \sigma(\mathbf{n}, \hat{\nu})$ change sign. Therefore S is unchanged. It is not difficult to see that the essential ingredient in guaranteeing the gauge invariance of S is that it has to be constructed from products of σ taken around *closed* paths of links. In order to keep the action S as local as possible one chooses primitive squares of four links. We come to the notion of the *plaquette* as a fundamental unity of the theory (see Fig. 2.6).

When our construction is generalized to systems with continuous symmetries, we will recognize the model as lattice version of theories with gauge symmetries. For the Abelian groups this has been done by K.G.Wilson [74]. Lattice gauge theories were independently invented by A.M. Polyakov [75]. The quantum Hamiltonian approach was developed by Kogut and Susskind [76].
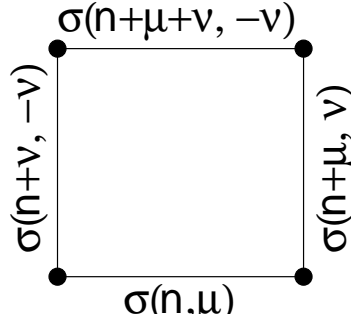
Figure 2.6.: A plaquette of spin variables.

2.4.2. Formulation of Quantum Electrodynamics on a lattice

Our aim is to try to understand similarities between quantization of the electromagnetic field and the approximate solution of the electrostatic problem. For this purpose let us consider "classical" Quantum Electrodynamics.

"Latticization"

We present our analysis in the $A_0 = 0$ gauge, where A_μ is the four-potential, because it is best suited to the Hamiltonian approach. Such an approach dates back to H.Weyl [77] and W.Heisenberg and W. Pauli [78], and is known as *temporal* or *Weyl* gauge. In this gauge the vector potential **A** and the electric field **E** are canonically conjugate variables.

The Hamiltonian for the photon field (or the free electrodynamic field) in the temporal gauge has the form

$$\mathcal{H} = \frac{1}{2} \int d\mathbf{r} \ \ E^2 + (\nabla \times \mathbf{A} \ ^2). \tag{2.18}$$

For simplicity we describe our notation in terms of a two-dimensional planar lattice. Its extension to a cubic lattice in three space dimensions is straightforward. We

Figure 2.7.: Labeling of sites and links in a two-dimensional lattice.

place our conjugate variables **A** and **E** on the links of the lattice, so that each site **n** = (n_x, n_y) has asso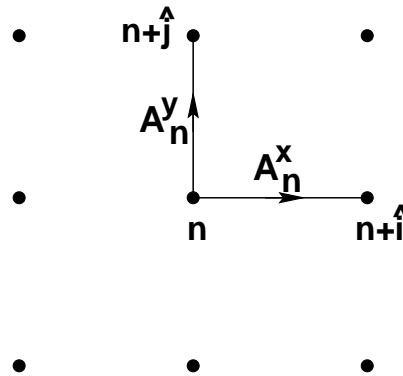ciated with it field components $A_{\mathbf{n}}^x$ and $A_{\mathbf{n}}^y$ residing on the links leaving the site **n** in $+x$ and $+y$ directions, respectively (see Fig. 2.7).

We then define the magnetic field $\mathbf{B_n}$ as the lattice curl

$$\mathbf{B_n} = (\nabla \times \mathbf{A})_{\mathbf{n}} \equiv \frac{1}{a} \left[A_{\mathbf{n}}^x + A_{\mathbf{n}+\hat{\imath}}^y - A_{\mathbf{n}+\hat{\jmath}}^x - A_{\mathbf{n}}^y \right] , \qquad (2.19)$$

where a is the lattice spacing. Like all pseudovectors **B** has one component, directed out of the plane in accordance with a right-hand rule and located at plaquette centers; plaquettes are labeled by their lower left-hand corners (Fig. 2.8). We also define the divergence of a vector (a scalar defined at each site; see Fig. 2.8)

$$(\nabla \cdot \mathbf{E}) = \frac{1}{a} \left[E_{\mathbf{n}}^x + E_{\mathbf{n}}^y - E_{\mathbf{n}-\hat{\imath}}^x - E_{\mathbf{n}-\hat{\jmath}}^y \right] . \qquad (2.20)$$
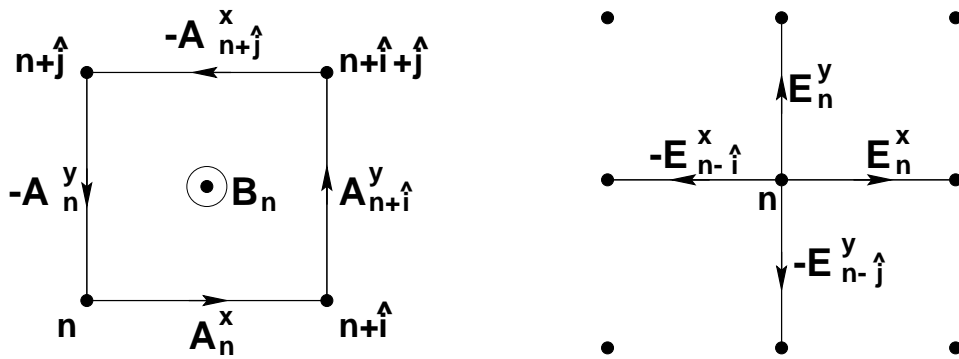
Figure 2.8.: Identification of the plaquette variable $\mathbf{B_n}$ in terms of link variables $\mathbf{A_n}$ (left). Divergence of $\mathbf{E_n}$ shown in terms of contributing links (right).

Our Hamiltonian from Eq. 2.18 can be "latticized" as following

$$\mathcal{H} = \frac{a^2}{2} \left[\sum_{links} (E_{\mathbf{n}}^a)^2 + \sum_{plaquettes} (B_{\mathbf{n}})^2 \right] . \qquad (2.21)$$

The canonical commutators become on the lattice (Latin superscripts are vector indices)

$$\left[A_{\mathbf{n}_1}^a, E_{\mathbf{n}_2}^b \right] = -i\frac{1}{a^2}\delta_{\mathbf{n}_1\mathbf{n}_2}\delta_{ab}. \qquad (2.22)$$

Equations 2.21 and 2.22 define a version of lattice Quantum Electrodynamics that is closely parallel to the continuum theory and is refered to as the *noncompact* version since the variable B can assume arbitrarily large values.

The Hilbert space and gauge fixing

We must next specify the Hilbert space on which our operators act. We interpret $\mathbf{A_n}$ and $\mathbf{E_n}$ as the operators of multiplication and differentiation on the space of square integrable functions of the variables $\mathbf{A_n}$.

The next step is to recognize that not all of the $\mathbf{E_n}$'s are truly quantum variables. First we notice that there is only one variable $B_\mathbf{n}$ but several variables $E_\mathbf{n}^a$ for each plaquette. Hence we would like to rewrite the kinetic part of the Hamiltonian in terms of variables conjugate to the $B_\mathbf{n}$'s plus those linear combinations of $\mathbf{E_n}$'s which commute with all of the $B_\mathbf{n}$'s and hence can be diagonalized along with $\mathcal{H}$. This is readily achieved if we note that certain linear combinations of the $\mathbf{E_n}$'s are the generators of time-independent gauge transformations, which commute with our Hamiltonian. To be specific, in the $A_0 = 0$ gauge, the Hamiltonian is unchanged if make the transformation

$$A_\mathbf{n}^a \to A_\mathbf{n}^a + (\nabla\Lambda)_\mathbf{n}^a, \tag{2.23}$$

where the lattice gradient is defined as

$$
\begin{aligned}
(\nabla\Lambda)_\mathbf{n}^x &= \frac{1}{a}\left(\Lambda_{\mathbf{n}+\hat{\imath}} - \Lambda_\mathbf{n}\right) \\
(\nabla\Lambda)_\mathbf{n}^y &= \frac{1}{a}\left(\Lambda_{\mathbf{n}+\hat{\jmath}} - \Lambda_\mathbf{n}\right)
\end{aligned}
\tag{2.24}
$$

From Eq. 2.22 it follows that this transformation is effected by the operator

$$U\left(\{\Lambda_\mathbf{n}\}\right) = \exp\left[i\sum_{\mathbf{n},a}(\nabla\Lambda)_\mathbf{n}^a E_\mathbf{n}^a\right] \equiv \exp\left(-i\sum_\mathbf{n}\Lambda_\mathbf{n}G_\mathbf{n}\right). \tag{2.25}$$

where $G_\mathbf{n}$ is the gauge generator. Noting, that for $\Lambda(\infty) = 0$,

$$\sum_\mathbf{n}(\nabla\Lambda)_\mathbf{n}^a E_\mathbf{n}^a = -\sum_\mathbf{n}\Lambda_\mathbf{n}(\nabla\cdot\mathbf{E})_\mathbf{n}, \tag{2.26}$$

we can identify the gauge generator G by

$$G_\mathbf{n} = (\nabla\cdot\mathbf{E})_\mathbf{n}. \tag{2.27}$$

Furthermore, the Heisenberg equations of motion are

$$
\begin{aligned}
i\frac{d}{dt}A^k(\mathbf{n}) &= A^k(\mathbf{n}), \mathcal{H} \\
&= \frac{a^2}{2}\left[A^k(\mathbf{n}), \sum_{\mathbf{n}'}E^k(\mathbf{n}')E^k(\mathbf{n}')\right] = -iE^k(\mathbf{n})
\end{aligned}
\tag{2.28}
$$

$$
\begin{aligned}
i\frac{d}{dt}E^k(\mathbf{n}) &= E^k(\mathbf{n}), \mathcal{H} \\
&= \frac{a^2}{2}\left[E^k(\mathbf{n}), \sum_{\mathbf{n}'}\epsilon_{jmp}\nabla^m A^p(\mathbf{n}')\epsilon_{jrs}\nabla^r A^s(\mathbf{n}')\right] \\
&= -\frac{i}{2}\epsilon_{jmp}\epsilon_{jrs}\sum_{\mathbf{n}'}\left\{\delta_{kp}\nabla^m\delta_{\mathbf{n}\mathbf{n}'}\nabla^r A^s(\mathbf{n}') + \delta_{ks}\nabla^r\delta_{\mathbf{n}\mathbf{n}'}\nabla^m A^p(\mathbf{n}')\right\} \\
&= i\epsilon_{kjl}\nabla^j\epsilon_{lmn}\nabla^m A^n(\mathbf{n}) = i(\nabla\times B)_\mathbf{n}^k
\end{aligned}
\tag{2.29}
$$

where the curl of $B(\mathbf{n})$ on the lattice is defined as following

$$
\begin{aligned}
(\nabla \times B)^x_{\mathbf{n}} &= \frac{1}{a} \left(B(\mathbf{n}) - B(\mathbf{n} - \hat{\jmath}) \right) \\
(\nabla \times B)^y_{\mathbf{n}} &= \frac{1}{a} \left(B(\mathbf{n} - \hat{\imath}) - B(\mathbf{n}) \right)
\end{aligned}
\tag{2.30}
$$

From the equations of motion it is clear that the gauge generators $G(\mathbf{n})$ commute with the Hamiltonian. Therefore we can diagonalize them and work within any individual eigensubspace. The eigenvalues of $G(\mathbf{n})$ may be interpreted as external charges $\rho(\mathbf{n})$, and in this way we see that the eigenvalue equation is nothing but Gauss's law, i.e.

$$
\left[\left(\nabla \cdot \mathbf{E} \right)(\mathbf{n}) - \rho(\mathbf{n}) \right] | \psi \rangle = 0,
\tag{2.31}
$$

for all states $| \psi \rangle$ in this sector of our Hilbert space. This is a very important consideration which we will use further. We want to stress that the invariance of the Hamiltonian under time-independent local gauge transformations leads to a conserved quantity $G(\mathbf{n})$ for each lattice point; in particular, if we impose Gauss's law $G(\mathbf{n}) - \rho(\mathbf{n}) = 0$ initially, it will remain zero for all times.

Restricting ourselves henceforth to any such eigensubspace we now decompose the electric field into a classical (longitudinal) and a quantum (transverse) part, writing

$$
\mathbf{E} = \mathbf{E}^{\parallel} + \mathbf{E}^{\perp}
\tag{2.32}
$$

where $\mathbf{E}^{\parallel}$ and $\mathbf{E}^{\perp}$ are defined by the conditions

$$
\nabla \times \mathbf{E}^{\parallel} = 0, \quad \nabla \cdot \mathbf{E}^{\perp} = 0.
\tag{2.33}
$$

The lattice curl and divergence in Eq. 2.33 are defined as in Eq. 2.19 and 2.20. Now, Eq. 2.33 implies that the longitudinal component can be presented as gradient of a scalar function

$$
\mathbf{E}^{\parallel} = -\nabla \phi
\tag{2.34}
$$

and, by Eq. 2.31, ϕ satisfies

$$
\nabla \cdot \mathbf{E} = \nabla \cdot \mathbf{E}^{\parallel} = -\nabla^2 \phi = \rho,
\tag{2.35}
$$

where the lattice Laplacian is defined to be

$$
\nabla^2 \phi \ (\mathbf{n}) = \frac{1}{a} \left[\phi(\mathbf{n} + \hat{\imath}) + \phi(\mathbf{n} - \hat{\imath}) + \phi(\mathbf{n} + \hat{\jmath}) + \phi(\mathbf{n} - \hat{\jmath}) - 4\phi(\mathbf{n}) \right].
\tag{2.36}
$$

As for the transversal part of the electric field $\mathbf{E}^{\perp}$, Eq. 2.33 implies

$$
\mathbf{E}^{\perp} = \nabla \times \theta,
\tag{2.37}
$$

where θ is a pseudovector (loop variable) defined on each plaquette of the lattice with

$$
\begin{aligned}
(\nabla \times \theta)^x (\mathbf{n}) &\equiv \frac{1}{a} \left[\theta(\mathbf{n}) - \theta(\mathbf{n} - \hat{\jmath}) \right] \\
(\nabla \times \theta)^y (\mathbf{n}) &\equiv \frac{1}{a} \left[-\theta(\mathbf{n}) + \theta(\mathbf{n} - \hat{\imath}) \right]
\end{aligned}
\tag{2.38}
$$

These equations can easily be inverted:

$$\theta(\mathbf{n}) = \sum_{j=-\infty}^{n_y} E^{\perp x}(n_x, j). \tag{2.39}$$

Summing up all our results, for each link of the lattice we have the electric field in this form

$$
\begin{aligned}
E^x(\mathbf{n}) &= \frac{1}{a}\left[-\left(\phi(\mathbf{n}+\hat{\imath})-\phi(\mathbf{n})\right)+\left(\theta(\mathbf{n})-\theta(\mathbf{n}-\hat{\jmath})\right)\right], \\
E^y(\mathbf{n}) &= \frac{1}{a}\left[-\left(\phi(\mathbf{n}+\hat{\jmath})-\phi(\mathbf{n})\right)-\left(\theta(\mathbf{n})-\theta(\mathbf{n}-\hat{\imath})\right)\right]
\end{aligned}
\tag{2.40}
$$

From Eq. 2.39 and 2.22 we can easily deduce the value of the commutator

$$[\theta(\mathbf{n}), B(\mathbf{n}')] = \frac{i}{a^2}\delta_{n_x n_x'}\delta_{n_y n_y'} \tag{2.41}$$

Thus θ and B are conjugate quantum variables. We now can rewrite the E^2 term in the Hamiltonian as

$$\mathcal{H} = \frac{1}{2}\sum_{links} E^2 = \frac{1}{2}\sum_{links} \ (E^{\parallel})^2 + 2\mathbf{E}^{\parallel}\cdot\mathbf{E}^{\perp} + (E^{\perp})^2 \tag{2.42}$$

In the continuum we have the property,

$$
\begin{aligned}
\int d^3r\,\mathbf{E}^{\parallel}\cdot\mathbf{E}^{\perp} &= \int d^3r\,(-\nabla\phi)\cdot\mathbf{E}^{\perp} \\
&= \int d^3r\,\phi\nabla\cdot\mathbf{E}^{\perp} = 0
\end{aligned}
\tag{2.43}
$$

and the same integration by parts is easily demonstrated on the lattice. Hence we are left with the usual Coulomb term plus the dynamical term written in terms of variables conjugate to the B's, i.e.

$$\mathcal{H} = \frac{1}{2}\sum_{links}\ (\nabla\phi)^2 + (\nabla\times\theta)^2 \ + \frac{1}{2}\sum_{plaquettes} B^2 \tag{2.44}$$

Introducing charges

To complete our formulation of Quantum Electrodynamics on a lattice we now specify the way in which quantum charges are introduced. Under local transformations the quantum fields transform as

$$
\begin{aligned}
\psi(r) &\rightarrow \exp\left[ie\Lambda(r)\right]\psi(r), \\
\psi^{\dagger}(r) &\rightarrow \exp\left[-ie\Lambda(r)\right]\psi^{\dagger}(r), \\
A(r) &\rightarrow A(r) + \nabla\Lambda(r),
\end{aligned}
\tag{2.45}
$$

hence it is easy to see that $\psi^\dagger(r + \xi)\psi(r)$ is not gauge invariant as long as $\xi \neq 0$. Therefore this operator must be modified if it is to be used in dynamical calculations which are to be consistent. Schwinger [79] suggested the operator

$$\psi^\dagger(r + \xi) \exp \ \ ie \int_r^{r+\xi} \mathbf{A}(r)d\mathbf{r} \ \ \psi(r), \tag{2.46}$$

because the line integral restores the desired local gauge invariance. So, if matter fields ψ were placed on a lattice, we receive

$$\psi^\dagger(r + \nu) \exp\left[iaeA_\nu(r)\right]\psi(r) \tag{2.47}$$

This gauge operator creates a pair of opposite charges at two separated points. Since the operator does not commute with the operator θ, the eigenvalues of this operator are changed when a state with pairs is created. This specific change can be computed directly from Gauss's law. The gauge operator creates a string of unit field strength along the link from $\mathbf{n}$ to $\mathbf{n} + \hat{\imath}$ and thereby changes $\nabla \cdot \mathbf{E}$ by $+1$ unit at $\mathbf{n}$ and by -1 unit at $\mathbf{n} + \hat{\imath}$. By 2.31 this means a change in the static Coulomb field owing to the additional field of a dipole pair with $+1$ unit of charge at $\mathbf{n}$ and -1 at $\mathbf{n} + \hat{\imath}$. According to 2.40 there must then be a compensating change in θ such that

$$(\nabla \times \theta)(\mathbf{n}) = \mathbf{E}^{string}(\mathbf{n}) - \mathbf{E}^{Coulomb}(\mathbf{n}). \tag{2.48}$$

In particular if we start with a state with no charges and $\theta(\mathbf{n}) = 0$, there will necessarily be a non–vanishing θ everywhere in the sector of states with charges present.

One-plaquette universe

We now turn to the problem of a very tiny universe made of a single square, as illustrated in 2.9. Our reason for doing so is that this very simple problem allows
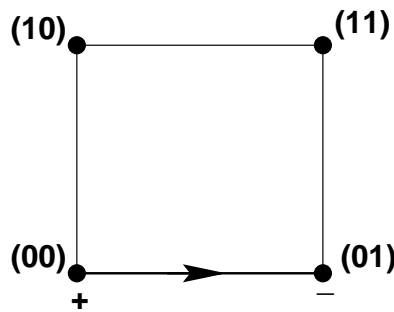

Figure 2.9.: A single-plaquette universe showing the charge configuration and notation discussed in the text.

us to present the physics of the more interesting problem of a lattice whose linear dimension is arbitrarily large.

For a single square the Hamiltonian 2.44 becomes

$$\mathcal{H} = \frac{1}{2} \sum_{links} (\nabla \phi)^2 + \frac{1}{2} \, 4\theta^2 \, + \frac{1}{2} B^2. \tag{2.49}$$

This is a trivial theory to solve. The energy of the ground state for any charge distribution is the energy of the Coulomb configuration corresponding to that distribution plus the ground-state energy of a harmonic oscillator of frequency $\omega = 2$.

Let us compute the expectation values of the electric field strengths created on the links of the plaquette by the presence of the dipole. It follows from Eq. 2.34 and 2.31 that the Coulomb field corresponding to this charge distribution is

$$
\begin{aligned}
E_{00}^{Coulomb,x} &= \frac{3}{4} \\
E_{00}^{Coulomb,y} &= E_{01}^{Coulomb,x} = -E_{10}^{Coulomb,y} = \frac{1}{4}
\end{aligned}
\tag{2.50}
$$

Since $e^{-iA_{00}^x}$ creates a unit string $E_{00}^x = 1$, Eq. 2.40 tells us that $\langle \psi | \theta | \psi \rangle = \frac{1}{4}$ at $t = 0$. So this state describes a coherent oscillator with $\omega = 2$. The time–dependent expectation values of the electric field are

$$
\begin{aligned}
\langle E_{00}^x(t) \rangle &= \frac{3}{4} + \frac{1}{4} \cos \omega t, \\
\langle E_{00}^y(t) \rangle &= \langle E_{01}^x(t) \rangle = -\langle E_{10}^y(t) \rangle = \frac{1}{4} - \frac{1}{4} \cos \omega t.
\end{aligned}
\tag{2.51}
$$

This state describes a static Coulomb configuration plus an *oscillating* photon cloud. Even though the cloud oscillates it is clear that the time-averaged value of the **E** field in this state is exactly the Coulomb value. The oscillating nature of the cloud is an artifact of our very small "universe"-the radiation cloud can not radiate away because it hits the nearby boundaries of this small system and is reflected back. In an infinite system the coherent cloud would simply radiate away, unshielding the Coulomb field of the two charges.

2.4.3. Electrostatics as a variational problem with constraint

After obtaining the knowledge of the quantum behavior of our system, we will try to map our considerations onto the classical case.

In a classical case for static charges we can neglect the magnetic component of the Hamiltonian. Gauss' law serves as the analog of gauge invariance in Quantum electrodynamics, so we will keep it for future use. The energy of a system of static charged particles in a uniform dielectric background is expressed as a function of the electric field **E**

$$\mathcal{U} = \epsilon_0 \int \frac{\mathbf{E}^2}{2} d^3 \mathbf{r}. \tag{2.52}$$

Combining this equation with Gauss' law

$$\nabla \cdot \mathbf{E} - \rho / \epsilon_0 = 0 \tag{2.53}$$

we can consider the problem of finding the energy of the system as a variational problem with constraint. It was done by Maggs and Rossetto [49] using the following approach.

One can introduce a Lagrange multiplier and construct the functional

$$\mathcal{A} = \int \; \epsilon_0 \frac{\mathbf{E}^2}{2} - \lambda(\mathbf{r})(\epsilon_0 \nabla \cdot \mathbf{E} - \rho) \; d^3\mathbf{r} \qquad (2.54)$$

Variation of this functional with respect to $\mathbf{E}$ gives $\mathbf{E} + \nabla\lambda = 0$. Therefore the Lagrange multiplier is identical to the electrostatic potential ϕ and the minimum energy is $\mathcal{U}_{Coulomb} = \frac{\epsilon_0}{2} \int (\nabla\phi)^2 d^3\mathbf{r}$. Again the cross term in Eq. 2.52 vanishes, as it is seen by integration by parts and we can write

$$\mathcal{U} = \frac{\epsilon_0}{2} \int \; (\nabla\phi)^2 + (\nabla \times \theta)^2 \; d^3\mathbf{r} \qquad (2.55)$$

We can understand a constrained electrostatics as the analogue of the Car–Parrinello method. While Gauss' law fixes only the longitudinal component of electric field strength $\mathbf{E}^{\parallel}$, the "Born–Oppenheimer surface" can be understood as the surface on which the transverse component of electric field vanishes, i.e. $\mathbf{E}^{\perp} = 0$. Therefore during the dynamics we allow the field to leave the "Born-Oppenheimer surface".

The additivity of the electrostatic energy with respect to the longitudinal and transversal part means the factorization of the statistical partition function [49]

$$\mathcal{Z}(\{\mathbf{r}\}) = \exp \; -\frac{\beta\epsilon_0}{2} \int (\nabla\phi)^2 d^3\mathbf{r} \; \int \mathcal{D}\mathbf{E}^{\perp} \exp \; -\frac{\beta\epsilon_0}{2} \int (\mathbf{E}^{\perp})^2 d^3\mathbf{r} \qquad (2.56)$$

where $\mathcal{D}\mathbf{E}^{\perp} = \prod_{\mathbf{r}} \delta(\nabla\mathbf{E} - \rho/\epsilon_0)\mathcal{D}\mathbf{E}$ performs the summation over all rotational degrees of freedom of the field described by the potential θ. All the dependence on the particle positions is in the prefactor characterized by the electrostatic potential ϕ found by solving Poisson's equation. This prefactor gives the Coulomb interaction between the particles. The remaining integral is independent of the positions of the charges and multiplies the standard partition function by a simple constant. This extra factor can be simply ignored.

Right now we are able to describe a local Monte–Carlo algorithm for the calculation of the electrostatic energy. Again we consider a lattice, the charges are living on the vertices of the lattice, i.e. the charge ρ is a function of the vertex position $\mathbf{n}$. The electric field is placed on the links of the lattice $\mathbf{E}(\mathbf{n} + \mathbf{a})$. Charges are allowed to hop from a site to a neighboring one, as described in Fig. 2.10 for the two-dimensional case.

As for Quantum Electrodynamics on the lattice we define lattice versions of divergence and curl:

$$(\nabla \cdot \mathbf{E}) (\mathbf{n}) = \frac{1}{a} \left(E^x(\mathbf{n}) + E^y(\mathbf{n}) - E^x(\mathbf{n} - \hat{\imath}) - E^y(\mathbf{n} - \hat{\jmath}) \right). \qquad (2.57)$$

$$(\nabla \times \mathbf{E}) (\mathbf{n})|_z = \frac{1}{a} \left(E^x(\mathbf{n}) + E^y(\mathbf{n} + \hat{\imath}) - E^x(\mathbf{n} + \hat{\jmath}) - E^y(\mathbf{n}) \right) \qquad (2.58)$$
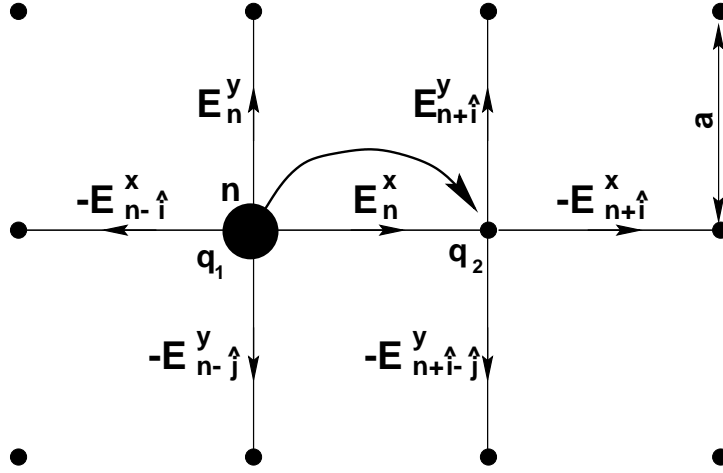
Figure 2.10.: The placement of the charges and electric field on the sites and links; the hopping of the charge from one site to a neighboring one (a - lattice spacing).

The discretized version of the energy is given by

$$\mathcal{U} = \frac{\epsilon_0 a^3}{2} \sum_{links} \mathbf{E}^2(\mathbf{n}).$$ (2.59)

where a is the lattice spacing.

Let us describe the process of moving of the charge from the site $\mathbf{n}$ in x-direction, i.e. to the site $\mathbf{n} + \hat{\imath}$. The Gauss law for these two sites before the hopping can be found with the help of Eq. 2.57

$$\rho_1 = \frac{1}{a^3} q_1 =$$
$$\frac{\epsilon_0}{a} \left(E^x(\mathbf{n}) + E^y(\mathbf{n}) - E^x(\mathbf{n} - \hat{\imath}) - E^y(\mathbf{n} - \hat{\jmath}) \right)$$
$$\rho_2 = \frac{1}{a^3} q_2 =$$
$$\frac{\epsilon_0}{a} \left(E^x(\mathbf{n} + \hat{\imath}) + E^y(\mathbf{n} + \hat{\imath}) - E^x(\mathbf{n}) - E^y(\mathbf{n} + \hat{\imath} - \hat{\jmath}) \right)$$

We can update the electric fields on the links after hopping in such a way, that the procedure will be as local as possible and after the hopping the Gauss' law will still be satisfied. If the amount of charge from the left site to the right site is δq, then we update the field on the link $(\mathbf{n}, x)$ by the amount $\frac{\delta q}{a^2 \epsilon_0}$. Let us check Gauss' law

after hopping.

$$q_1 + \delta q =$$

$$a^2 \epsilon_0 \quad E^x(\mathbf{n}) + E^y(\mathbf{n}) - E^x(\mathbf{n} - \hat{\imath}) - E^y(\mathbf{n} - \hat{\jmath}) + \frac{\delta q}{a^2 \epsilon_0}$$

$$q_2 - \delta q =$$

$$a^2 \epsilon_0 \quad E^x(\mathbf{n} + \hat{\imath}) + E^y(\mathbf{n} + \hat{\imath}) - E^x(\mathbf{n}) - E^y(\mathbf{n} + \hat{\imath} - \hat{\jmath}) - \frac{\delta q}{a^2 \epsilon_0}$$

So Gauss' law is unchanged after this updating. But if we calculate the curl of the electric field, we will easily see, that it has nonzero value. It means, that after the update of the field on the link we leave the Born-Oppenheimer surface.

On the other hand we see a strong analogy with the quantum approach. The hopping of the charge can be considered as the creation of 2 charges with opposite values. We have already seen that this operation leads to the generation of a "string" field on the link which connects these two charges. Furthermore, this pair changes the transverse field, i.e. field θ, which lives on the plaquette. Therefore using this process of generation of "particle-antiparticle" pairs and restricting accordingly the possible moves, we can reduce the transverse part of the electrostatic energy and finally obtain the solution of our electrostatic problem. Of course in the classical case the analog of local gauge invariance is Gauss' law and we have to satisfy it at each hopping process.

The Monte Carlo algorithm can be implemented as following

1. At time $t = 0$ start with the system where the constraint is satisfied.

2. Displace the charge and update correspondingly the electric field on the connecting link. Accept or reject this move according to the Metropolis criterion [80]. This is the trial move for the particles;

3. Update all the field values of a single plaquette while conserving the constraint at each vertex. This is done by adding a random increment Δ to the fields $E^x(\mathbf{n})$ and $E^y(\mathbf{n} + \hat{\imath})$ and simultaneously decreasing by the same Δ fields $E^x(\mathbf{n} + \hat{\jmath})$ and $E^y(\mathbf{n})$. Gauss' law is still satisfied. This is the trial move for the fields.

4. The two moves are not sufficient to equilibrate a system with periodic boundary conditions in all situations. This problem is linked with the solution $\phi = -\overline{\mathbf{E}} \cdot \mathbf{r}$ or $\mathbf{E} = \overline{\mathbf{E}}$ of the Laplace equation on a torus, where $\overline{\mathbf{E}}$ is an arbitrary constant vector. The motion of the charges generates fluctuations in $\overline{\mathbf{E}}$, while updates of the field conserve this component $\overline{\mathbf{E}}$. In order to be absolutely sure that the algorithm is ergodic a third possible Monte-Carlo move is introduced, which shifts $\overline{\mathbf{E}}$. In large systems fluctuations in this single mode should give a small contribution to the thermodynamics if the initial conditions are typical; in such cases this update can be eliminated.

The total complexity is of the order of $\mathcal{O}(N)$, so the method is as local as possible. Great.

2.5. What one should definitely not do

Inspired by the success of the Monte Carlo method, we want to construct a Molecular Dynamics algorithm for charged systems. One has to construct some artificial dynamics where Gauss' law will play the role of a constraint.

2.5.1. The Lagrangian of the constrained system of charges and fields

In order to describe the dynamics of the charged system one has to construct the equations of motion. The first step in this direction is to postulate the Lagrangian. The usual Lagrangian for the charged system is

$$\mathcal{L}_0 = \sum_{i \in charges} \frac{m_i}{2} \dot{\mathbf{r}}_i^2 - \sum_{i<j} \mathcal{U}_{LJ}(r_{ij}) - a^3 \sum_{j \in links} \frac{\epsilon_0}{2} \mathbf{E}_j^2 \qquad (2.60)$$

where a is the lattice spacing, m_i the masses of the particles, $\dot{\mathbf{r}}_i$ their velocities, $\mathcal{U}_{LJ}$ the pair–wise interaction potential between the particles (LJ means Lennard–Jones potential), $\mathbf{E}$ the electric field on the links. We can find the equations of motion from the Lagrangian and finally solve them. But for each time step we would have to find the electric field $\mathbf{E}$ by solving (on the lattice) the equations of electrostatics, i. e.

$$\nabla \cdot \mathbf{E} = \frac{1}{\epsilon_0} \rho, \qquad \nabla \times \mathbf{E} = 0 \qquad (2.61)$$

In other words, we would have to implement some sort of Poisson equation solver, which is complicated and costly, as outlined in Sec. 2.3.3. As discussed before, Eq. 2.61 means that we have to keep the system on both the constraint surface (Gauss' law) and the Born–Oppenheimer surface (vanishing transversal component).

In the Car–Parrinello method [81, 82] we abandon the requirement of staying strictly on the Born–Oppenheimer surface, and rather replace this by some artificial dynamics. In the Car–Parrinello method we include the electric fields as *additional* degrees of freedom via an extended Lagrangian formalism which enables us to systematically derive equations of motion for them. The time derivatives of these extra variables, therefore, generate extra kinetic energy terms to which we will refer as the "fictitious" kinetic energy. The full kinetic energy, which contains the contribution from the translation of the charged particles as well as the translation of the electric fields is:

$$\mathcal{T} = \sum_{i \in charges} \frac{m_i}{2} \dot{\mathbf{r}}_i^2 + a^3 \sum_{j \in links} \frac{\mu_j}{2} \dot{\mathbf{E}}_j^2 \qquad (2.62)$$

where j labels the links, $\dot{\mathbf{E}}_j$ is the "velocity" of the electric field and μ_j is the inertia associated with the electric field velocity. Further we will not use mixtures of particles and define the mass of the particles as m. The same is true for the fields (it is difficult to imagine for which purpose we need different masses for different fields on the links); we hence use μ without indexing.

Our extended Lagrangian can be written as the difference of kinetic and potential terms:

$$
\mathcal{L} = \sum_{i \in charges} \frac{m_i}{2} \dot{\mathbf{r}}_i^2 + a^3 \sum_{j \in links} \frac{\mu_j}{2} \dot{\mathbf{E}}_j^2 -
$$
$$
\sum_{i<j} \mathcal{U}_{LJ}(r_{ij}) - a^3 \sum_{j \in links} \frac{\epsilon_0}{2} \mathbf{E}_j^2 - \sum_{\mathbf{n} \in sites} \lambda(\mathbf{n}) \ (\nabla \cdot \mathbf{E})(\mathbf{n}) - \frac{\rho(\mathbf{n})}{\epsilon_0}
$$

(2.63)

where we have put the constraint on each vertex $\mathbf{n}$ with the help of Lagrange multiplier $\lambda(\mathbf{n})$.

2.5.2. Introducing units

We have to take care about units which we will use for our system. Usually it is very convenient in the simulation to use Lennard–Jones units. Therefore we have to adjust the electric units to Lennard–Jones units. The pair-wise Lennard–Jones potential for particles i and j has the following form

$$
\mathcal{U}_{LJ}(r_{ij}) = 4\epsilon_{LJ} \left\{ \left(\frac{\sigma}{r_{ij}} \right)^{12} - \left(\frac{\sigma}{r_{ij}} \right)^{6} + \frac{1}{4} \right\}
$$

(2.64)

for $r_{ij} < 2^{1/6}\sigma$ ($\mathcal{U}_{LJ}$ is zero otherwise), where r_{ij} is the distance between two particles. Using ϵ_{LJ} as the unit of energy and σ as the unit of length, we can rewrite the Lennard–Jones potential in dimensionless form (tilde means dimensionless quantity)

$$
\tilde{\mathcal{U}}_{LJ}(\tilde{r}_{ij}) = 4 \left\{ \left(\frac{1}{\tilde{r}_{ij}} \right)^{12} - \left(\frac{1}{\tilde{r}_{ij}} \right)^{6} + \frac{1}{4} \right\}
$$

(2.65)

Furthermore we can write down dimensionless time and velocity. Together with energy and length we have this transformation mapping

$$
\mathcal{U} \ \rightarrow \ \tilde{\mathcal{U}} = \frac{\mathcal{U}}{\epsilon_{LJ}}
$$
$$
\mathbf{r} \ \rightarrow \ \tilde{\mathbf{r}} = \frac{\mathbf{r}}{\sigma}
$$
$$
t \ \rightarrow \ \tilde{t} = \frac{t}{\sqrt{\frac{m\sigma^2}{\epsilon_{LJ}}}} = \sqrt{\frac{\epsilon_{LJ}}{m\sigma^2}} t
$$
$$
\mathbf{p} \ \rightarrow \ \tilde{\mathbf{p}} = \frac{p}{\frac{m\sigma}{\sqrt{\frac{m\sigma^2}{\epsilon_{LJ}}}}} = \frac{\mathbf{p}}{\sqrt{m\epsilon_{LJ}}}
$$

where $\mathbf{p}$ is the momentum of the particle.

It is a simple, but a little bit tedious algebra to show the transformation rules for the electric field and the velocity of the electric field. The result is

$$\mathbf{E} \rightarrow \tilde{\mathbf{E}} = \frac{\mathbf{E}}{\sqrt{\frac{\epsilon_{LJ}}{\epsilon_0 \sigma^3}}}$$

$$\dot{\mathbf{E}} \rightarrow \dot{\tilde{\mathbf{E}}} = \frac{\sqrt{m\epsilon_0 \sigma^5}}{\epsilon_{LJ}} \dot{\mathbf{E}}$$

After the transformation to Lennard-Jones units our Lagrangian (without constraint term) receives the form

$$\tilde{\mathcal{L}} = \sum_{i \in charges} \frac{\tilde{\mathbf{p}}_i^2}{2} + \tilde{a}^3 \frac{\mu}{2} \frac{\epsilon_{LJ}^2}{m\sigma^2\epsilon_0} \sum_{j \in links} \dot{\tilde{\mathbf{E}}}_j^2 - \sum_{i<j} \tilde{\mathcal{U}}_{LJ}(\tilde{r}_{ij}) - \frac{\tilde{a}^3}{2} \sum_{j \in links} \tilde{\mathbf{E}}_j^2$$

where $\tilde{a}$ is the dimensionless lattice spacing. From the last equation we can deduce that we are forced to introduce some reduced mass of the field, i.e.

$$\tilde{\mu} = \frac{\epsilon_{LJ}^2}{m\sigma^2\epsilon_0} \mu$$

Further we have to transform Gauss' law to dimensionless form. Usually the strength of the electrostatic interactions is expressed by the Bjerrum length [83]. It is the distance at which two unit charges have an interaction energy equal to $k_B T$ (T is the thermodynamic temperature)

$$l_B = \frac{e^2}{4\pi\epsilon_0 k_B T} \tag{2.66}$$

where e is the unit charge.

For a charge q on a lattice site, we can introduce a dimensionless charge

$$\tilde{q} = \frac{q}{\sqrt{4\pi\epsilon_0 k_B T l_B}} \tag{2.67}$$

($\tilde{q} = 1$ cooresponding to $q = e$ and a dimensionless charge density

$$\tilde{\rho} = \frac{\tilde{q}}{\tilde{a}^3}. \tag{2.68}$$

Gauss' law

$$\frac{1}{a} E \sim \frac{1}{\epsilon_0} \rho \tag{2.69}$$

is then transformed to the dimensionless form

$$\frac{1}{\tilde{a}} \tilde{E} \sim \tilde{\rho} \sqrt{4\pi k_B \tilde{T} \tilde{l}_B} \tag{2.70}$$

From now on, we will assume LJ units throughout, and drop the tilde.

2.5.3. The simulation technique

From the extended Lagrangian we obtain the equations of motion for particles and for fields:

$$m\frac{d^2\mathbf{r}_i}{dt^2} = -\sum_{j\neq i}\frac{\partial U_{LJ}(|\mathbf{r}_i - \mathbf{r}_j|)}{\partial r_i}$$

$$-a^3\sum_{n\in sites}\lambda(n)\frac{\partial}{\partial \mathbf{r}_i}\left[\nabla\cdot\mathbf{E} - \frac{\rho}{\epsilon_0}\right](n)$$

$$\mu\frac{d^2\mathbf{E}_k}{dt^2} = -\epsilon_0\mathbf{E}_k - \sum_{n\in sites}\lambda(n)\frac{\partial}{\partial \mathbf{E}_k}\left[\nabla\cdot\mathbf{E} - \frac{\rho}{\epsilon_0}\right](n) \quad (2.71)$$

where index i goes over all particles and index k over all links. It means that from the Lagrangian with holonomic constraints we came to the unconstrained formulation of Molecular Dynamics.

Introducing the Hamiltonian

$$\mathcal{H} = \sum_i \mathbf{p}_i\dot{\mathbf{r}}_i + \sum_{i\in links}\mathbf{p}_i^E\dot{\mathbf{E}}_i - \mathcal{L} \quad (2.72)$$

the equations of motion can be recast in a more suitable for the time-discretization form

$$\frac{d\mathbf{r}_i}{dt} = \frac{\mathbf{p}_i}{m} \quad (2.73)$$

$$\frac{d\mathbf{E}_k}{dt} = \frac{\mathbf{p}_k^E}{\mu} \quad (2.74)$$

$$\frac{d\mathbf{p}_i}{dt} = -\sum_{j\neq i}\frac{\partial U_{LJ}(|\mathbf{r}_i - \mathbf{r}_j|)}{\partial r_i}$$

$$-a^3\sum_{n\in sites}\lambda(n)\frac{\partial}{\partial \mathbf{r}_i}\left[\nabla\cdot\mathbf{E} - \frac{\rho}{\epsilon_0}\right](n) \quad (2.75)$$

$$\frac{d\mathbf{p}_k^E}{dt} = -\epsilon_0\mathbf{E}_k - \sum_{n\in sites}\lambda(n)\frac{\partial}{\partial \mathbf{E}_k}\left[\nabla\cdot\mathbf{E} - \frac{\rho}{\epsilon_0}\right](n) \quad (2.76)$$

The constrained Verlet algorithm

Eqs. 2.73 - 2.76 can be written in the compact form:

$$\dot{q} = M^{-1}p \quad (2.77)$$

$$\dot{p} = -\nabla_q V(q) - g'(q)^T\lambda \quad (2.78)$$

$$g(q) = 0 \quad (2.79)$$

Here $q \in \mathbf{R}^{3N+N_{sites}}$ and $p \in \mathbf{R}^{3N+N_{sites}}$ are the vectors of Cartesian positions and momenta (N – the number of particles, N_{sites} – number of lattice sites), M is a

$3N + N_{sites}$–dimensional positive diagonal mass matrix of the form

$$M = diag(\underbrace{m, m, m, \ldots, m}_{3N \text{ elements}}, \; \underbrace{\mu, \mu, \mu, \ldots, \mu}_{3N_{sites} \text{ elements}}), \qquad (2.80)$$

$g : \mathbf{R}^{3N+N_{sites}} \to \mathbf{R}^{N_{sites}}$ is the mapping which gives N_{sites} holonomic constraints, g' is the matrix of partial derivatives with respect to the positions q, and $\lambda \in \mathbf{R}^{N_{sites}}$ is a vector of time-dependent Lagrange multipliers. These equations form a system of differential-algebraic equations (DAEs) of index three: three differentiations of Eq. 2.79 with respect to time are required to reduce the equations to a system of ordinary differential equations [84]. The solution manifold underlying Eq. 2.77 - Eq. 2.79 is

$$\mathcal{M} = \left\{ (q, p) | g(q) = 0, g'(q)M^{-1}p = 0 \right\}.$$

The so called *hidden* constraint $g'(q)M^{-1}p = 0$ is obtained through time differentiation of the position constraint.

A computational approach for unconstrained problems that remains the basis for modern Molecular Dynamics simulations is a discretization that is often referred to as the *Verlet method* [85] when applied in Molecular Dynamics. When rewritten as a one-step discretization incorporating half–steps in the momenta,

$$p(t_n + \frac{h}{2}) = p(t_n) - \frac{h}{2}\nabla_q V(q(t_n))$$

$$q(t_n + h) = q(t_n) + hM^{-1}p(t_n + \frac{h}{2})$$

$$p(t_n + h) = p(t_n + \frac{h}{2}) - \frac{h}{2}\nabla_q V(q(t_n + h))$$

it is called the *velocity Verlet algorithm*. Due to its evident simplicity and efficiency, the Verlet method continues to be popular in Molecular Dynamics. It is known that the method is symplectic, i.e. conserves the wedge product $dq \wedge dp$ of differentials [58]. The property of being symplectic reproduces a corresponding property for the true flow map of a Hamiltonian system, and may explain the good performance of the method for long time interval simulations [86]. In particular, the property of being symplectic implies the Liouville property of conservation of volume in phase space.

The Verlet method was adapted to allow for bond constraints by Ryckaert et al [87], and the resulting discretization scheme is referred to as the Verlet method with SHAKE–type constraints, or simply SHAKE. An alternative velocity–level formulation for the constrained case, RATTLE, was proposed by Andersen [88].

The SHAKE algorithm can be written in this form

$$p(t_n + \frac{h}{2}) = p(t_n) - \frac{h}{2}\nabla_q V(q(t_n)) - \frac{h}{2}g'(q(t_n))^T \lambda(t_n) \tag{2.81}$$

$$q(t_n + h) = q(t_n) + hM^{-1}p(t_n + \frac{h}{2}) \tag{2.82}$$

$$0 = g(q(t_n + h)) \tag{2.83}$$

$$p(t_n + h) = p(t_n + \frac{h}{2})$$
$$- \frac{h}{2}\nabla_q V(q(t_n + h)) - \frac{h}{2}g'(q(t_n + h))^T \lambda(t_n + h) \tag{2.84}$$

and the RATTLE algorithm correspondingly

$$p(t_n + \frac{h}{2}) = p(t_n) - \frac{h}{2}\nabla_q V(q(t_n)) - \frac{h}{2}g'(q(t_n))^T \lambda(t_n) \tag{2.85}$$

$$q(t_n + h) = q(t_n) + hM^{-1}p(t_n + \frac{h}{2}) \tag{2.86}$$

$$0 = g(q(t_n + h)) \tag{2.87}$$

$$p(t_n + h) = p(t_n + \frac{h}{2})$$
$$- \frac{h}{2}\nabla_q V(q(t_n + h)) - \frac{h}{2}g'(q(t_n + h))^T \mu(t_n + h) \tag{2.88}$$

$$0 = g'(q(t_n + h)) M^{-1}p(t_n + h) \tag{2.89}$$

At each step of discretization like RATTLE or SHAKE, a system of nonlinear algebraic equations must be solved. Assuming that the nonlinear equations are solved exactly at each step, SHAKE and RATTLE are globally second order accurate. The two methods are equivalent at time steps in position and at half step in momenta and, moreover, the RATTLE method is a symplectic discretization. The SHAKE algorithm is essentially symplectic [89] in that the wedge product is preserved, but the computed solution does not conserve the hidden constraint $g'(q)M^{-1}p = 0$. Symplectic discretization schemes for ordinary differential equations are discussed in [90], and symplectic methods for constrained problems are discussed in [91]. The SHAKE and RATTLE discretizations have been generalized to families of higher order schemes by Reich [92] through concatenation of steps with appropriately chosen step sizes. Regardless of which discretization is used, it is necessary to solve the nonlinear equations at each step accurately in order to retain the desirable theoretical properties.

The SHAKE iteration for the nonlinear equations

As has already been mentioned both the SHAKE and the RATTLE algorithms lead to identical results in terms of the q variable (see Ref. [89]). So, we decided to use the SHAKE version, because the implementation of that method is a little bit simpler than for RATTLE.

It has been also shown [89] that equations 2.82 - 2.84 is a second–order, time–reversible, symplectic discretization of the equation system 2.77 - 2.79. In addition, the method conserves angular momentum [93] and can be viewed as the exact solution of a perturbed constrained Hamiltonian system [92].

But SHAKE requires an efficient technique for solving the nonlinear equations at each step. In fact, the original paper [87] describing the SHAKE discretization presented an iterative solver for the nonlinear equations, and the term SHAKE typically is used to refer to the overall procedure consisting of discretization together with the iterative solver used in satisfying the constraints (*coordinate resetting*).

Substituting Eq. 2.81 in Eq. 2.82 leads to the equations

$$
\begin{aligned}
q(t_n + h) &= q(t_n) + hM^{-1}(p(t_n) - \frac{h}{2}\nabla_q V(q(t_n)) - \frac{h}{2}g'\left(q(t_n)\right)^T \lambda(t_n)) \\
0 &= g(q(t_n + h))
\end{aligned}
$$

Denoting $Q \equiv q(t_n + h)$, $G \equiv g'(q(t_n))$ and $\Lambda \equiv \frac{h^2}{2}\lambda(t_n)$ we can write the nonlinear system as

$$
g\left(\overline{Q} - M^{-1}G^T\Lambda\right) = 0, \tag{2.90}
$$

where

$$
\overline{Q} \equiv q(t_n) + hM^{-1}(p(t_n) - \frac{h}{2}\nabla_q V(q(t_n))) \tag{2.91}
$$

represents the result of an unconstrained step of size h.

The system of nonlinear equations (Eq. 2.90) can be written in terms of individual unknowns as

$$
g\left(\overline{Q} - M^{-1}\sum_{i=1}^{N_{sites}}\Lambda_i G_i^T\right) = 0, \tag{2.92}
$$

where Λ_i is the ith component of Λ, and $G_i^T = \nabla_q g_i(q(t_n))$. In the SHAKE iteration, we cycle through the constraints one by one, adjusting one multiplier at each step.

This results in the following scheme:

1. We initialize $Q = \overline{Q}$ as the unconstrained coordinate, which corresponds to the initial guess $\Lambda = 0$.

2. We compute the correction of the ith component $\Delta\Lambda_i$ needed to satisfy the ith linearized constraint equation:

$$
\Delta\Lambda_i \leftarrow \frac{g_i(Q)}{g_i'(Q)M^{-1}G_i^T}, \tag{2.93}
$$

3. Update Q by

$$
Q \leftarrow Q - M^{-1}G_i^T\Delta\Lambda_i. \tag{2.94}
$$

4. This cycle should be repeated until all constraint residuals $g_i(Q)$ are below a prescribed value.

Initialization procedure

We have already seen that in order to be able to propagate our constrained system, we have to solve the system of nonlinear equations. Solving them iteratively means that we have only local convergence. Therefore an initial solution must be pretty close to the constraint surface. This leads to the problem of initialization of our fields.

We search for some solution of Gauss' equation in three-dimensional space by means of a simple procedure. For a given charge distribution on the lattice which satisfies the condition of overall neutrality, we find a particular solution of Gauss' law as the result of the following recursive procedure (see Fig. 2.11):

1. In each plane perpendicular to the z-axis, find the average charge. Place this charge on each vertex of that plane.

2. On the links which go to the plane $z = 0$ (in z-direction) set the field to zero.

3. On the links which go out of the plane $z = 0$, put a field which is larger or smaller by the amount of plane charge in between.

4. Proceed throughout the box.

5. At the end, we must again wind up at zero field because of overall neutrality and the periodic boundary conditions.

6. Calculate the average field in z direction and subtract that value from all the fields we have found.

7. For each vertex, subtract the plane charge from the charge value.

8. Find the average charge in each line in x direction.

9. Find the fields in y direction, where the line charge gives the change in electric field.

10. Do subtraction analogous to before.

11. Find the field in x direction, and subtract again the average field.

12. Put charges back on to the lattice.

Let us check Gauss' law. According to the construction at each vertex $\mathbf{n}$ of the lattice we have

$$E_z^2 - E_z^1 = \frac{q_{plane}}{\epsilon_0 a^2}$$
$$E_y^2 - E_y^1 = \frac{q_{wire}}{\epsilon_0 a^2}$$
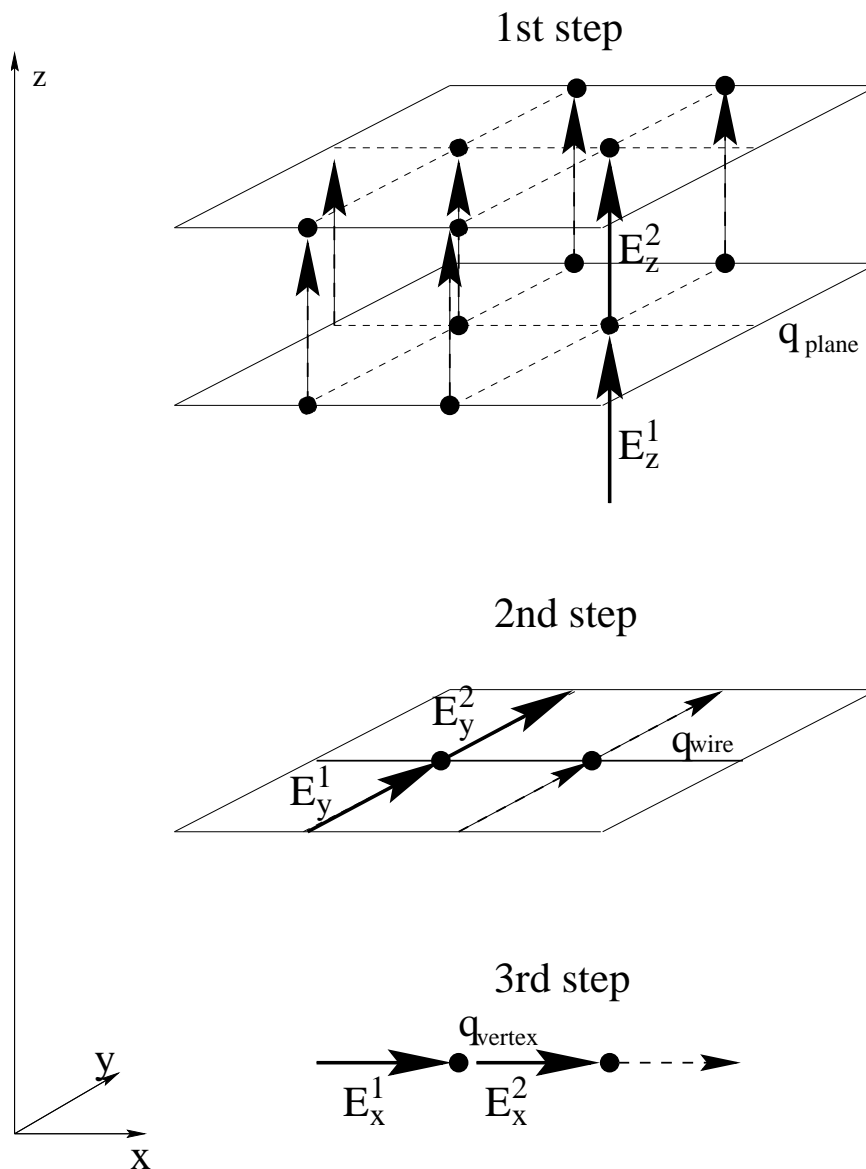$$E_x^2 - E_x^1 = \frac{q_{vertex}}{\epsilon_0 a^2}$$

Figure 2.11.: The Recursive treatment of spacial dimensions for the calculation of some Gauss' law solution.(1st step) The charge in the plane $z = z_{plane}$ is $q_{plane} = \frac{1}{N}\sum_i q(\mathbf{r}_i)\delta(z_i - z_{plane})$, N is the number of charges in plane $z = z_{plane}$. Update the z-field according to the formula $E_z^2 = E_z^1 + \frac{q_{plane}}{\epsilon_0 a^2}$.(2nd step) Subtract the charge q_{plane} from the each charge on sites of z_{plane}. The charge of the wire $y = y_{wire}, z = z_{plane}$ is $q_{wire} = \frac{1}{N}\sum_i q(\mathbf{r}_i)\delta(z_i - z_{plane})\delta(y_i - y_{wire})$, N now meaning the number of charges in the wire. Update y-field $E_y^2 = E_y^1 + \frac{q_{wire}}{\epsilon_0 a^2}$. (3rd step) Subtract the charge q_{wire} from the each charge on the sites of (y_{wire}, z_{plane}). Update x field $E_x^2 = E_x^1 + \frac{q_{vertex}}{\epsilon_0 a^2}$

Since the total charge is given by

$$q_{plane} + q_{wire} + q_{vertex}$$

these equations yield Gauss' law directly.

Charge interpolation scheme

The simulation runs a coupled system of point charges q_i living in the continuum, and electric fields on the lattice. Therefore we have to interpolate charges to the vertices of the lattice. As can be seen from Eq. 2.93 for the calculation of a new Λ we need to calculate the derivative of the constraint. The derivative g' is defined also by the derivative of the charge with respect to the coordinate, i.e. $\frac{\partial}{\partial \mathbf{r}_i}\rho(\mathbf{n})$. This leads to the requirement that the interpolation scheme must be at least continuously differentiable. The simple linear interpolation does not satisfy this condition - the first derivative has jumps and we have taken a smoother one: suppose a charge q_0 is somewhere in the cube at coordinates x, y, z with $0 \leq x \leq a, 0 \leq y \leq a$, and $0 \leq z \leq a$. Then the charge on the vertex (i, j, k), where each index can be zero or one, is given by

$$q(i,j,k) = q_0 \cos^2\left\{\frac{\pi}{2} \quad \frac{x}{2} - i\right\} \ \cos^2\left\{\frac{\pi}{2} \quad \frac{y}{2} - j\right\} \ \cos^2\left\{\frac{\pi}{2} \quad \frac{z}{2} - k\right\}$$

This interpolation function is infinitely differentiable, and satisfies the condition of $\sum_{i,j,k} q(i,j,k) = q_0$.

Why it was a bad idea to implement such an algorithm

As shown in [94], the SHAKE algorithm can be viewed as a 1-step nonlinear Gauss-Seidel-Newton iteration in the framework developed by Ortega and Rheiboldt [95]. Local convergence to a solution Q^* is guaranteed precisely when standard Gauss-Seidel iteration converges for the linear system of equations

$$A_n x = b,$$

where $A_n = g'(q(t_n+h))M^{-1}g'(q(t_n))$. If the unconstrained approximation $\overline{q}(t_n+h)$ is sufficiently close to $q(t_n + h)$ (i. e. for sufficiently small time step h), SHAKE iteration converges with an asymptotic rate of convergence of approximately

$$\rho \ (D + L)^{-1}U \ ,$$

where $A_n = L + D + U$ is the splitting of A_n into strictly lower triangular, diagonal, and strictly upper triangular parts and $\rho(\cdot)$ is the spectral radius of a matrix.

The matrix $B_n = g'(q(t_n))M^{-1}g'(q(t_n)) = A_n + \mathcal{O}(h)$ has a very special structure and in some cases can be easily analyzed. In the case of molecules one can consider only the bond length constraints, and it can be shown that the matrix is

nearly constant along solutions, so also the matrix A_n is nearly constant along solutions. It can also be seen that the SHAKE iteration will converge very slowly for chainlike structures unless successive bonds are nearly perpendicular, and degraded convergence would be anticipated for molecules with high connectivity.

For our case of constrained electrostatics it is much harder to analyze the structure of the matrix B_n, so we decided to perform the simulation. The preliminary results have shown that the convergence rate is indeed very poor and the method in the proposed form can not compete with existing methods at all. Apparently, the necessary number of iterations increases strongly with the system size.

A natural improvement to Gauss–Seidel iteration is based on the use of overrelaxation. In this method, we update the iterate at each step by forming a weighted combination of the previous iterate and the Gauss–Seidel step: in essence, we exaggerate each Gauss–Seidel correction by a *relaxation parameter* ω, changing the update of Λ from

$$\Lambda_i \leftarrow \Lambda_i + \Delta\Lambda_i$$

to

$$\Lambda_i \leftarrow \Lambda_i + \omega\Delta\Lambda_i$$

The parameter ω can be a fixed value obtained through some preliminary experiment, or it can be obtained automatically during the integration by a simple adaptive algorithm [94].

This adjustment is essentially free of cost. And it can mean substantial speedups in coordinate resetting. Since the method is just alternative nonlinear equation solver to the SHAKE iteration, the converged numerical solution will be identical (up to roundoff error) to that computed by SHAKE iteration.

For our simulation we have tried this "overrelaxation" method, but still there was not a big improvement in the convergence rate. *Pech gehabt.*

A few words of encouragement

Our artificial Lagrangian and the method of Ryckaert et al [87] can not be considered as an alternative to the existing methods of simulation of charged systems. But there are some good ideas, which we will use in our further attempts. Among them is definitely the initialization scheme for the electric field which will be used unchanged in the new method.

3. Maxwell equations Molecular Dynamics

3.1. Introduction

Despite the numerical ineffiency of the method described at the end of the previous chapter, its development brought to light some useful ideas which will be employed in the following chapter:

1. The method will be devoleped in the framework of the Car–Parrinello method.

2. The discretization method of electromagnetic fields will not be changed as well.

3. The initial solution of the Gauss equation will be implemented along the lines of the previous chapter.

Nevertheless we have to modify the interpolation scheme for the charges and to choose a better constraint function, which will allow constructing a more robust method.

It has been already mentioned in the previous chapter, that the idea of "Maxwell equations Molecular Dynamics" (MEMD) was suggested recently by A. C. Maggs [49, 50]. The development outlined below was done in rather close contact with him. He has made a couple of very important observations, which have deepened our insight into the approach significantly, and contributed to the answer of a number of very important questions:

1. Is Maxwell dynamics the only possible way to propagate the fields? The answer is no; it is also possible to propagate them in a *diffusive* fashion. This has been implemented by means of a Monte Carlo algorithm [49, 50] for a lattice gas of charges.

2. If we restrict attention on Hamiltonian or quasi–Hamiltonian dynamics of the system, and want wave–like propagation of the signal, is then Maxwell–style dynamics the only choice? The answer is a cautious yes; one can show that the Maxwell equations arise in a very natural way if one derives the method along the lines of CP.

3. Is there a contradiction between the Lorentz covariance of the ME, and the strictly nonrelativistic setup of MD? The answer is no; the Lorentz covariance actually has to do with the fact that the value of c is the same in all reference frames. This, however, is not the case here: In our context, c means nothing but the propagation velocity of electromagnetic waves *relative to the discretization lattice* which provides an absolute reference frame (an "ether").

4. Is it necessary to use a large value of c to avoid violation of a quasi–static behavior? The answer is no as long as just static properties of the system in thermal equilibrium are considered — the values of these properties turn out to be completely independent of c.

In what follows, we will essentially re–derive the MEMD algorithm outlined in Ref. [51], and discuss some details of our implementation (Ref. [52]). We will answer to these questions:

1. Is it necessary to apply a thermostat to the system? Ref. [51] claims yes, in order to avoid unwanted conserved quantities. Our belief is no, based upon the fact that the particle dynamics provides lots of nonlinearities into the equations of motion. For more details, see below.

2. How is MEMD implemented? We try to provide somewhat more detail.

3. How does MEMD perform, in particular in comparison with existing methods? In this respect, there is also so far only little information available.

We will present some benchmark results, comparing MEMD with P³M for the same system. It turns out that our implementation of MEMD is quite competitive with P³M for large charge densities, while for very dilute systems P³M is better. However, we believe that our MEMD implementation can be further improved by combining it with a direct evaluation of Yukawa–like forces on short length scales, roughly along the lines as suggested in Ref. [51].

3.2. Lagrangian treatment of dynamics

We are facing the same problem as before: calculate the electric field for a moving charge distribution. As the initial condition of Cauchy problem (time $t = 0$) we choose the exact solution of Gauss' law, i.e. $\mathbf{E}(t = 0) = \mathbf{E}_0$, such that

$$\epsilon_0 \nabla \cdot \mathbf{E}_0 = \rho_0 \equiv \rho(t = 0)$$

where ρ_0 is the initial charge distribution. For the solution at a later time t we use incremental updates

$$\mathbf{E}(t) = \mathbf{E}_0 + \mathbf{E}', \qquad \mathbf{E}'(t = 0) \equiv 0 \tag{3.1}$$

and $\mathbf{E}$ again satisfies Gauss' law

$$\epsilon_0 \nabla \cdot E(t) = \rho(t)$$

In order to find the increment of the electric field $\mathbf{E}'$ we multiply the left- and right-hand side of the Eq. 3.1 by $\epsilon_0 \nabla \cdot$:

$$\nabla \cdot \mathbf{E}' = \frac{1}{\epsilon_0} \left[\rho(t) - \rho_0 \right] \tag{3.2}$$

Trying to solve the last equation directly will lead us to the same problems as before. Therefore we want to investigate the case of a kinematic constraint, i.e. the constraint which is the time derivative of Eq. 3.2:

$$\nabla \cdot \dot{\mathbf{E}}' = \frac{1}{\epsilon_0} \dot{\rho} = -\frac{1}{\epsilon_0} \nabla \cdot \mathbf{j} \tag{3.3}$$

where the charge conservation law $\dot{\rho} + \nabla \cdot \mathbf{j} = 0$ was used. In the construction of the method we will use the constraint

$$\nabla \cdot \left[\epsilon_0 \dot{\mathbf{E}}' + \mathbf{j} \right] = 0 \tag{3.4}$$

The simplistic solution of 3.4

$$\mathbf{E}' = -\frac{1}{\epsilon_0} \int_0^t d\tau \, \mathbf{j}(\tau) \tag{3.5}$$

does not give the right answer. Consider the case of a ring current in a metal where $\mathbf{j} \neq 0$, $\rho = 0$ and $\dot{\rho} = 0$. From Gauss' law we can immediately conclude that for this problem the electric field is zero, $\mathbf{E} \equiv 0$. On the other hand the solution of Eq. 3.5 would give a field, which increases linearly in time. In our problem the energy is bounded, therefore it is an unphysical behavior. Hence we have to introduce another field $\mathbf{E}''$ and the general solution of Eq. 3.4 has the form

$$\mathbf{E}' = -\frac{1}{\epsilon_0} \int_0^t d\tau \, \mathbf{j}(\tau) + \mathbf{E}'' \tag{3.6}$$

Taking the time derivative of last equation and multiplying by ∇, we find:

$$\epsilon_0 \cdot \dot{\mathbf{E}}' + \mathbf{j} = \epsilon_0 \cdot \dot{\mathbf{E}}'' \quad \Rightarrow \quad \nabla \cdot \dot{\mathbf{E}}'' = 0 \tag{3.7}$$

The time evolution of the vector field $\mathbf{E}''$ is given by the following equation

$$\frac{\partial}{\partial t} \left(\nabla \cdot \mathbf{E}'' \right) = 0 \tag{3.8}$$

If we specify $\mathbf{E}'' = 0$ as the initial condition, we obtain

$$\nabla \cdot \mathbf{E}'' = 0 \tag{3.9}$$

for all times $t > 0$. Hence from the Helmholtz theorem [96] we conclude that the vector field $\mathbf{E}''$ is of purely solenoidal nature:

$$\mathbf{E}'' = \nabla \times \boldsymbol{\Theta}$$

As $\mathbf{E}''$ violates the condition $\nabla \times \mathbf{E} = 0$, the general solution of Eq. 3.4 contains a transversal component.

Therefore the most general form of constraint Eq. 3.4 is

$$\epsilon_0 \dot{\mathbf{E}} + \mathbf{j} - \epsilon_0 \nabla \times \dot{\boldsymbol{\Theta}} = 0 \tag{3.10}$$

A simple illustrative example, given in [50], helps to understand the nature of the kinematic constraint. Consider two gears described by the rotation angles ϕ and ψ. Setting the gears in a contact and imposing on them the potential energy $g(\phi)$ and $h(\psi)$ we can write the Lagrangian

$$L = \frac{\dot{\phi}^2}{2} + \frac{\dot{\psi}^2}{2} - g(\phi) - h(\psi) + A(\dot{\phi} + \dot{\psi}) \tag{3.11}$$

where the $\dot{\phi} + \dot{\psi} = 0$ is the rolling constraint.

From this Lagrangian one can simply obtain the equations of motion

$$p_\phi = \dot{\phi} + A \tag{3.12}$$

$$\frac{\partial^2 \phi}{\partial t^2} = -\frac{dg}{d\phi} - \frac{dA}{dt} \tag{3.13}$$

Later we will see, that if we identify the Lagrange multiplier A with the vector potential, these equations are very similar to the equations of electromagnetism. Such a description of electromagnetic fields in terms of rotors (or wheels) was known to FitzGerald in the nineteenth century as a mechanical analogy of the ether [97]. In two dimensions it can be represented as an array of wheels, connected by elastic bands, Fig. 3.1. The spinning of the wheels represented a magnetic field. The elastic bands served to convey motion from one wheel to the next.

In the following we construct an electromechanical model of electromagnetism using the arguments described above. We study a Car–Parrinello–style (CP–style) dynamics, where the equation of motion for $\boldsymbol{\Theta}$ is of second order in time. We thus need to supply an initial condition for $\dot{\boldsymbol{\Theta}}$, too; we choose $\dot{\boldsymbol{\Theta}}(t = 0) = 0$. The most straightforward way to generate a coupled dynamics is to add a kinetic energy term $(1/2)(\epsilon_0/c^2) \int d^3\mathbf{r}\, \dot{\boldsymbol{\Theta}}^2$ to the system Lagrangian; here the prefactor is a mass–like parameter, to be freely chosen in analogy to the electron mass in CP. c will later on turn out to be the speed of light.
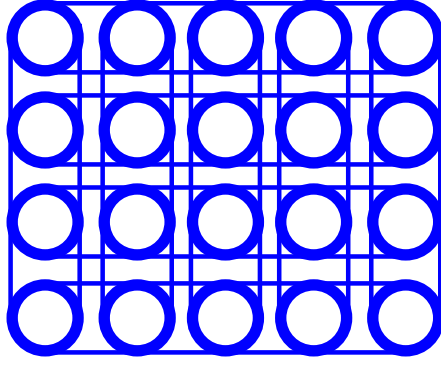
Figure 3.1.: FitzGerald's wheel–and–band model of the ether.

The starting point is the Lagrangian treatment of mechanics with a phenomeno-logical Lagrangian

$$
\begin{aligned}
L = \sum_i \frac{m_i}{2} \mathbf{v}_i^2 - U \\
+ \frac{1}{c^2} \frac{\epsilon_0}{2} \int d^3\mathbf{r}\, \dot{\boldsymbol{\Theta}}^2 - \frac{\epsilon_0}{2} \int d^3\mathbf{r}\, \mathbf{E}^2 \\
+ \int d^3\mathbf{r}\, \mathbf{A}\, \left[\epsilon_0 \dot{\mathbf{E}} - \epsilon_0 \nabla \times \dot{\boldsymbol{\Theta}} + \mathbf{j} \right] ,
\end{aligned} \tag{3.14}
$$

where the Lagrange multiplier $\mathbf{A}$ imposes the kinematic constraint; the particle masses are m_i, their velocities are $\mathbf{v}_i$ and the interparticle potential (of *non–electromagnetic type*) is U. Inserting the charge current of point particles

$$
\mathbf{j} = \sum q_i \delta(\mathbf{r} - \mathbf{r}_i) \mathbf{v}_i \tag{3.15}
$$

into Eq. 3.14 we obtain

$$
\begin{aligned}
L = \sum_i \frac{m_i}{2} \mathbf{v}_i^2 - U + \sum_i q_i \mathbf{A}(\mathbf{r}_i) \cdot \dot{\mathbf{r}}_i \\
+ \frac{1}{c^2} \frac{\epsilon_0}{2} \int d^3\mathbf{r}\, \dot{\boldsymbol{\Theta}}^2 - \frac{\epsilon_0}{2} \int d^3\mathbf{r}\, \mathbf{E}^2 + \int d^3\mathbf{r}\, \mathbf{A}\, \left[\epsilon_0 \dot{\mathbf{E}} - \epsilon_0 \nabla \times \dot{\boldsymbol{\Theta}} \right]
\end{aligned} \tag{3.16}
$$

We find the equations of motion by the usual variational calculus. Variation with respect to $\dot{\mathbf{r}}_i$ gives us

$$
\frac{\partial L}{\partial \dot{r}_i^\alpha} = m_i \dot{r}_i^\alpha + q_i A^\alpha(\mathbf{r}_i) \tag{3.17}
$$

Further we calculate the time derivative of Eq. 3.17

$$
\frac{d}{dt} \frac{\partial L}{\partial \dot{r}_i^\alpha} = m_i \ddot{r}_i^\alpha + q_i \dot{A}^\alpha(\mathbf{r}_i) + q_i \frac{\partial A^\alpha}{\partial r_i^\beta} \dot{r}_i^\beta \tag{3.18}
$$

Variation with respect to $\mathbf{r}_i$ yields

$$\frac{\partial L}{\partial r_i^\alpha} = -\frac{\partial U}{\partial r_i^\alpha} + q_i \dot{r}_i^\beta \frac{\partial A^\beta}{\partial r_i^\alpha} \tag{3.19}$$

Combining Eqs. 3.18 and 3.19 results in the equation of motion for the particle

$$m_i \ddot{r}_i^\alpha = -\frac{\partial U}{\partial r_i^\alpha} - q_i \dot{A}^\alpha + q_i \dot{r}_i^\beta \left(\frac{\partial A^\beta}{\partial r_i^\alpha} - \frac{\partial A^\alpha}{\partial r_i^\beta} \right) \tag{3.20}$$

If we introduce the vector

$$\mathbf{B} = \nabla \times \mathbf{A} \tag{3.21}$$

then the last equation written in vector notation transforms to

$$m_i \ddot{\mathbf{r}}_i = -\frac{\partial U}{\partial \mathbf{r}_i} - q_i \dot{\mathbf{A}} + q_i \, \mathbf{v}_i \times \mathbf{B} \tag{3.22}$$

where we have used the usual rule of vector calculus

$$(\mathbf{v} \times \mathbf{B})^\alpha = \epsilon^{\alpha\beta\gamma} \epsilon^{\gamma\mu\nu} v^\beta \partial_\mu A^\nu = v^\beta \left(\partial_\alpha A^\beta - \partial_\beta A^\alpha \right)$$

In order to find the equations of motion for the electromagnetic fields we variate the Lagrangian density $\mathcal{L}$, which is by definition satisfies $L = \int d^3 \mathbf{r} \, \mathcal{L}$.

Variation in $\dot{\boldsymbol{\Theta}}$ yields

$$\begin{aligned} \frac{\partial \mathcal{L}}{\partial \dot{\boldsymbol{\Theta}}} &= \frac{\epsilon_0}{c^2} \dot{\boldsymbol{\Theta}} - \epsilon_0 \nabla \times \mathbf{A} \\ &= \frac{\epsilon_0}{c^2} \dot{\boldsymbol{\Theta}} - \epsilon_0 \mathbf{B} \end{aligned} \tag{3.23}$$

(note $\int d^3 \mathbf{r} \, \mathbf{A} \cdot (\nabla \times \boldsymbol{\Theta}) = \int d^3 \, \mathbf{r} \boldsymbol{\Theta} \cdot (\nabla \times \mathbf{A})$) and the equation of motion is

$$0 = \frac{d}{dt} \frac{\partial \mathcal{L}}{\partial \dot{\boldsymbol{\Theta}}} = \frac{\epsilon_0}{c^2} \ddot{\boldsymbol{\Theta}} - \epsilon_0 \dot{\mathbf{B}} \tag{3.24}$$

or

$$\frac{1}{c^2} \ddot{\boldsymbol{\Theta}} = \dot{\mathbf{B}} \tag{3.25}$$

The next variation in $\mathbf{E}$ gives us the relation between vectors the $\dot{\mathbf{A}}$ and $\mathbf{E}$:

$$\dot{\mathbf{A}} = -\mathbf{E} \tag{3.26}$$

Therefore Eq. 3.22 can be rewritten in a more appropriate form

$$m_i \ddot{\mathbf{r}}_i = -\frac{\partial U}{\partial \mathbf{r}_i} + q_i \left(\mathbf{E} + \mathbf{v} \times \mathbf{B} \right) \tag{3.27}$$

which we recognize as the sum of the nonelectromagnetic force and the conventional Lorentz force.

Using the natural initial condition $\dot{\boldsymbol{\Theta}}(t = 0) = 0$ we can write the following identity

$$\frac{1}{c^2}\dot{\boldsymbol{\Theta}} = \mathbf{B} \tag{3.28}$$

With that, using the constraint equation, we obtain another Maxwell equation, namely Ampere's law

$$\frac{\partial \mathbf{E}}{\partial t} = c^2 \nabla \times \mathbf{B} - \frac{1}{\epsilon_0}\mathbf{j} \tag{3.29}$$

From relation 3.26 we derive Faraday' law

$$\frac{\partial \mathbf{B}}{\partial t} = \nabla \times \dot{\mathbf{A}} = -\nabla \times \mathbf{E} \tag{3.30}$$

Note that Eq. 3.26 and 3.21 can be considered as a kind of special gauge and the vector $\mathbf{A}$ can be considered as a vector potential. This gauge has the name of temporal or Weyl gauge, in which the scalar electrostatic potential $\phi \equiv 0$ (see [98]).

To summarize: The requirement of local updates, combined with treating the deviations from the BOS (Born–Oppenheimer surface) in the CP manner, has led us in a natural way to standard electromagnetism, where the temporal gauge turns out to be the most appropriate one for our purposes. It should be stressed that this is a consistent non–relativistic setting, where the equations of motion are valid in one particular chosen frame of reference.

From Eq. 3.14 the equation of motion for the field degree of freedom $\mathbf{A}$ can be derived:

$$\frac{\partial^2}{\partial t^2}\mathbf{A} = -c^2 \nabla \times \nabla \times \mathbf{A} + \frac{1}{\epsilon_0}\mathbf{j} \tag{3.31}$$

This is the usual wave equation. Equation 3.22 with 3.31 supply the full description of the coupled system of charged particles plus electromagnetic field.

Note that the same equations of motion can be derived from a slightly different Lagrangian (see [52]), written in terms of $\mathbf{A}$ as the (only) field degree of freedom, which is common practice in electromagnetism [99]. To derive the same equations of motion, namely Eq. 3.20 and 3.31, it is sufficient to consider the Lagrangian

$$\begin{aligned} L = \sum_i \frac{m_i}{2}\mathbf{v}_i^2 - U + \frac{\epsilon_0}{2}\int d^3\mathbf{r}\,\dot{\mathbf{A}}^2 \\ - \frac{\epsilon_0\,c^2}{2}\int d^3\mathbf{r}\,(\nabla \times \mathbf{A})^2 + \int d^3\mathbf{r}\,\mathbf{A}\cdot\mathbf{j} \end{aligned} \tag{3.32}$$

This Lagrangian has a very nice property: Because it is unconstrained, we can easily construct the whole Hamiltonian formalism.

3.3.   Hamiltonian description of the coupled system

As was already mentioned in the previous section, the Hamilton description for our system can be derived from the Lagrangian 3.32 by means of usual Legendre

transformation. In order to construct the Hamiltonian for our system, we have to introduce canonically conjugate momenta. We introduce new variables

$$\mathbf{P}_i = m_i \dot{\mathbf{r}}_i + q_i \mathbf{A}(\mathbf{r}_i) \tag{3.33}$$

$$\mathbf{p}_A = \epsilon_0 \dot{\mathbf{A}} \tag{3.34}$$

where $\mathbf{P}_i$ are the canonically conjugate particle momenta, and $\mathbf{p}_A$ play the role of field momenta. The Hamiltonian has the following form

$$\mathcal{H} = \sum_i \frac{1}{2m_i} [\mathbf{P}_i - q_i \mathbf{A}(\mathbf{r}_i)]^2 + U$$
$$+ \frac{1}{2\epsilon_0} \int d^3\mathbf{r} \, \mathbf{p}_A^2 + \frac{\epsilon_0 c^2}{2} \int d^3\mathbf{r} \, (\nabla \times \mathbf{A})^2 \tag{3.35}$$

and the equations of motion (derived from the latter Hamiltonian) are

$$\frac{d}{dt}\mathbf{r}_i = \frac{1}{m_i} (\mathbf{P}_i - q_i \mathbf{A}(\mathbf{r}_i)) \tag{3.36}$$

$$\frac{d}{dt}P_i^\alpha = -\frac{\partial U}{\partial r_i^\alpha} + \frac{q_i}{m_i} \left[P_i^\beta - q_i A^\beta(\mathbf{r}_i) \right] \frac{\partial A^\beta}{\partial r_i^\alpha} \tag{3.37}$$

$$\frac{d}{dt}\mathbf{A} = \frac{1}{\epsilon_0}\mathbf{p}_A \tag{3.38}$$

$$\frac{d}{dt}\mathbf{p}_A = \sum_i \frac{q_i}{m_i} (\mathbf{P}_i - q_i \mathbf{A}(\mathbf{r}_i)) \, \delta(\mathbf{r} - \mathbf{r}_i) - \epsilon_0 c^2 \nabla \times \nabla \times \mathbf{A} \tag{3.39}$$

3.4. A Liouville like theorem for non-Hamiltonian dynamics

The Hamiltonian dynamics has a couple of very desirable properties: Firstly, it conserves the phase–space volume and the energy, the latter being given by

$$\mathcal{H} = \sum_i \frac{m_i}{2} \dot{\mathbf{r}}_i^2 + U \tag{3.40}$$
$$+ \frac{\epsilon_0}{2} \int d^3\mathbf{r} \, \mathbf{E}^2 + \frac{\epsilon_0 c^2}{2} \int d^3\mathbf{r} \, \mathbf{B}^2.$$

Furthermore, one can show that the total momentum, given by

$$\mathbf{P} = \sum_i m_i \dot{\mathbf{r}}_i + \frac{1}{c^2} \int d^3\mathbf{r} \, \mathbf{E} \times \mathbf{H}, \tag{3.41}$$

where $\mathbf{H} = \epsilon_0 c^2 \mathbf{B}$, is conserved as well. For the proof one can employ the dynamic equations for the particles and fields, and make use of the identity

$$\int d^3\mathbf{r} \, \mathbf{X} \times (\nabla \times \mathbf{X}) = \int d^3\mathbf{r} \, \mathbf{X} \, (\nabla \cdot \mathbf{X}), \tag{3.42}$$

which holds for any vector field $\mathbf{X}$ as long as partial integration with vanishing boundary terms can be applied.

Now we want to modify our equations of motion of particles 3.36 and 3.37. If we omit the magnetic part of the Lorentz force, we destroy the Hamiltonian structure of the system. But on the other hand the particle part of the equations of motion will be easier, which is important for the numerical implementation. The energy, as given by Eq. 3.40, is still conserved.

The new equations of motion have the form

$$\dot{\mathbf{r}}_i = \frac{1}{m_i}\mathbf{p}_i \tag{3.43}$$

$$\dot{\mathbf{p}}_i = -\frac{\partial U}{\partial \mathbf{r}_i} + q_i\mathbf{E}(\mathbf{r}_i) \tag{3.44}$$

$$\dot{\mathbf{A}} = -\mathbf{E} \tag{3.45}$$

$$\dot{\mathbf{E}} = c^2\nabla \times (\nabla \times \mathbf{A}) - \frac{1}{\epsilon_0}\mathbf{j}, \tag{3.46}$$

where $\mathbf{p}_i$ are kinematic momenta of the particles.

We should investigate the phase flow for the modified system. Suppose we are given a system of n ordinary differential equations

$$\dot{\mathbf{x}} = \mathbf{f}(\mathbf{x}), \qquad \mathbf{x} = (x_1, \dots, x_n), \tag{3.47}$$

whose solution may be extended to the whole time axis. Let $\{g^t\}$ be the corresponding group (or the map) of time transformations:

$$g^t(\mathbf{x}) = \mathbf{x} + \mathbf{f}(\mathbf{x})t + \mathcal{O}\left(t^2\right), \qquad (t \to 0) \tag{3.48}$$

It can be shown that if $\nabla\cdot\mathbf{f} = \partial f_i/\partial x_i \equiv 0$ then the one–parameter map g^t conserves the volume in $\mathbf{x}$-space [58].

If we consider Hamilton equations then the right-hand sides of them give a vector field: at each point $(\mathbf{p}, \mathbf{q})$ of phase space there is a $2n$-dimensional vector $(-\partial\mathcal{H}/\partial\mathbf{q}, \partial\mathcal{H}/\partial\mathbf{p})$. Therefore for Hamilton system we have

$$\nabla \cdot \mathbf{f} = \frac{\partial}{\partial p}\left(-\frac{\partial\mathcal{H}}{\partial q}\right) + \frac{\partial}{\partial q}\left(\frac{\partial\mathcal{H}}{\partial p}\right) \equiv 0 \tag{3.49}$$

This is the Liouville theorem: the phase flow conserves the volume in phase space.

Applying the general approach to our system, the divergence of the flow is given by this expression

$$\nabla \cdot \mathbf{f}_{coul} = -\frac{\partial}{\partial\mathbf{A}}\mathbf{E} + \frac{\partial}{\partial\mathbf{E}}\left(c^2\nabla \times (\nabla \times \mathbf{A}) - \frac{1}{\epsilon_0}\mathbf{j}\right)$$
$$+ \frac{\partial}{\partial\mathbf{r}_i}\frac{1}{m_i}\mathbf{p}_i + \frac{\partial}{\partial\mathbf{p}_i}\left(q_i\mathbf{E}(\mathbf{r}_i) - \frac{\partial U}{\partial\mathbf{r}_i}\right) \tag{3.50}$$

From the last equation it is immediately seen that

$$\nabla \cdot \mathbf{f}_{coul} \equiv 0. \tag{3.51}$$

However, momentum conservation does *not* hold for our modified dynamics. The momentum carried away by the electromagnetic waves is not completely balanced by the particle momenta. Rather, we have the relation

$$\sum_i \mathbf{p}_i = \text{const.} + O\left(c^{-2}\right). \tag{3.52}$$

This is not a catastrophe, since momentum conservation is usually only important in studies of dynamics. However, for such calculations one has to use a fairly large value of c anyways, since otherwise the electromagnetic field is not in its quasi–static limit, and the particle trajectories get too much distorted. Furthermore, one must expect that momentum conservation is also violated as a result of the lattice discretization, which breaks the translational invariance of the system.

We now assume that the dynamics is sufficiently nonlinear to make the system ergodic. This seems reasonable for the case of a many–charge system, in particular if the potential U has a strongly repulsive core to facilitate "collisions". We therefore assume that the system has no further important conservation law except for the fact that it stays on the constraint surface, and that the energy $\mathcal{H}$ is conserved.

Hence our map conserves the phase space volume and can be considered as a quasi–Liouville operator, which conserves the measure

$$d\mu = \prod_{\mathbf{r}} d\mathbf{E}_{\mathbf{r}}\, d\mathbf{A}_{\mathbf{r}} \prod_i d\mathbf{r}_i\, d\mathbf{p}_i \tag{3.53}$$

3.5. Thermalized electrodynamics

Making use of the fact that thermodynamic ensembles are equivalent in the large–system limit, we can emply the canonical ensemble. Coupling the particles with a Gaussian noise, we write equations of motion for the thermalized electrodynamics

$$\dot{\mathbf{r}}_i = \frac{1}{m_i}\mathbf{p}_i \tag{3.54}$$

$$\dot{\mathbf{p}}_i = -\frac{\partial U}{\partial \mathbf{r}_i} + q_i \mathbf{E}(\mathbf{r}_i) - \frac{\zeta}{m_i}\mathbf{p}_i + \mathbf{f}_i \tag{3.55}$$

$$\dot{\mathbf{A}} = -\mathbf{E} \tag{3.56}$$

$$\dot{\mathbf{E}} = c^2 \nabla \times (\nabla \times \mathbf{A}) - \frac{1}{\epsilon_0}\mathbf{j}, \tag{3.57}$$

where ζ is the particle friction constant, and $\mathbf{f}_i$ is a random force satisfying the standard fluctuation–dissipation theorem:

$$\left\langle f_i^{\alpha}(t) f_j^{\beta}(t') \right\rangle = 2\zeta k_B T \delta_{ij}\delta_{\alpha\beta}\delta(t - t'), \tag{3.58}$$

where α and β denote Cartesian indices.

With $\beta = 1/(k_B T)$, where k_B is Boltzmann's constant and T the absolute temperature, we may therefore write the partition function as

$$
\begin{aligned}
\mathcal{Z} \;=\; & \int d\mathbf{r}_i \int d\mathbf{p}_i \int \mathcal{D}\mathbf{A} \int \mathcal{D}\mathbf{E} \exp\left(-\beta\mathcal{H}\right) \\
& \times \delta\left(\nabla \cdot \mathbf{E} - \frac{1}{\epsilon_0}\rho\right),
\end{aligned}
\tag{3.59}
$$

where $\mathcal{H}$ is given by Eq. 3.40. It is now straightforward to integrate out the momenta, the $\mathbf{A}$ field, and the transversal component of the $\mathbf{E}$ field. The integration over the longitudinal component of $\mathbf{E}$ cancels with the delta function, such that the only remaining degrees of freedom are the particle coordinates, for whose potential of mean force we hence find

$$
\mathcal{H}_{conf} = U + \frac{\epsilon_0}{2}\int d^3\mathbf{r}\,\mathbf{E}^2;
\tag{3.60}
$$

here $\mathbf{E}$ is nothing but the solution of the standard electrostatic problem

$$
\nabla \cdot \mathbf{E} \;=\; \frac{1}{\epsilon_0}\rho
\tag{3.61}
$$
$$
\nabla \times \mathbf{E} \;=\; 0,
\tag{3.62}
$$

i. e. the Coulomb field. Inserting this field into Eq. 3.60, we find the standard Coulomb Hamiltonian,

$$
\mathcal{H}_{conf} = U + \frac{1}{2}\frac{1}{4\pi\epsilon_0}\int d^3\vec{r}\int d^3\vec{r}'\,\frac{\rho(\vec{r})\rho(\vec{r}')}{|\vec{r}-\vec{r}'|}.
\tag{3.63}
$$

This demonstrates that the particles behave statistically in the same way as if they would directly interact Coulombically.

3.6.   Discretized electromagnetic Lagrangian

For implementation on the computer, the equations need to be discretized with respect to both space and time. For the moment, we will only consider the spatial discretization, and consider time still as a continuous variable. The issue of time discretization will be discussed later.

The Lagrangian Eq. 3.32 is simple enough in order to start the discretization. It involves only the vector potential, velocities and coordinates of charged particles. We consider a domain of physical space as being an affine space and divide it into subdomains of contiguous cells of cubic shape. The charges live on the vertices of our lattice which has the spacing a. The electric fields $E(l)$ and vector potentials $A(l)$ live on the edges or links and are aligned with them. We need also the operator $\nabla \times$. It gives the vector, which lives on the faces of the cube or on the
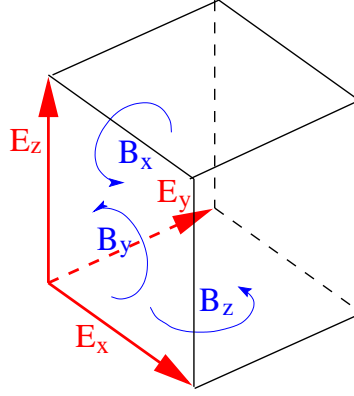
Figure 3.2.: Spatial elements of a cell complex. The electric field is aligned to the edges of the cell, $\mathbf{B}$ is the plaquette variable, $\mathbf{B} = \nabla \times \mathbf{A}$, where the operation of $\nabla \times$ understood in the discretized sense.

plaquettes, Fig. 3.2. Within the framework of the discretized electromagnetic fields the counterpart of the Lagrangian 3.32 has the form

$$
\begin{aligned}
L = &\sum_i \frac{m_i}{2} \dot{\mathbf{r}}_i^2 + \frac{\epsilon_0}{2} a^3 \sum_l \dot{A}(l)^2 \\
&- \frac{\epsilon_0}{2} c^2 a^3 \sum_p \left[(\nabla \times \mathbf{A})(p) \right]^2 + a^3 \sum_l A(l) j(l)
\end{aligned}
\tag{3.64}
$$

where we have discarded the trivial interparticle potential.

Let us calculate the analogies of derivatives on the lattice sites and links. We have to replace derivatives with finite differences.

$$
\frac{\partial L}{\partial A(l)} = a^3 j(l) - \frac{1}{2} \epsilon_0 c^2 a^3 \frac{\partial}{\partial A(l)} \sum_p \left[(\nabla \times \mathbf{A})(p) \right]^2
\tag{3.65}
$$

Let p^1, p^2, p^3 and p^4 be the four plaquettes which encircle the link l as shown on Fig. 3.3. Using the usual rules of vector analysis, the *curl*-operator can be written as

$$
\nabla \times \mathbf{A} = \begin{pmatrix} \partial_x \\ \partial_y \\ \partial_z \end{pmatrix} \times \begin{pmatrix} A_x \\ A_y \\ A_z \end{pmatrix} = \begin{pmatrix} \partial_y A_z - \partial_z A_y \\ \partial_z A_x - \partial_x A_z \\ \partial_x A_y - \partial_y A_x \end{pmatrix}
\tag{3.66}
$$

Note that the $\nabla \times \mathbf{A}$ which lies on the plaquette p_1 is a vector with only one nonzero component in y-direction. Therefore the discretized analog of the *curl* operator will
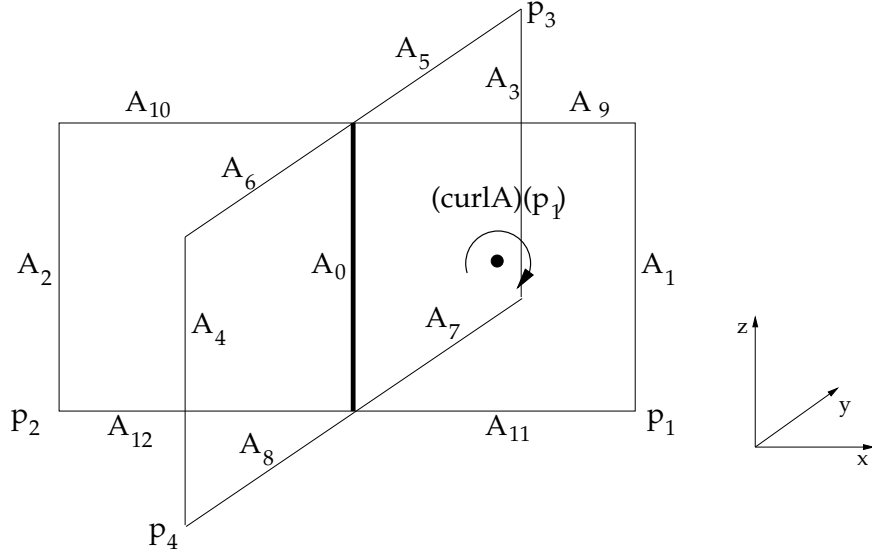
Figure 3.3.: Calculation of the discretized curl operator.

be

$$(\nabla \times \mathbf{A})\,(p_1) \;=\; \frac{1}{a}\left[A_9 - A_{11} - A_1 + A_0\right] \tag{3.67}$$

$$(\nabla \times \mathbf{A})\,(p_2) \;=\; \frac{1}{a}\left[A_{10} - A_{12} - A_0 + A_2\right] \tag{3.68}$$

$$(\nabla \times \mathbf{A})\,(p_3) \;=\; \frac{1}{a}\left[A_3 - A_0 - A_5 + A_7\right] \tag{3.69}$$

$$(\nabla \times \mathbf{A})\,(p_4) \;=\; \frac{1}{a}\left[A_0 - A_4 - A_6 + A_8\right] \tag{3.70}$$

From the last equations it is simple algebra to obtain finite differences of $\nabla \times \mathbf{A}$ on the lattice:

$$
\begin{aligned}
\frac{\partial}{\partial A_0} \sum_p \left[(\nabla \times \mathbf{A})\,(p)\right]^2 &= \\
&= \frac{2}{a^2}\left[A_9 - A_{11} - A_1 + A_0 - A_{10} + A_{12} + A_0 - A_2\right. \\
&\quad \left. - A_3 + A_0 + A_5 - A_7 + A_0 - A_4 - A_6 + A_8\right] = \\
&= \frac{2}{a^2}\left[4A_0 - A_1 - A_2 - A_3 - A_4 + A_5\right. \\
&\quad \left. - A_6 - A_7 + A_8 + A_9 - A_{10} - A_{11} + A_{12}\right]
\end{aligned}
\tag{3.71}
$$

On the other hand the z-component of $\nabla \times \nabla \times A$ on the link 0 is

$$
\begin{aligned}
\left[\nabla \times (\nabla \times \mathbf{A})\right](0) &= \frac{1}{a} \left[(\nabla \times \mathbf{A})(p_1) - (\nabla \times \mathbf{A})(p_2) \right. \\
&\quad \left. - (\nabla \times \mathbf{A})(p_3) + (\nabla \times \mathbf{A})(p_4) \right] \\
&= \frac{1}{a^2} \left[4A_0 - A_1 - A_2 - A_3 - A_4 + A_5 \right. \\
&\quad \left. - A_6 - A_7 + A_8 + A_9 - A_{10} - A_{11} + A_{12} \right]
\end{aligned}
\tag{3.72}
$$

Comparing the Eq. 3.71 and 3.72 we come to the conclusion that they are equal. Therefore the following is valid

$$
\frac{\partial}{\partial A(l)} \sum_p \left[(\nabla \times \mathbf{A})(p) \right]^2 \equiv 2 \left[\nabla \times (\nabla \times \mathbf{A}) \right](l)
\tag{3.73}
$$

$$
\frac{\partial L}{\partial A(l)} = a^3 j(l) - \epsilon_0 c^2 a^3 \left[\nabla \times (\nabla \times \mathbf{A}) \right](l)
\tag{3.74}
$$

$$
\frac{\partial L}{\partial \dot{A}(l)} = \epsilon_0 a^3 \dot{A}(l)
\tag{3.75}
$$

Combining the last two equations we obtain the wave equation for the vector field on the link

$$
\frac{\partial^2}{\partial t^2} A(l) = -c^2 \left[\nabla \times (\nabla \times \mathbf{A}) \right](l) + \frac{1}{\epsilon_0} j(l)
\tag{3.76}
$$

If we set $E(l) = -A(l)$ we obtain the equations of motion in the "grid temporal gauge"

$$
\dot{A}(l) \;=\; -E(l)
\tag{3.77}
$$

$$
\dot{E}(l) \;=\; c^2 \left[\nabla \times (\nabla \times \mathbf{A}) \right](l) - \frac{1}{\epsilon_0} j(l)
\tag{3.78}
$$

3.6.1. Coupling the matter with the discretized electromagnetism

We have not yet specified the interpolation procedure for the charge currents. Therefore let us consider the coupling term in the Lagrangian. At first we will pursue the "vakonomic" approach [100], which is particularly suitable for the case of continous time variable and later we will switch our attention to the case of discrete time step.

Current assignment for continuous time

The particle motion generates currents on the surrounding links. We use a linear interpolation scheme for $\mathbf{j}$, where the current is distributed onto the twelve links which surround the cube in which the particle is. The assignment scheme uses

the fact that the charge interpolation scheme, or the charge assignment scheme, in the case of linear interpolation factorizes in the product of three one-dimensional functions. If we label the nodes of the unit cube by triples of numbers (i, j, k), then the charge assignment scheme may be written as

$$U_{ijk}(\xi, \eta, \zeta) = w_i(\xi)w_j(\eta)w_k(\zeta) \tag{3.79}$$

and the charge assigned to node (i, j, k), where $i, j, k = 0$ or 1, is

$$Q_{ijk} = qw_i(\xi)w_j(\eta)w_k(\zeta) \tag{3.80}$$

where $w_0(x) = 1 - x/a$, $w_1(x) = x/a$ and (ξ, η, ζ) is the displacement of the particle from the element corner $(0, 0, 0)$ (see Table 3.6.1). Inspection of Eq. 3.80 reveals

Table 3.1.: Fraction of the particle in each of the eight corners of cell

Weighting fraction	Cell corner
$(1 - \xi)\,(1 - \eta)\,(1 - \zeta)$	i, j, k
$\xi\,(1 - \eta)\,(1 - \zeta)$	$i + 1, j, k$
$(1 - \xi)\,\eta\,(1 - \zeta)$	$i, j + 1, k$
$(1 - \xi)\,(1 - \eta)\,\zeta$	$i, j, k + 1$
$(1 - \xi)\,\eta\,\zeta$	$i, j + 1, k + 1$
$\xi\,(1 - \eta)\,\zeta$	$i + 1, j, k + 1$
$\xi\,\eta\,(1 - \zeta)$	$i + 1, j + 1, k$
$\xi\,\eta\,\zeta$	$i + 1, j + 1, k + 1$

the assignment scheme to be the same as area weighting [43, 101].

Now we formally define the currents on the links of a cell as following ansatz

$$j_x(j, k) \equiv j(i, j, k \to i + 1, j, k) = \frac{q}{a^3} v_x w_j(\eta)w_k(\zeta) \tag{3.81a}$$

$$j_y(i, k) \equiv j(i, j, k \to i, j + 1, k) = \frac{q}{a^3} v_y w_i(\xi)w_k(\zeta) \tag{3.81b}$$

$$j_z(i, j) \equiv j(i, j, k \to i, j, k + 1) = \frac{q}{a^3} v_z w_i(\xi)w_j(\eta) \tag{3.81c}$$

where $\mathbf{v} = (v_x, v_y, v_z)$ is the velocity of the point charge q.

This assignment scheme can be viewed as a two–dimensional interpolation of the current (see Fig. 3.4).

Let us check the charge conservation for this scheme. Using Eq. 3.80 for the time derivative we can write

$$\frac{\partial}{\partial t}\rho(i, j, k) =$$

$$\frac{q}{a^3} \quad -\frac{\partial \xi}{\partial t}w_j(\eta)w_k(\zeta) - \frac{\partial \eta}{\partial t}w_i(\xi)w_k(\zeta) - \frac{\partial \zeta}{\partial t}w_i(\xi)w_j(\eta) \quad =$$

$$-\frac{q}{a^4}\left\{v_x w_j(\eta)w_k(\zeta) + v_y w_i(\xi)w_k(\zeta) + v_z w_i(\xi)w_j(\eta)\right\} \tag{3.82}$$
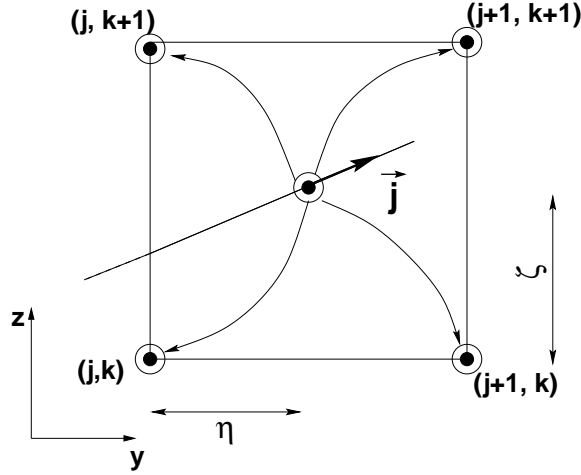
Figure 3.4.: The current assignment scheme as the interpolation of the current in two dimensions. The cut of the cell is in the yz-plane.

On the other hand the divergence of the current in corner (i, j, k) has the following form

$$
\begin{aligned}
\left[\nabla \cdot \mathbf{j}\right](i, j, k) &= \frac{1}{a} \left\{ j(i, j, k \rightarrow i+1, j, k) + \right. \\
&\quad + j(i, j, k \rightarrow i, j+1, k) + j(i, j, k \rightarrow i, j, k+1) \left. \right\} = \\
&= \frac{q}{a^4} \left\{ v_x w_j(\eta) w_k(\zeta) + v_y w_i(\xi) w_k(\zeta) + v_z w_i(\xi) w_j(\eta) \right\}
\end{aligned}
\tag{3.83}
$$

Therefore we have an exact charge conservation scheme at each vertex of the lattice.

Derivation from vakonomic approach

As we have already mentioned, there exist two approaches of obtaining of the equations of motions. The first one is the vakonomic method [100], which considers the Lagrange multiplier as an additional degree of freedom. We have already used this method in order to derive the equations of motion in the continuum case. And now we focus on the discrete equations. On the other hand the principle of virtual work, or D'Alembert principle of imposing nonholonomic constraints, can also give the equations of motion. In general, for a nonholonomic constraint, they are not equivalent [102].

In order to derive the "discretized Lorentz force" we consider the case of one charge and reduced Lagrangian

$$
\lambda = \frac{1}{q} a^3 \sum_l A(l) j(l)
\tag{3.84}
$$

This is the normalized interaction term. Written explicitly in terms of links it is

transformed to

$$
\begin{aligned}
\lambda = \; & A(0,0,0;1,0,0)v_x w(y,0)w(z,0) \\
& + A(0,1,0;1,1,0)v_x w(y,1)w(z,0) \\
& + A(0,0,1;1,0,1)v_x w(y,0)w(z,1) \\
& + A(0,1,1;1,1,1)v_x w(y,1)w(z,1) \\
& + A(0,0,0;0,1,0)v_y w(x,0)w(z,0) \\
& + A(1,0,0;1,1,0)v_y w(x,1)w(z,0) \\
& + A(0,0,1;0,1,1)v_y w(x,0)w(z,1) \\
& + A(1,0,1;1,1,1)v_y w(x,1)w(z,1) \\
& + A(0,0,0;0,0,1)v_z w(x,0)w(y,0) \\
& + A(1,0,0;1,0,1)v_z w(x,1)w(y,0) \\
& + A(0,1,0;0,1,1)v_z w(x,0)w(y,1) \\
& + A(1,1,0;1,1,1)v_z w(x,1)w(y,1)
\end{aligned}
\tag{3.85}
$$

where we have slightly changed the indexing of the interpolation function w. Let us consider the x-direction. The last two can be made by analogy. So

$$
\begin{aligned}
\frac{\partial \lambda}{\partial x} = \frac{1}{a} \big\{ & -A(0,0,0;0,1,0)v_y w(z,0) \\
& +A(1,0,0;1,1,0)v_y w(z,0) \\
& -A(0,0,1;0,1,1)v_y w(z,1) \\
& +A(1,0,1;1,1,1)v_y w(z,1) \\
& -A(0,0,0;0,0,1)v_z w(y,0) \\
& +A(1,0,0;1,0,1)v_z w(y,0) \\
& -A(0,1,0;0,1,1)v_z w(y,1) \\
& +A(1,1,0;1,1,1)v_z w(y,1) \big\}
\end{aligned}
\tag{3.86}
$$

$$
\begin{aligned}
\frac{d}{dt}\frac{\partial\lambda}{\partial\dot{x}} &= \frac{d}{dt}\{A(0,0,0;1,0,0)w(y,0)w(z,0)\\
&\quad +A(0,1,0;1,1,0)w(y,1)w(z,0)\\
&\quad +A(0,0,1;1,0,1)w(y,0)w(z,1)\\
&\quad +A(0,1,1;1,1,1)w(y,1)w(z,1)\}\\
&= \Big\{\dot{A}(0,0,0;1,0,0)w(y,0)w(z,0)\\
&\quad +\dot{A}(0,1,0;1,1,0)w(y,1)w(z,0)\\
&\quad +\dot{A}(0,0,1;1,0,1)w(y,0)w(z,1)\\
&\quad +\dot{A}(0,1,1;1,1,1)w(y,1)w(z,1)\Big\}\\
&\quad +\frac{1}{a}A(0,0,0;1,0,0)\left[-v_yw(z,0)-v_zw(y,0)\right]\\
&\quad +\frac{1}{a}A(0,1,0;1,1,0)\left[+v_yw(z,0)-v_zw(y,1)\right]\\
&\quad +\frac{1}{a}A(0,0,1;1,0,1)\left[-v_yw(z,1)+v_zw(y,0)\right]\\
&\quad +\frac{1}{a}A(0,1,1;1,1,1)\left[+v_yw(z,1)+v_zw(y,1)\right]
\end{aligned}
\tag{3.87}
$$

After an easy but tedious algebra and using the equality $\dot{A}(l) = -E(l)$ we can write the Euler–Lagrange equation

$$
\begin{aligned}
\frac{d}{dt}\frac{\partial\lambda}{\partial\dot{x}}-\frac{\partial\lambda}{\partial x} &= -\{E(0,0,0;1,0,0)w(y,0)w(z,0)\\
&\quad +E(0,1,0;1,1,0)w(y,1)w(z,0)\\
&\quad +E(0,0,1;1,0,1)w(y,0)w(z,1)\\
&\quad +E(0,1,1;1,1,1)w(y,1)w(z,1)\}\\
&\quad +\frac{1}{a}v_yw(z,0)\left[A(0,1,0;1,1,0)-A(0,0,0;1,0,0)\right.\\
&\quad +A(0,0,0;0,1,0)-A(1,0,0;1,1,0)]\\
&\quad +\frac{1}{a}v_yw(z,1)\left[A(0,1,1;1,1,1)-A(0,0,1;1,0,1)\right.\\
&\quad -A(1,0,1;1,1,1)+A(0,0,1;0,1,1)]\\
&\quad +\frac{1}{a}v_zw(y,0)\left[A(0,0,1;1,0,1)-A(0,0,0;1,0,0)\right.\\
&\quad -A(1,0,0;1,0,1)+A(0,0,0;0,0,1)]\\
&\quad +\frac{1}{a}v_zw(y,1)\left[A(0,1,1;1,1,1)-A(0,1,0;1,1,0)\right.\\
&\quad -A(1,1,0;1,1,1)+A(0,1,0;0,1,1)]
\end{aligned}
\tag{3.88}
$$

The expression in the first brackets of the latter equation can be understood as an

average of the x-component of the electric force over the grid cell:

$$F_x^e = -q\left\{E(0,0,0;1,0,0)w(y,0)w(z,0) + E(0,1,0;1,1,0)w(y,1)w(z,0)\right.$$
$$\left. + E(0,0,1;1,0,1)w(y,0)w(z,1) + E(0,1,1;1,1,1)w(y,1)w(z,1)\right\} \quad (3.89)$$

Analogous, this can be written for the y ans z components of the electric force:

$$\begin{aligned}
F_y^e &= -q\left\{E(0,0,0;0,1,0)w(x,0)w(z,0)\right. & (3.90)\\
&\quad + E(1,0,0;1,1,0)w(x,1)w(z,0)\\
&\quad + E(0,0,1;0,1,1)w(x,0)w(z,1)\\
&\quad \left. + E(1,0,1;1,1,1)w(x,1)w(z,1)\right\}\\
F_z^e &= -q\left\{E(0,0,0;0,0,1)w(y,0)w(x,0)\right. & (3.91)\\
&\quad + E(0,1,0;0,1,1)w(y,1)w(x,0)\\
&\quad + E(1,0,0;1,0,1)w(y,0)w(x,1)\\
&\quad \left. + E(1,1,0;1,1,1)w(y,1)w(x,1)\right\}
\end{aligned}$$

The second part of the equation 3.88 can be rewritten by means of the discretized *curl*-operator as

$$\begin{aligned}
F_x^m/q = \frac{1}{a}\left\{v_y\left[w(z,0)B_z(0) + w(z,1)B_z(1)\right]\right.\\
\left. - v_z\left[w(y,0)B_y(0) + w(y,1)B_y(1)\right]\right\}
\end{aligned} \quad (3.92)$$

where $B_z(i)$ is the z-component of the magnetic field, lying in the $z = i$ plaquette; $B_y(i)$ is the y-component of the magnetic field, lying in the $y = i$ plaquette, and $i = 0, 1$. This is the discretized analog of the usual magnetic part of the Lorentz force.

Magnetic self–force

Due to the finite grid spacing, we have to expect that the lattice structure of our system leads to artefacts in the magnetic force calculation. In order to check this, we simulate a wire with a current in a box (see Fig. 3.5). Measuring the force which acts on the charged particles we can measure the total force on the wire.

The resulting force is given in the Fig. 3.6. It is clearly seen that the magnetic self-force vanishes only in the situation of perfect symmetry – the wire traverses through the center of the grid cell.

3.6.2. Principle of virtual work

There is an alternative approach of the treatment of constrained systems. Our kinematic constraint 3.4 can be transformed to the following form

$$d\mathbf{E} + \frac{1}{\epsilon_0}\mathbf{j}dt - \nabla \times d\mathbf{\Theta} = 0 \quad (3.93)$$

This is an example of a nonholonomic constraint [103]. One can consider the constraints as certain additional external forces, namely the forces which have to be exerted by the constraints in order to compel the system to fulfill the kinematical conditions. These forces must satisfy a certain principle. It is presented as an axiom of mechanics which is not derivable from the other basic axioms. It has the name of D'Alembert and is typically stated as follows: The work done by the forces of constraint is zero on motions allowed by the constraint. One can say that the Principle of Virtual Work is satisfied by the curve c, if there exists external forces F_i^c which do no work on the constraints and are such that

$$\frac{d}{dt} \; \frac{\partial L}{\partial \dot{q}^i} \; - \frac{\partial L}{\partial q^i} = F_i^c \tag{3.94}$$

where L is the Lagrange function of the mechanical system.

This principle is more elementary than the variational principles because it requires no integration with respect to the time. It uses the notion of "virtual displacements" and is of great use in Mechanics [104]. It will serve for us as other derivation of the equations of motion.

Since the sources of the electromagnetic field are charges and these are scalar quantities, it follows that all the integral quantities of electromagnetism are scalars. These are charge, charge flux, electric and magnetic fluxes, electric and magnetic voltages. The laws of electromagnetism, when one uses integral quantities, are all relation between scalar variables and then they are expressed by scalar equations [105]. For example, the Faraday's electromagnetic induction law has the
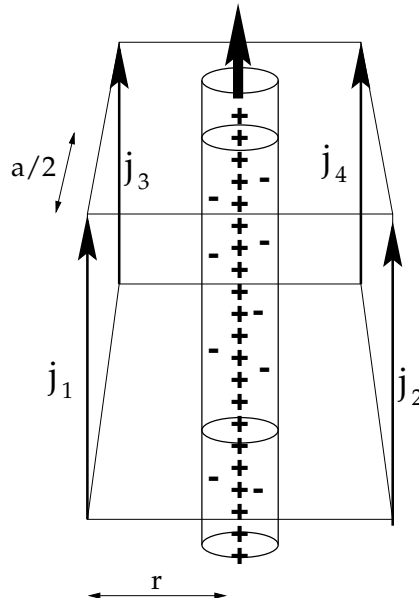

Figure 3.5.: Electric wire placed in the grid cell. Positive particles are moving with velocity v in z-direction, generating currents on the links of the grid cube. They interact with each other according to the Bio-Savart Law.
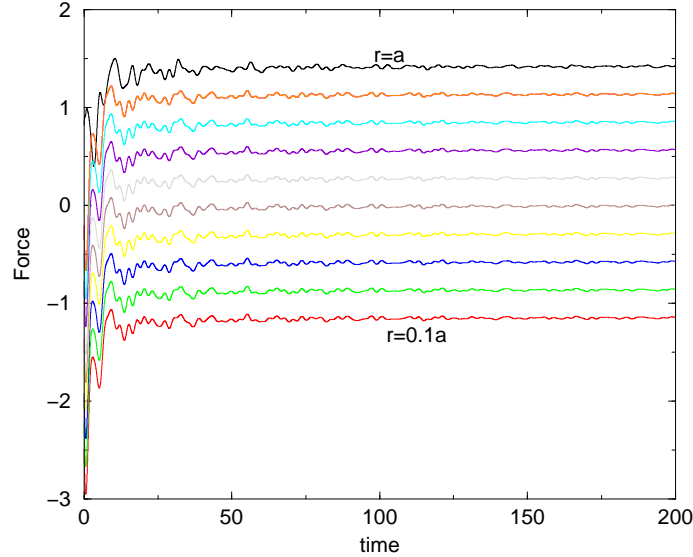
Figure 3.6.: Magnetic self-force as a function of the wire displacement in the grid cell. Time is measured in Lennard-Jones units, force is measured in units of $q^2/(\epsilon_0 a^2)$, where a is the grid-spacing. The lowest curve corresponds to the wire close to the left boundary of the grid cell $r = 0.1a$, and the highest curve is placed on the right boundary of the grid cell $r = 1a$; $c = 1$, $L = 11$.

following form

$$\int_{\partial A} \mathbf{E} \cdot d\mathbf{l} = - \iint_A \frac{\partial}{\partial t} \mathbf{B} \cdot d\mathbf{A} \tag{3.95}$$

where A and ∂A are correspondingly surface area and its boundary. At the same time this law can be rewritten as

$$\mathcal{E}[\partial \mathbf{A}] = -\frac{\partial}{\partial t} \Psi[\mathbf{A}] \tag{3.96}$$

where $\mathcal{E}$ is the electromotive force and Ψ is the magnetic flux; i.e. the electromotive force impulse (or the electric voltage) referred to the boundary of a surface endowed with inner orientation during a time interval is opposite to the magnetic flux variation across the surface in the same interval.

Therefore following [106] we can define the electric state of the system by the electric flux map

$$\phi : \mathcal{C}_2(M) \to R \tag{3.97}$$

which associates a real number, the electric flux, to any surface in manifold M.

Although the electric flux map 3.97 determines completely the fluxes in the system, it does not give the local value of the electric induction field, which is needed for the calculation of the electric energy. In this context fields can be considered as secondary quantities obtained by a kind of interpolation. The properties of

that interpolation process are not trivial. In the case of the electric induction fields, the selection of a set of facets of $C_2(M)$ is involved, as well as an accuracy and convergence analysis. The interpolation with Whitney facet elements is an example of such an interpolation [107]. Taking into account that in our coupled system charges can also change fields we can write the electric induction field $\mathbf{D}$ as a function of electric flux and the positions of the charges

$$\mathbf{D} = \mathbf{D}(\phi, \mathbf{r}_i) \tag{3.98}$$

Since fluxes and particle positions are independent of each other, they are suitable variables for the definition of the energy functional of the coupled electromagnetic system. One has

$$\Psi(\phi, \mathbf{r}_i) = \int \rho^{\Psi} \left(\mathbf{D}(\phi, \mathbf{r}_i) \right) \, d^3\mathbf{r} \tag{3.99}$$

where the energy density $\rho^{\Psi} \left(\mathbf{D}(\phi, \mathbf{r}_i) \right)$ depends on the map ϕ through the interpolated field $\mathbf{D}$. According to the principle of virtual work, the definition of forces follows now from the variation $\delta\Psi$ of those energy functionals and the factorization of the result thereof under the form of a mechanical work monomial $\mathbf{f} \cdot \delta\mathbf{x}$.

Let us now consider the virtual displacement of the charge. Under this displacement only the interpolated charges on the eight nodes of the surrounding cube are changed. Therefore only that cube gives contribution to the force onto the particle. We consider the changes of the fields in the unit cube M, Fig. 3.7. Let $O \equiv (0,0,0)$,
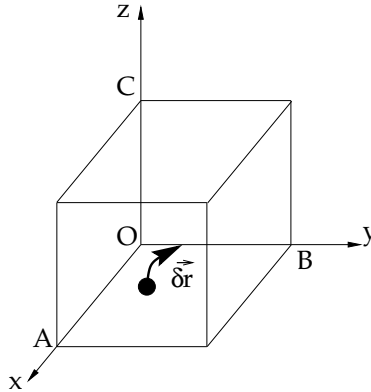

Figure 3.7.: Theoretical setup for the calculation of the force using the virtual work principle.

$A \equiv (1,0,0)$, $B \equiv (0,1,0)$ and $C \equiv (0,0,1)$ be four particular points of the cube M. Given a set of points O, A, B, C, an affine combination is defined to be the point [108]:

$$\alpha_0 \, O + \alpha_1 \, A + \alpha_2 \, B + \alpha_3 \, C \tag{3.100}$$

where the α_i are scalars and

$$\alpha_0 + \alpha_1 + \alpha_2 + \alpha_3 = 1 \tag{3.101}$$

Then the point $\mathbf{r}$ inside a cube can be written in barycentric coordinates as

$$\mathbf{r} = (1 - \alpha - \beta - \gamma)O + \alpha A + \beta B + \gamma C \tag{3.102}$$

Let ϕ_x, ϕ_y and ϕ_z be the electric fluxes obtained by applying the electric flux map to the particular parallelogram facets OBC, OCA and OAB of M. If the cube is small enough, the induction field $\mathbf{D}$, to first approximation, is the uniform vector field that satisfies

$$\phi_x = (\mathbf{s} \times \mathbf{t}) \cdot \mathbf{D}, \quad \phi_y = (\mathbf{t} \times \mathbf{r}) \cdot \mathbf{D}, \quad \phi_z = (\mathbf{r} \times \mathbf{s}) \cdot \mathbf{D} \tag{3.103}$$

where $\mathbf{r} = A - O$, $\mathbf{s} = B - O$ and $\mathbf{t} = C - O$ are three linearly independent vectors.

By inverting these relations one finds the expression for the interpolated induction field

$$\mathbf{D} = \frac{\mathbf{r}}{V}\phi_x + \frac{\mathbf{s}}{V}\phi_y + \frac{\mathbf{t}}{V}\phi_z \tag{3.104}$$

where V is the volume of the cube:

$$V = (\mathbf{r} \times \mathbf{s}) \cdot \mathbf{t} = (\mathbf{s} \times \mathbf{t}) \cdot \mathbf{r} = (\mathbf{t} \times \mathbf{r}) \cdot \mathbf{s} \tag{3.105}$$

The variation of $\mathbf{D}$ can be obtained by the variation of the fluxes

$$\delta \mathbf{D} = \frac{\mathbf{r}}{V}\delta\phi_x + \frac{\mathbf{s}}{V}\delta\phi_y + \frac{\mathbf{t}}{V}\delta\phi_z \tag{3.106}$$

In order to find the variations of fluxes we can use Gauss' law in integral form [105]

$$\delta\phi_x[\partial V] = \delta Q_x[V], \quad \delta\phi_y[\partial V] = \delta Q_y[V], \quad \delta\phi_z[\partial V] = \delta Q_z[V] \tag{3.107}$$

where δQ_x, δQ_y and δQ_z are the changes of the charge through the facets (or plaquettes) OBC, OCA and OAB respectively.

The general expression for the energy density in the continuum involves two vectors – the electric field intensity $\mathbf{E}$ and the electric induction field $\mathbf{D}$. Though they are both vectors, they have a completely different origin. It was Maxwell himself who advised to be very careful in assigning a certain physical quantity to a mathematical object. As it turns out, the mathematical images of $\mathbf{D}$ and $\mathbf{E}$ are different from each other. Using the language of differential forms, one can say that $\mathbf{D}$ is a 2–form and $\mathbf{E}$ is a 1–form. For our simple case of a cubic lattice and vacuum conditions we can express this difference by placing the $\mathbf{E}$ field on the links of the primary lattice and $\mathbf{D}$ on the plaquettes of the dual lattice [109], Fig. 3.8.

The expression for the density energy in the continuum has the form

$$\rho = \frac{\mathbf{E} \cdot \mathbf{D}}{2} \tag{3.108}$$

and it has the same form in the lattice theory [110]. In the situation of no dielectric matter we can write

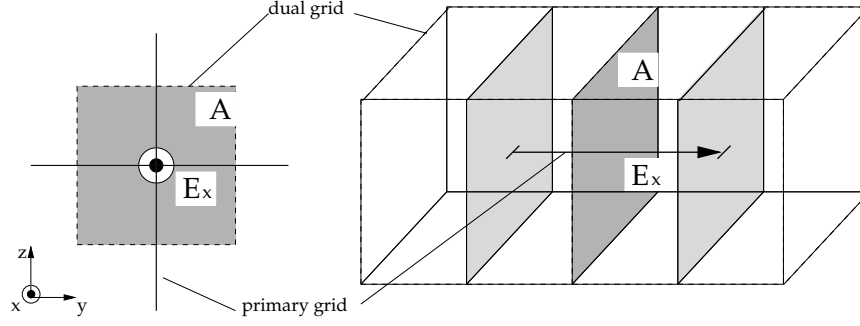$$\Psi = V\frac{|\mathbf{D}|^2}{2\epsilon_0} \tag{3.109}$$

Figure 3.8.: Calculation of the discrete electric energy. A is the area on the dual lattice, and E_x is the electric field on the link of the primary lattice.

Therefore the variation of the energy functional is given by this relation

$$\delta\Psi = \frac{V}{\epsilon_0}\mathbf{D}\cdot\delta\mathbf{D} = \mathbf{E}\cdot(\mathbf{r}\delta\phi_x + \mathbf{s}\delta\phi_y + \mathbf{t}\delta\phi_z) \tag{3.110}$$

Finally the force acting on the charge is given by

$$\mathbf{F} = -\mathbf{E}\left[\mathbf{r}\frac{\delta Q_x}{\delta x} + \mathbf{s}\frac{\delta Q_y}{\delta y} + \mathbf{t}\frac{\delta Q_z}{\delta z}\right] \tag{3.111}$$

The calculation of the force depends on the calculation of the charge differences. This is directly connected to the choice of the current assignment scheme. Because the variations of positions are infinitesimal, for the linear interpolation scheme the forces are given by Eqs. 3.89 – 3.91.

3.6.3. Current assignment based on the charge fluxes

In the following subsection we will give a geometric derivation of the current assignment scheme. In order to assign currents to the links we can use the integral form of the continuity equation

$$\int_{\partial V}\mathbf{j}d\mathbf{s} = \int_V \frac{\partial}{\partial t}\rho\,dV \tag{3.112}$$

i. e. the flux $J = \int_{\partial V}\mathbf{j}d\mathbf{s}$ through the boundary of the volume V is equal to the change of the charge inside this volume. Let us consider the fluxes which are caused by the changing of the charge on each vertex of the cell during one time step h.

The primary cells are indexed by the integral position coordinates $x = ia$, $y = ja$, $z = ka$ of their left–forward–low corners. Its indexing generates the indexing of the dual cells by the position coordinates of their centers. In an equidistant grid, the address of the cell, or the triple of numbers (i, j, k), a particle with coordinates (x_p, y_p, z_p) is located in, is defined by

$$i = \left[\frac{x_p}{a}\right], \qquad j = \left[\frac{y_p}{a}\right], \qquad k = \left[\frac{z_p}{a}\right]$$

where the brackets [] mean the integer part of the number and a is the mesh size.

Then the location of a given particle (i.e. the center of the particle cube) inside this cell can be written as $x/a = i + \xi$, $y/a = j + \eta$, $z/a = k + \zeta$, where ξ, η, ζ lie between 0 and 1, and the Table 3.6.1 shows what fractions of the particle lie on each of the eight cell corners.
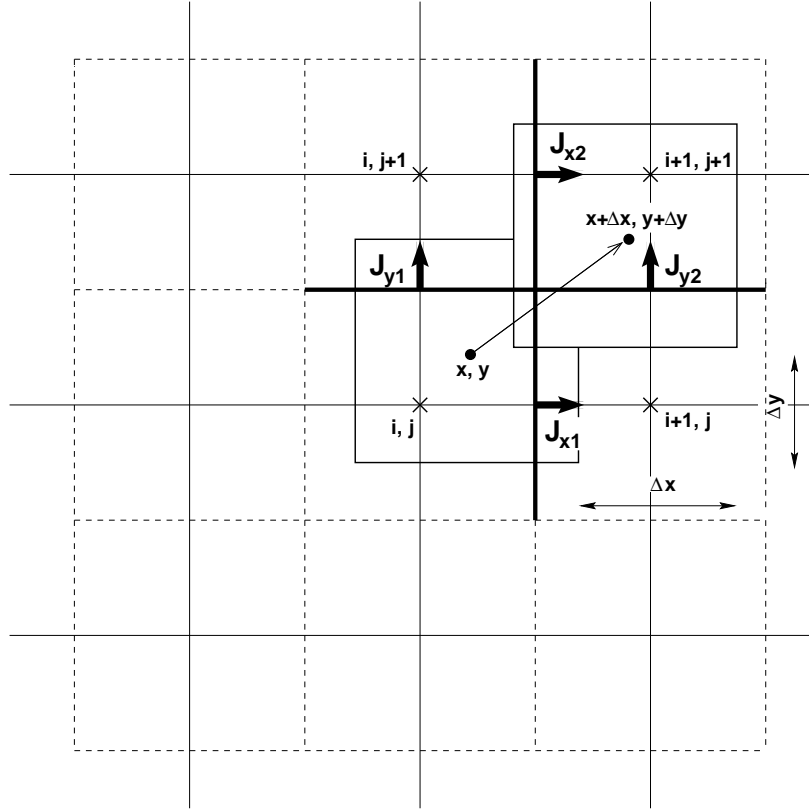

Figure 3.9.: Two–dimensional case of the current assignment scheme. The motion of the charge creates currents across the four cell boundaries of dual lattice. A move as shown will create the four fluxes J_{x1}, J_{x2}, J_{y1} and J_{y2} as given in the text. The coordinates describing the location of the charge center at the start of the move are measured relative to the "local origin".

Each particle cube straddles twelve dual cell faces, four for each of the three orientations: x-facing, y-facing and z-facing. Consider a particle which moves straight from $(i + \xi_1, j + \eta_1, k + \zeta_1)$ to $(i + \xi_2, j + \eta_2, k + \zeta_2)$ linearly with time, covering a displacement $\Delta\xi = \xi_2 - \xi_1, \Delta\eta = \eta_2 - \eta_1, \Delta\zeta = \zeta_2 - \zeta_1$ in the time h. The total flux transported in to the dual cell indexed $(i + 1, j + 1, k + 1)$ across its

x-facing boundary shared with the dual cell indexed $(i, j + 1, k + 1)$ is

$$\frac{q}{h} \int_{\xi_1}^{\xi_2} \eta(t)\zeta(t)d\xi = \frac{q}{h} \int_0^1 (\eta_1 + \lambda\Delta\eta)(\zeta_1 + \Delta\zeta)\Delta\xi d\lambda =$$
$$= \frac{q\Delta\xi}{h} \left[\frac{1}{3}\Delta\eta\Delta\zeta + \frac{1}{2}(\eta_1\Delta\zeta + \zeta_1\Delta\eta) + \eta_1\zeta_1 \right] \tag{3.113}$$

This is the contribution to J_x at the link $(i, j + 1, k + 1) \rightarrow (i + 1, j + 1, k + 1)$, which corresponds to J_{x2} in Fig. 3.9.

Further, the total flux transported into the dual cell indexed $(i + 1, j, k + 1)$ across its x-facing boundary shared with the dual cell indexed $(i, j, k + 1)$ is

$$\frac{q}{h} \int_{\xi_1}^{\xi_2} (1 - \eta(t))\zeta(t)d\xi = \frac{q}{h} \int_0^1 (1 - \eta_1 - t\Delta\eta)(\zeta_1 + \Delta\zeta)\Delta\xi d\lambda =$$
$$= \frac{q\Delta\xi}{h} \left[-\frac{1}{3}\Delta\eta\Delta\zeta + \frac{1}{2}\{(1 - \eta_1)\Delta\zeta - \zeta_1\Delta\eta\} + (1 - \eta_1)\zeta_1 \right] \tag{3.114}$$

And quite similar we derive the fluxes J_x on the links $(i, j, k) \rightarrow (i + 1, j, k)$ and $(i, j + 1, k) \rightarrow (i + 1, j + 1, k)$:

$$J_x \{(i, j, k) \rightarrow (i + 1, j, k)\} = \frac{q\Delta\xi}{h} \left[\frac{1}{3}\Delta\eta\Delta\zeta - \right.$$
$$\left. -\frac{1}{2}\{(1 - \eta_1)\Delta\zeta + (1 - \zeta_1)\Delta y\} + (1 - \eta_1)(1 - \zeta_1) \right] \tag{3.115}$$

$$J_x \{(i, j + 1, k) \rightarrow (i + 1, j + 1, k)\} = \frac{q\Delta\xi}{h} \left[-\frac{1}{3}\Delta\eta\Delta\zeta + \right.$$
$$\left. +\frac{1}{2}\{(1 - \zeta_1)\Delta\eta - \eta_1)\Delta z\} + \eta_1(1 - \zeta_1) \right] \tag{3.116}$$

The four contributions to J_y and J_z are obtained from Eqs. 3.114 – 3.116 by the cyclic rotation

$$i, \Delta\xi, \xi \Rightarrow j, \Delta\eta, \eta \Rightarrow k, \Delta\zeta, \zeta \tag{3.117}$$

A similar assignment scheme was used in [111] in the simulation of plasma physics.

Note that the terms of the order $\mathcal{O}(t^2)$ are necessary for the exact charge conservation. The same current updating scheme can be derived if one integrates over the time step Eqs. 3.81a– 3.81c.

Let us check the charge conservation for this scheme. By linear superposition, conservation of charge for one trajectory moving through a single time step implies the same for the sum of all trajectories. Addition of the three fluxes from a single

charge into the dual cell indexed $(i+1,\ j+1,\ k+1)$ yields

$$
(J_x + J_y + J_z)\{(i,j,k) \to (i+1,j+1,k+1)\} = \frac{q}{h}\ \{
$$

$$
\Delta\xi\Delta\eta\Delta\zeta + \frac{\Delta\xi}{2}\left(\eta_1\Delta\zeta + \zeta_1\Delta\eta\right) + \eta_1\zeta_1\Delta\xi +
$$

$$
+ \frac{\Delta\eta}{2}\left(\xi_1\Delta\zeta + \zeta_1\Delta\xi\right) + \xi_1\zeta_1\Delta\eta + \tag{3.118}
$$

$$
+ \frac{\Delta\zeta}{2}\left(\xi_1\Delta\eta + \eta_1\Delta x\right) + \xi_1\eta_1\Delta\zeta\ \} =
$$

$$
\frac{q}{h}\left\{(\xi_1 + \Delta\xi)(\eta_1 + \Delta\eta)(\zeta_1 + \Delta\zeta) - \xi_1\,\eta_1\,\zeta_1\right\}
$$

On the other hand, the difference between the particle fractions protruding into the dual cell before and after the move is

$$
\Delta Q(i+1, j+1, k+1) = q\left\{(\xi_1 + \Delta\xi)(\eta_1 + \Delta\eta)(\zeta_1 + \Delta\zeta) - \xi_1\,\eta_1\,\zeta_1\right\} \tag{3.119}
$$

This, then confirms the rigorous charge conservation.

Note that if we suppose that the current on the link is constant then the flux on the same link can be written as $J = \mathbf{j}\cdot\mathbf{s} = ja^2$. Moreover, the change of particle position can be written as the velocity times time step, i.e. $\Delta\xi = \frac{v_x h}{a}$, $\Delta\eta = \frac{v_y h}{a}$, $\Delta\zeta = \frac{v_z h}{a}$. In this case we have from Eq. 3.113

$$
j(i, j+1, k+1 \to i+1, j+1, k+1) =
$$

$$
\frac{qv_x}{a^3}\ \frac{1}{3}\frac{v_y v_z h^2}{a^2} + \frac{h}{2a}\left(\eta_1 v_z + \zeta_1 v_y\right) + \eta_1\ \zeta_1 \tag{3.120}
$$

Therefore for sufficiently small time step we have the equivalence of two assignment schemes (for continuous and discretized time variable), i.e.

$$
\lim_{h \to 0} j(i, j+1, k+1 \to i+1, j+1, k+1) = \frac{q}{a^3}v_x\eta_1\zeta_1 \tag{3.121}
$$

3.7. Self–energy artefacts

In the continuum the solution of the Maxwell equations for point charges is singular at the point where a charge is. The point charge carries along with it a potential which at short distances diverges as the Coulomb potential, and which therefore has the electrostatic energy

$$
\frac{1}{2}\int\limits_{\{|\mathbf{r}-\mathbf{r}_i(t)|\leq R\}} d^3\mathbf{r}\,\mathbf{E}(\mathbf{r}, t)^2 \propto \int_0^R dr r^2\ {r^{-2}}^2 = \int_0^R dr r^{-2} = \infty \tag{3.122}
$$

where we assume the nonrelativistic case (velocity of the particle is much smaller than speed of light, $v \ll c$). Taking literally such an object would have an infinite

mass and cannot respond to external forces. It would maintain its velocity forever, which is not what we want in our simulations.

Our spatial lattice with lattice spacing a, on which we interpolate charges, introduces an efficient "cut–off" for this self–interaction of the charged particle with its own field. On the lattice the charge is no more a point object and has a characteristic diameter of the order of the lattice spacing. Therefore the singularities are removed from the theory.

Nevertheless the force exerted on a particle by its own field depends on the value of the lattice spacing and with $a \to 0$ goes to infinity. Furthermore, the self energy $\mathcal{U}_{self}$ of an interpolated charge distribution $\rho_{int}(\mathbf{r})$ becomes a function of its position with respect to the mesh. In general,

$$\mathcal{U}_{self} = \frac{1}{2} \int d^3r \rho_{int}(\mathbf{r})\phi(\mathbf{r}) \tag{3.123}$$

where the $\phi(\mathbf{r})$ is the solution of the Poisson equation for the given interpolated charge distribution. The solution of Poisson equation can be written as a convolution of the charge distribution with the Green function, i. e. the function which satisfies the homogeneous Poisson equation:

$$\Delta_{(\mathbf{r}')}G\left(\mathbf{r} - \mathbf{r}'\right) = -\delta\left(\mathbf{r} - \mathbf{r}'\right)$$

Therefore Eq. 3.123 can be written as

$$\mathcal{U}_{self} = \frac{1}{2\epsilon_0} \int d^3r d^3r' G\left(\mathbf{r} - \mathbf{r}'\right) \rho_{int}(\mathbf{r})\rho_{int}(\mathbf{r}') \tag{3.124}$$

The last relation is a convolution and, therefore, takes on a very simple form when Fourier transformed in space:

$$\begin{aligned} \mathcal{U}_{self} &= \frac{1}{2\epsilon_0} \int \frac{d^3k d^3r d^3r'}{(2\pi)^3} G(\mathbf{k})e^{i\mathbf{k}(\mathbf{r}-\mathbf{r}')}\rho_{int}(\mathbf{r})\rho_{int}(\mathbf{r}') \\ &= \frac{1}{2\epsilon_0} \int \frac{d^3k}{(2\pi)^3} G(\mathbf{k})S_{int}(\mathbf{k}) \end{aligned} \tag{3.125}$$

where $S_{int}(\mathbf{k})$ is the structure factor of the interpolation of the charge to the lattice. For the Coulomb interaction, the Green function is $G_{coulomb}(\mathbf{r} - \mathbf{r}') = 1/(4\pi|\mathbf{r} - \mathbf{r}'|)$ and its Fourier transform $G(\mathbf{k}) = 1/k^2$. Introduction of the lattice spacing a leads to an upper bound of the potential amplitude ΔU_{self}, which has the order $\mathcal{O}(q^2/\epsilon_0 a)$ where q is the charge of the particle. It is not difficult to see that this potential is periodic.

Let us now consider a single particle with charge q in a large one–dimensional system. Place the particle between adjacent mesh points located at $x = 0$ and $x = a$ and apply the linear interpolation scheme. Then the self energy is

$$\mathcal{U}_{self} = \frac{a}{2}\left(\rho_0\phi_0 + \rho_1\phi_1\right) \tag{3.126}$$

The mesh-defined potential is given by the solution of the set of algebraic equations

$$\phi_{i-1} - 2\phi_i + \phi_{i+1} = -\frac{\rho_i a^2}{\epsilon_0} \tag{3.127}$$

Solving Eq. 3.127 for an isolated charge ρ_0 at grid point 0, taking $\phi_0 = 0$ and using the symmetry of the problem, gives

$$\phi_i = -\frac{\rho_0 a}{2\epsilon_0} |x_i| \tag{3.128}$$

For the Eq. 3.126 using the superposition principle we obtain:

$$\mathcal{U}_{self} = -\frac{q^2}{4\epsilon_0}(1 - \frac{x}{a})x = \frac{q^2}{4a\epsilon_0}\left(x - \frac{a}{2}\right)^2 + const \tag{3.129}$$

This is a simple harmonic oscillator potential well. It yields an oscillation frequency

$$\omega_{self} = \left(\frac{q^2}{2m\epsilon_0 a}\right)^{1/2} \tag{3.130}$$

where m is the particle mass. Using the definition of the plasma frequency $\omega_p^2 = nq^2/\epsilon_0 m$ the frequency ω_{self} has the form

$$\omega_{self} = \frac{\omega_p}{\sqrt{2na}} \tag{3.131}$$

If the number of particles per cell is large, then ω_{self} is much smaller than the plasma frequency. This is the case of plasma simulations (see Ref. [101]).

The well–depth energy $\Delta\mathcal{U}_{self}$ may be compared to the thermal energy:

$$\frac{\Delta\mathcal{U}_{self}}{k_b T} = \frac{q^2 a}{16\epsilon_0 k_b T} = \frac{a}{16n\lambda_D^2} \tag{3.132}$$

where $\lambda_D = \sqrt{\epsilon_0 k_b T/nq^2}$ is the Debye length.

Dimensional arguments indicate that in three dimension this ratio will be of the order

$$\frac{\Delta\mathcal{U}_{self}}{k_B T} \propto \frac{1}{N_c}\left(\frac{a}{\lambda_D}\right)^2$$

where $N_c = nV_c$ is the number of particles per cell $V_c = a^3$. Note that this ratio is desirably small when N_c is large. Re–writing

$$\frac{\Delta\mathcal{U}_{self}}{k_B T} \propto \frac{1}{na\lambda_D^2},$$

we see that for dilute systems and fine meshes the self–energy plays an important role. Due to the presence of this periodic potential, the particle is "trapped" in the center of the grid cell where the self energy is lowest(see Fig. 3.10).
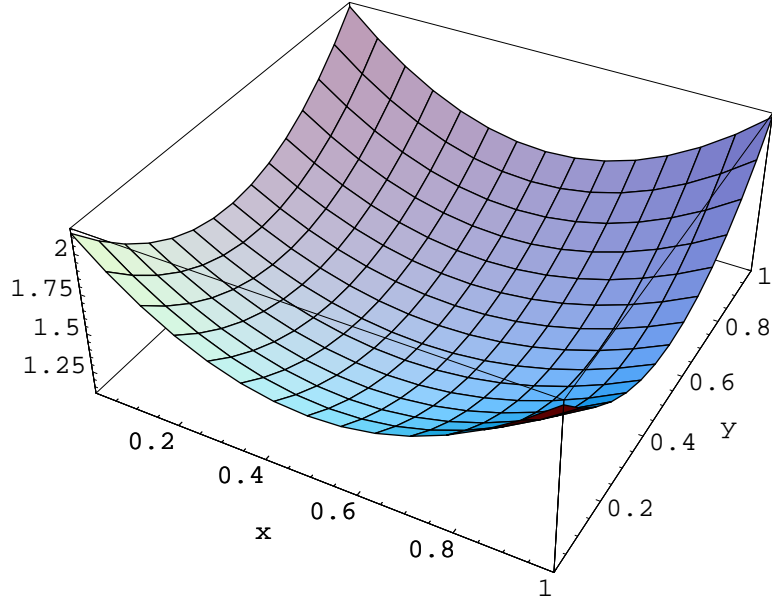
Figure 3.10.: Self–energy along $z = 0.5$ of a grid cube for the pure Coulomb inter-
action. The energy was calculated using the lattice Green function.
Coordinates x and y are normalized to the lattice spacing a.

The conventional remedy to the situation consists simply in spreading out the
charge over a wider range of lattice sites, thereby reducing the self-energy artefacts.
This is typically done with a convolution step that distributes charges over several
hundred sites using Gaussian distributions [112] after interpolation to the grid.
These convolutions are easy to perform in Fourier space, but are complicated and
time consuming in real space. They would also drastically reduce the speed of the
algorithm.

3.7.1.   Dynamic subtraction of lattice artefacts

Recently Maggs and Rottler [113] have introduced a dynamic correction that leads
to an effective convolution of the charge distribution with minimal computational
overhead.

The idea is similar to the introduction of "strong interaction" in quantum elec-
trodynamics. In the same spirit the interpolated charge cloud is stabilized by
Yukawa interactions.

In order to understand the latter, let us first consider the functional

$$\mathcal{F} = -\frac{\epsilon_0}{2} \int d^3\mathbf{r} \, (\nabla\psi)^2 + \int d^3\mathbf{r} \, \rho\psi \tag{3.133}$$

and study, for fixed ρ,

$$\frac{\delta\mathcal{F}}{\delta\psi} = 0. \tag{3.134}$$

It is straightforward to see that (i) this variational problem is equivalent to the Poisson equation for the electrostatic potential ψ, and that (ii) insertion of the solution into $\mathcal{F}$ yields $\mathcal{F} = +(1/2) \int d^3\mathbf{r}\,\rho\psi$, i. e. the correct electrostatic energy. However, this functional is useless for dynamic simulations where one would try to simulate a coupled dynamics of ρ and ψ. The reason is that the $\nabla\psi$ term has the wrong sign, such that arbitrarily large variations of ψ are favored and the simulation would be inherently unstable (the partition function for integrating out the ψ field would not exist).

A well–behaved theory, however, is obtained by just turning the sign of the $\nabla\psi$ term:

$$\mathcal{F} = +\frac{\epsilon_0}{2} \int d^3\mathbf{r}\ (\nabla\psi)^2 + \int d^3\mathbf{r}\,\rho\psi. \tag{3.135}$$

This results in $+\nabla^2\psi = \rho/\epsilon_0$, and insertion into the functional yields again $\mathcal{F} = +(1/2) \int d^3\mathbf{r}\,\rho\psi$. Since, however, ψ is just the negative of the real (physical) electrostatic potential, one obtains a theory which describes attraction between like charges and repulsion between unlike charges. We now introduce an additional field degree of freedom ψ, and couple this to the original method (Lagrangian) via

$$\mathcal{L} \ \rightarrow \ \mathcal{L} + \frac{\epsilon_0}{2c_\psi^2} \int d^3\mathbf{r}\ \dot{\psi}^2 \tag{3.136}$$
$$-\frac{\epsilon_0}{2} \int d^3\mathbf{r}\ (\nabla\psi)^2 - \int d^3\mathbf{r}\,\rho\psi.$$

Here c_ψ is another dynamical parameter of dimension velocity. It can be set identical to c, but need not. This modified method would result in an additional potential of mean force between the charges which would *exactly cancel* the original Coulomb potential (including self–terms). This is apparently not useful. However, we can introduce a slightly modified coupling with a screening parameter $\mu > 0$:

$$\mathcal{L} \ \rightarrow \ \mathcal{L} + \frac{\epsilon_0}{2c_\psi^2} \int d^3\mathbf{r}\ \dot{\psi}^2 \tag{3.137}$$
$$-\frac{\epsilon_0}{2} \int d^3\mathbf{r}\ (\nabla\psi)^2 - \frac{\epsilon_0}{2} \int d^3\mathbf{r}\ \mu^2\psi^2 - \int d^3\mathbf{r}\,\rho\psi.$$

This introduces an additional potential of mean force between the charges, which, in the continuum limit, would read

$$U_Y(r) = -\frac{1}{4\pi\epsilon_0} \frac{q_1 q_2}{r} \exp(-\mu r), \tag{3.138}$$

such that unlike charges repel each other with a screened Coulomb interaction.

In the simulation the charges are coupled simultaneously to the unconstrained scalar field

$$\mathcal{F}_Y[\psi] = \int d^3r \left\{ \frac{\epsilon_0}{2}\ (\nabla\psi)^2 + \mu^2\psi^2\ + \rho\psi \right\} \tag{3.139}$$

as well as to constrained vector field Eq. 2.54. The total partition function then
reads

$$\mathcal{Z}(\mathbf{r}) = \mathcal{Z}_{coulomb}(\mathbf{r}) \times \mathcal{Z}_Y(\mathbf{r}) \times const \tag{3.140}$$

where

$$\mathcal{Z}_Y(\mathbf{r}) = \int \mathcal{D}\psi e^{-\mathcal{F}_Y[\psi](\mathbf{r})/k_B T} \tag{3.141}$$

and implies an effective interaction between two charges q_1 and q_2 given by

$$U(r) = \frac{q_1 q_2}{4\pi\epsilon_0 r}\ \ 1 - e^{-\mu r} \tag{3.142}$$

At large separation there is a pure Coulomb interaction; at short distances the
potential has been regularized.

Using the standard calculus of variations, from the Eq. 3.139 the Yukawa–
Helmholz can be derived

$$\Delta\psi_Y - \mu^2 \psi_Y = \frac{\rho}{\epsilon_0} \tag{3.143}$$

The corresponding Green's function for the last equation is

$$G_Y(\mathbf{k}) = -\frac{1}{\mathbf{k}^2 + \mu^2} \tag{3.144}$$

Summing up the Green's functions for the pure Coulomb and Yukawa scalar fields
we obtain the Green's function for the regularized potential

$$G(\mathbf{k}) = \frac{1}{\mathbf{k}^2} - \frac{1}{\mathbf{k}^2 + \mu^2} = \frac{\mu^2}{\mathbf{k}^2 \left(\mathbf{k}^2 + \mu^2\right)} \tag{3.145}$$

By inserting Eq. 3.145 into Eq. 3.123, we find that the self–energy is now finite
for $a \to 0$. The additional factor in the last equation can be considered as the
convolution function with the initial interpolated charge distribution. Then one
writes the structure factor $S_{conv}(\mathbf{k})$ of it

$$S_{conv}(\mathbf{k}) = \frac{\mu^2}{\mathbf{k}^2 + \mu^2} \tag{3.146}$$

By reducing μ one obtains better smoothing of the pure Coulomb interaction. At
the same time this weakens the original Coulomb interactions on a local scale, and
can be corrected by adding $-U_Y$ to the standard interparticle potential. Here one
can use the continuum version of the potential; this will only serve to decrease the
influence of lattice artifacts.

From numerical integration Maggs and Rottler [113] have obtained a variation
of the periodic energy barrier which is of the order $(\mu a)^2$ for small μ. In order to
enhance the convergence of such a coupling they have introduced another uncon-
strained field:

$$\mathcal{F}_v[\mathbf{h}] = \int \left\{ \frac{\epsilon_0 \mathbf{h}(\mathbf{r})^2}{2} - \frac{(\epsilon_0 \nabla \mathbf{h}(\mathbf{r}) - \rho(\mathbf{r}))^2}{2\mu^2} \right\} d^3 r \tag{3.147}$$

This is a vector field. The corresponding Green function has the form

$$G(\mathbf{k}) = -\frac{\mu^2}{(\mathbf{k}^2 + \mu^2)(\mathbf{k}^2 + 2\mu^2)} \tag{3.148}$$

By coupling the charges to three fields, respectively a constrained vector, a scalar and an unconstrained, we obtain the following interaction potential

$$\mathcal{V}(r) = \frac{q_1 q_2}{4\pi\epsilon_0 r} \left[1 - 2e^{-\mu r} + e^{-\sqrt{2}\mu r} \right] \tag{3.149}$$

The inhomogeneity in the self-energy is smaller than when using only the scalar Yukawa field, and the barrier now varies as $(\mu a)^4$ for small μ.

3.7.2. Direct subtraction of the self–energy

Instead of decreasing the self–energy barrier by choosing appropriate convolution functions there exists another approach. The main idea is to directly subtract the self–energy of the charge interpolated cloud.

Let consider the electrostatic problem of one charge placed at $\mathbf{r} = (0,0,0)$ in an infinite lattice. The Green's function for this problem satisfies the following equation

$$\Delta_{(\mathbf{r}')} G(\mathbf{r} - \mathbf{r}') = -\frac{1}{a^2} \delta_{\mathbf{r},\mathbf{r}'} \tag{3.150}$$

Then the electrostatic potential ϕ can be found as convolution with the Green function

$$\phi(\mathbf{r}) = \frac{a^2}{\epsilon_0} \sum_{\mathbf{r}'} G(\mathbf{r} - \mathbf{r}')\rho(\mathbf{r}') \tag{3.151}$$

Taking into account the fact that the charge distribution of a point charge is the delta function, Eq. 3.151 can be rewritten as

$$\phi(\mathbf{r}) = \frac{q}{a\epsilon_0} G(\mathbf{r}) \tag{3.152}$$

where a is the lattice spacing. The Laplace operator on the left hand side of Eq. 3.150 for the cubic lattice transforms to finite–differencing operator

$$\Delta_{(\mathbf{r})} f(\mathbf{r}) = \frac{1}{a^2} \sum_{\mathbf{n}} [f(\mathbf{r} + \mathbf{n}) - f(\mathbf{r})] \tag{3.153}$$

where the $\mathbf{n}$ are the vectors form site $\mathbf{r}$ to its nearest neighbors ($\mathbf{n} = \pm\mathbf{a}_i, i = 1,\ldots,3$ for a three–dimensional lattice) and $\mathbf{a}_i$ are independent primitive translation vectors.

To find the lattice Green's function defined by Eq. 3.150 we take periodic boundary conditions at the edges of the cube. Consider a cube with L lattice points along

each side. Thus the total number of sites in the 3-dimensional cube is L^3. Substituting the Fourier transform

$$G(\mathbf{r}) = \frac{1}{L^3} \sum_{\mathbf{k} \in BZ} G(\mathbf{k}) e^{i\mathbf{k}\mathbf{r}} \tag{3.154}$$

of the lattice Green's function into Eq. 3.150, we find

$$G(\mathbf{k}) = \frac{1}{\epsilon(\mathbf{k})}, \tag{3.155}$$

for the three–dimensional cube where we have defined

$$\epsilon(\mathbf{k}) = 2 \sum_{i=1}^{3} (1 - \cos \mathbf{k}\mathbf{a}_i). \tag{3.156}$$

Owing to the periodic boundary conditions, the wave vector $\mathbf{k}$ in Eq. 3.154 is limited to the first Brillouin zone and is given by

$$\mathbf{k} = \frac{m_1}{L}\mathbf{b}_1 + \frac{m_2}{L}\mathbf{b}_2 + \frac{m_3}{L}\mathbf{b}_3 \tag{3.157}$$

where m_1, m_2, m_3 are integers such that $-L/2 \le m_i \le L/2$ for $i = 1, 2, 3$, and $\mathbf{b}_j$ are reciprocal lattice vectors defined by $\mathbf{a}_i\mathbf{b}_j = 2\pi\delta_{ij}$. Here we assumed that L is an even integer, which will be irrelevant in the limit $L \to \infty$. Alternatively we may shift these vectors by half a period and obtain an equivalent range which is valid for any values of L. The mathematical description of the crystal lattice and the concept of the Brillouin zone can be found in many books on solid state physics (see Ref. [114], [115], [116]).

Finally, with the help of the inverse Fourier transform, the lattice Green's function takes the form

$$G(\mathbf{r}) = \frac{1}{L^3} \sum_{\mathbf{k} \in BZ} \frac{e^{i\mathbf{k}\mathbf{r}}}{\epsilon(\mathbf{k})}. \tag{3.158}$$

If we take the limit $L \to \infty$ then the discrete summation over $\mathbf{k}$ can be substituted by an integral (see [114]):

$$\frac{1}{L^3} \sum_{\mathbf{k} \in BZ} \mapsto a^3 \int_{\mathbf{k} \in BZ} \frac{d^3k}{(2\pi)^3}. \tag{3.159}$$

Thus the lattice Green's function is

$$G(\mathbf{r}) = a^3 \int_{\mathbf{k} \in BZ} \frac{d^3k}{(2\pi)^3} \frac{e^{i\mathbf{k}\mathbf{r}}}{\epsilon(\mathbf{k})} \tag{3.160}$$

Using Eqs. 3.152 and 3.158 the electrostatic potential from the point charge on a cubic lattice is

$$\phi(\mathbf{r}) = \frac{q}{L^3\epsilon_0 a} \sum_{\mathbf{k} \in BZ} \frac{e^{i\mathbf{k}\mathbf{r}}}{\epsilon(\mathbf{k})} \tag{3.161}$$

Writing the electric field on the link as the difference of potentials on the ends of that link $E_i(\mathbf{r}) = -\frac{1}{a}[\phi(\mathbf{r} + \mathbf{a}_i) - \phi(\mathbf{r})]$ for the Fourier transformed component of the electric field we obtain

$$\hat{E}_i(\mathbf{k}) = -\frac{1}{a}\hat{\phi}(\mathbf{k}) \ \ e^{i\mathbf{k}\mathbf{a}_i} - 1 \tag{3.162}$$

The Parseval's theorem allows us to write the electrostatic self–energy in the form

$$\mathcal{U}_{self} = \frac{\epsilon_0 a^3}{2} \sum_{\mathbf{r}} \sum_{i=1}^{3} E_i(\mathbf{r})^2 = \frac{\epsilon_0 a^3}{2L^3} \sum_{\mathbf{k}} \sum_{i=1}^{3} \hat{E}_i(\mathbf{k})\hat{E}_i^*(\mathbf{k}) \tag{3.163}$$

Inserting 3.162 into the last equation, we obtain

$$\mathcal{U}_{self} = \frac{\epsilon_0 a^2}{2L^3} \sum_{i=1}^{3} \sum_{\mathbf{k}} \hat{E}_i(\mathbf{k})\hat{\phi}^*(\mathbf{k}) \ \ 1 - e^{-i\mathbf{k}\mathbf{a}_i} \tag{3.164}$$

Transforming back into real space, the self-energy is

$$\mathcal{U}_{self} = \frac{\epsilon_0 a^2}{2} \sum_{i=1}^{3} \sum_{\mathbf{r}} (E_i(\mathbf{r}) - E_i(\mathbf{r} - \mathbf{a}_i))\phi(\mathbf{r}) = \frac{1}{2} \sum_{\mathbf{r}} q(\mathbf{r})\phi(\mathbf{r}) \tag{3.165}$$

where we have used the expression for the Gauss law on the lattice:

$$\sum_{i=1}^{3} (E_i(\mathbf{r}) - E_i(\mathbf{r} - \mathbf{a}_i)) = \frac{q(\mathbf{r})}{\epsilon_0 a^2} \tag{3.166}$$

We see that the lattice electrostatic energy has the same expression as in the continuum. The self–energy of a point charge is the value of the electrostatic potential at the point where the particle is:

$$\mathcal{U}_{self} = \frac{1}{2}q \cdot \phi(0) = \frac{q^2 a^2}{2\epsilon_0} \int_{\mathbf{k}\in BZ} \frac{d^3k}{(2\pi)^3} \frac{1}{\epsilon(\mathbf{k})} \tag{3.167}$$

In order to calculate this lattice integral we can calculate the sum for different values of L and then take the limit of infinite lattice size.

$$\mathcal{U}_{self}(L) = \frac{q^2}{8L^3\epsilon_0 a} \sum_{p_1=0}^{L-1} \sum_{p_2=0}^{L-1} \sum_{p_3=0}^{L-1} \frac{1}{\sin^2 \ \frac{\pi}{L}p_1 \ + \sin^2 \ \frac{\pi}{L}p_2 \ + \sin^2 \ \frac{\pi}{L}p_3} \tag{3.168}$$

where $\mathbf{p} = (p_1, p_2, p_3) \neq \mathbf{0}$. The numerical values along with the fit are presented on the Fig. 3.11.

Moreover, the integral 3.167 can be evaluated analytically. Eq. 3.158 can be simplified if we specify the lattice point as $\mathbf{r} = l_1\mathbf{a}_1 + l_2\mathbf{a}_2 + l_3\mathbf{a}_3$:

$$G(l_1, l_2, l_3) = \int_{-\pi}^{\pi} \frac{dx_1}{2\pi} \int_{-\pi}^{\pi} \frac{dx_2}{2\pi} \int_{-\pi}^{\pi} \frac{dx_3}{2\pi} \frac{e^{i(l_1x_1+l_2x_2+l_3x_3)}}{2\sum_{i=1}^{3}(1 - \cos x_i)} \tag{3.169}$$

In our case we are searching for the value of Green's function at point $(0,0,0)$. The exact value for the cubic lattice function was given in the paper [117]:

$$
\begin{aligned}
2G(0,0,0) &= \frac{2\sqrt{2}}{\pi^2} k'_+ k'_- K_+ K_- \\
&= \frac{4}{\pi^2}(18 + 12\sqrt{2} - 10\sqrt{3} - 7\sqrt{6})K_-^2 \approx 0.5054620197
\end{aligned}
\tag{3.170}
$$

where $K_{\pm} = \mathbf{K}(k_{\pm})$ is the complete elliptic integral of the first kind with modulus

$$
k_{\pm} = (2 - \sqrt{3})(\sqrt{3} \pm \sqrt{2})
$$

Therefore the self-energy equals

$$
\frac{a\epsilon_0}{q^2}\mathcal{U}_{self} = \frac{1}{2}G(0,0,0) \approx 0.126365505
$$

which is in good agreement with the numerical calculations.

We are ready to calculate the self–energy for the interpolated charge cloud. In general inserting the discrete charge distribution $\rho(\mathbf{r}) = a^{-3}\sum_i q_i \delta_{\mathbf{r},\mathbf{R}_i}$ into the Eq. 3.151 for the electrostatic potential we have

$$
\phi(\mathbf{r}) = \frac{1}{\epsilon_0 a}\sum_{\mathbf{r}'} G(\mathbf{r} - \mathbf{r}')\sum_i q_i \delta_{\mathbf{r}',\mathbf{R}_i} = \frac{1}{\epsilon_0 a}\sum_i q_i G(\mathbf{r} - \mathbf{R}_i)
\tag{3.171}
$$

Further, inserting the last equation into Eq. 3.165 we calculate the self-energy

$$
\mathcal{U}_{self} = \frac{1}{2}\sum_i q_i \phi(\mathbf{R}_i) = \frac{1}{2a\epsilon_0}\sum_i \sum_j q_i q_j G(\mathbf{R}_i - \mathbf{R}_j)
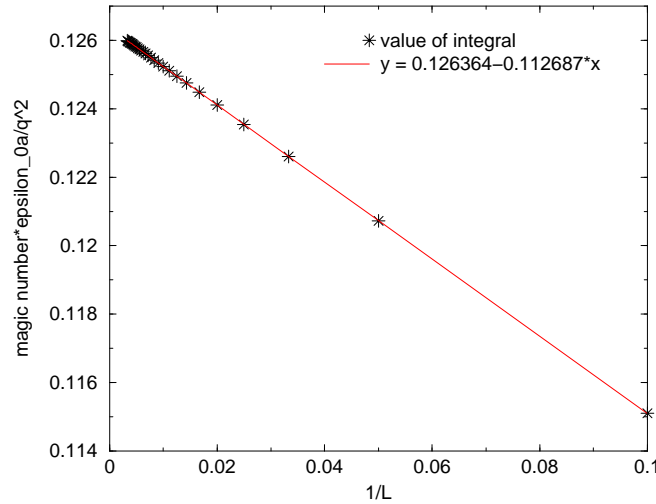\tag{3.172}
$$

Figure 3.11.: Self-energy magic number. Numerical calculation of the lattice sum (Eq. 3.168). Taking the limit $L \to \infty$ gives the value of the integral 3.167, which is approximately 0.126364.

For the finite lattice using Eq. 3.158 this yields

$$\mathcal{U}_{self} = \frac{1}{2a\epsilon_0 L^3} \sum_{\mathbf{k}} \frac{\sum_i \sum_j q_i q_j e^{i\mathbf{k}(\mathbf{R}_i - \mathbf{R}_j)}}{\epsilon(\mathbf{k})} \qquad (3.173)$$

Using the explicit expression for $\epsilon(\mathbf{k})$ (Eq. 3.156) one can write

$$\mathcal{U}_{self} = \frac{1}{4a\epsilon_0 L^3} \sum_{\mathbf{k}} \frac{\sum_i \sum_j q_i q_j \cos \mathbf{k}(\mathbf{R}_i - \mathbf{R}_j)}{\sum_{i=1}^{3}(1 - \cos \mathbf{k}\mathbf{a}_i)} \qquad (3.174)$$

For the simple cubic lattice in three dimensions the linear interpolation will give 8 charges which are placed at the corners of the cube with edge length a (see Fig. 3.12). Therefore in our case the self-energy is a symmetric bilinear form defined
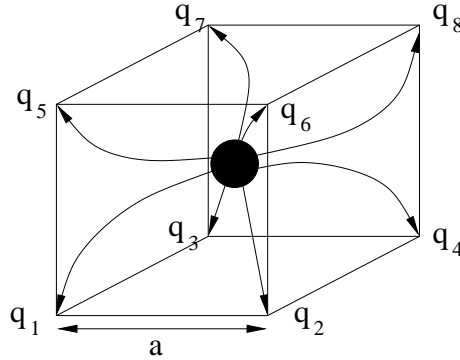

Figure 3.12.: Charge assignment scheme for the cubic lattice. The order of the interpolation scheme is 1 (nearest neighbors).

by the matrix $\{\alpha_{ij}\}$, the elements of which do not depend on the position of the charge. In our algorithm the values of the coefficients

$$\alpha_{ij} = \frac{1}{4a\epsilon_0 L^3} \sum_{\mathbf{k}} \frac{\cos \mathbf{k}(\mathbf{R}_i - \mathbf{R}_j)}{\sum_{i=1}^{3}(1 - \cos \mathbf{k}\mathbf{a}_i)} \qquad (3.175)$$

are calculated during the initialization step and are used in the calculation of the self-force. The value of the self-force which has to be subtracted from the overall forces is given by the following ansatz

$$\mathbf{F}_{self} = -\frac{\partial \mathcal{U}_{self}}{\partial \mathbf{r}} = -\sum_i \sum_j \alpha_{ij} \left(q_i \frac{\partial q_j}{\partial \mathbf{r}} + q_j \frac{\partial q_i}{\partial \mathbf{r}} \right) . \qquad (3.176)$$

Note that for the infinite lattice the analytic expression for the value of the electrostatic potential (and therefore also the value of the self-energy) can be obtained. For example, using the enumeration of cube sites shown in Fig. 3.12 the

electrostatic potential at the front left bottom corner of the cube is

$$
\begin{aligned}
\phi(0) = \frac{1}{\epsilon_0 a} \{ & q_1 G(0,0,0) + (q_2 + q_3 + q_5)G(1,0,0) \\
& + (q_4 + q_6 + q_7)G(1,1,0) + q_8 G(1,1,1) \}
\end{aligned}
\tag{3.177}
$$

where $G(l_1, l_2, l_3)$ is given by Eq. 3.169 and we have used the symmetry of the task. We have already calculated the value $G(0,0,0)$ (Eq. 3.170). Again, due to the symmetry and using Gauss' law we obtain

$$
G(1,0,0) = G(0,0,0) - \frac{1}{6}
\tag{3.178}
$$

The value $G(1,1,0)$ is calculated in [117]:

$$
G(1,1,0) = \frac{5}{4}G(0,0,0) - \frac{1}{4}G(2,0,0) - \frac{1}{4}
$$

where $G(2,0,0)$ can be found using the recurrence formula of Horiguchi and Morita [118]:

$$
G(2,0,0) = \frac{10}{3}G(0,0,0) + \frac{1}{\pi^2 G(0,0,0)} - 1.
$$

The recursion scheme developed by Duffin and Shelly [119] allows us to determine the last value $G(1,1,1)$:

$$
G(1,1,1) = r_1 G(0,0,0) + \frac{r_2}{\pi^2 G(0,0,0)}
$$

where $r_1 = -1/8$ and $r_2 = 3/16$.

3.8. Implementation

For the field propagation one is forced to choose whether to implement the electric fields $E(l)$ and the vector potentials $A(l)$ on the links or the electric field $E(l)$ and magnetic flux $B(p)$. The latter algorithm was used in Ref. [51].

In the implementation of the algorithm we assume that particles with masses m_i live in the continuum (off–lattice approach). Particles have charges q_i and interact between themselves also by a Lennard–Jones potential. The Lennard–Jones potential of scale σ is truncated at its minimum, $r_c = 2^{1/6}\sigma$.

The charges are interpolated on the lattice with grid spacing a using the linear interpolation scheme. All electromagnetic fields live on the links of the lattice, therefore the electric field $\mathbf{E}$ is associated with $3L^3/a^3$ links, where L is the dimension of the simulation box.

In order to start the simulation for the given random distribution of charges we have to calculate the initial electrostatic field, i. e. the exact solution of the electrostatic problem. For this purpose we use the hierarchical scheme described in

section 2.5.3. For the overall system, we use a checkerboard decomposition which allows easy parallelization.

The value of speed of light has always satisfied the stability criterion $h \ll a/c$.

Ideally, one would like to run MEMD via an integrator which leaves the phase–space volume invariant and is time–reversible, such as the Verlet algorithm in standard MD [39]. Since the equations of motion (even in the lattice–discretized case) have these properties, it is indeed possible to construct such a scheme. An analog to the Verlet algorithm for MEMD would be the following integrator, based upon a time step h:

1. Update the particle momenta by half a time step.

2. Update the $\mathbf{A}$ field by half a time step.

3. Update the particle positions by half a time step.

4. Update the electric field by a full time step.

5. Update the particle positions by half a time step.

6. Update the $\mathbf{A}$ field by half a time step.

7. Update the particle momenta by half a time step.

Here, "update" means the simple Euler rule $x(t + h) = x(t) + \dot{x}(t)h$. The time consuming part (update of the particle momenta, update of the electric field) is arranged in such a way that only one "force calculation" per time step is necessary. This scheme does conserve the phase–space volume and is time–reversible. Since the updates of $\mathbf{A}$ and of the particle momenta are interchangeable due to the omission of magnetic forces, we can replace this by an equivalent scheme:

1. Update the particle momenta by half a time step.

2. Update the $\mathbf{A}$ field by a *full* time step, from $t - h/2$ to $t + h/2$.

3. Update the particle positions by half a time step.

4. Update the electric field by a full time step.

5. Update the particle positions by half a time step.

6. Update the particle momenta by half a time step.

However, this algorithm suffers a severe disadvantage: The update of the electric field (step 4) is based upon a particle configuration (in real space and velocity space) which has so far only progressed by half a time step. As a consequence, Gauss' law is not satisfied within machine accuracy, but rather only within the accuracy of the time discretization. This is very undesirable, and hence we have modified the scheme as follows:

1. Update the particle momenta by half a time step.

2. Update the **A** field by a full time step, from $t - h/2$ to $t + h/2$.

3. Update the particle positions by *a full* time step.

4. Update the electric field by a full time step.

5. Update the particle momenta by half a time step.

In order to update the electric field on the link l we calculate charge fluxes (see section 3.6.3):

$$E(l;\, t_n + h) = E(l;\, t_n)$$
$$+ c^2 h \left(\nabla \times \nabla \times \mathbf{A} \right) \left[l;\, t_n + \frac{h}{2} \right] - \frac{h}{a^2 \epsilon_0} J \left[l;\, t_n + \frac{h}{2} \right], \tag{3.179}$$

where the flux J is given at half time step, the operation of *curl* understood in the discretized sense, and a is the lattice spacing. Note that the calculation of $J(l;\, t_n + h/2)$ requires knowledge of both the initial and the final positions of the particles, see Sec. 3.6.3. Thus the continuity equation 3.112 is satisfied exactly, and this ensures that the system stays on the constraint surface, as discussed above in detail.

For the particles velocities we use the electric force from Eqs. 3.89 – 3.91:

$$\mathbf{p}_i \left[t_n + \frac{h}{2} \right] = \mathbf{p}_i(t_n) + \frac{h}{2} \left\{ \mathbf{F}_{LJ}(t_n) + \mathbf{F}^e(t_n) \right\} \tag{3.180}$$

where $\mathbf{F}_{LJ}$ is the force derived from the Lennard–Jones potential.

However, this scheme does no longer satisfy time–reversal symmetry (this is obvious since the updates of the particle positions and of the electric field do not commute), and probably also violates phase–space volume conservation, since $\mathbf{j}$ is no longer just a simple function on phase space. Nevertheless, we considered it as most important to keep the system on its constraint surface.

We have added a Langevin thermostat to the particles:

$$\frac{d}{dt} \mathbf{p}_i = -\frac{\partial U}{\partial \mathbf{r}_i} + q_i \mathbf{E}(\mathbf{r}_i) - \frac{\gamma}{m_i} \mathbf{p}_i + \xi_i, \tag{3.181}$$

where γ is the particle friction constant, and ξ_i is a random force satisfying the standard fluctuation–dissipation theorem:

$$\left\langle \xi_i^\alpha(t) \xi_j^\beta(t') \right\rangle = 2\gamma k_B T \delta_{ij} \delta_{\alpha\beta} \delta(t - t'), \tag{3.182}$$

where α and β denote Cartesian indices. This puts the system into the canonical ensemble. For large systems, one can rely on the equivalence of ensembles, and there

is no fundamental statistical–mechanical need for such a thermostat — it is just a matter of technical convenience: Usually a Langevin thermostat tends to stabilize the simulation due to its inherent feedback mechanism, such that larger time steps are feasible. It should be noted that such thermostatted dynamics violates time reversibility and phase–space volume conservation.

3.8.1. Intersection with lattice cube boundaries

When a particle during one time step intersects the boundary of the grid cell, it will generate currents on more than four links per direction. In this case we have automated the particle splitting procedure. We calculate the intersection points with each cell face and split the trajectory of the particles on the segments. On each segment the currents are interpolated onto the links and the update of the electric field is completed.

3.8.2. Data structure

For the implementation of the parallel version we have used the domain decomposition strategy. The computational domain is split into a set of blocks, where each block has its own fields and particles and communicates with other blocks and boundaries via its glue-patches, Fig. 3.13. The standard MPI-interface [120], [121]
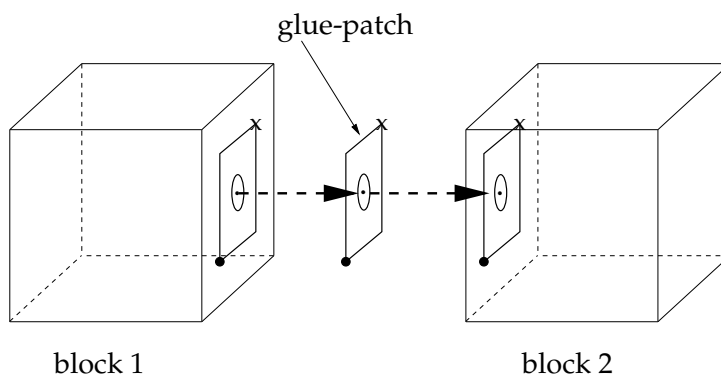

Figure 3.13.: All interior boundary conditions are applied by passing data between blocks via glue-patches.

was used for the communication between blocks, i. e. processes. This standard is available virtually for all platforms which provides a portability of the code.

All the field variables which live on one site of the lattice (electric fields, charges, vector fields plus auxiliaries) are found in structures of type `t_site`. Each node of the parallel machine has an array of such structures called `lattice`, with as many elements as there are sites on the node. In scalar mode there is only one node. The site structure looks like this:

```
typedef struct
```

```
    /* coordinates of this site */
    short      r[SPACE_DIM];
    /* interpolated charge */
    double     charge;
    /* 3d vector of electric field */
    t_dvector field;
    /* rotor of vector field */
    t_dvector curlA;
    /* vector field */
    t_dvector A;
    /* 3d vector of electric flux */
    t_dvector flux;
    /* additional variables for Yukawa fields */
    double     addDOF_p[ADD_DOF_DIM];
    double     addDOF_v[ADD_DOF_DIM];
    double     addDOF_f[ADD_DOF_DIM];
  t_site;
```

At run time space for the lattice sites is allocated dynamically, typically as an array `lattice[i]`, each element of which is a site structure. Thus, to refer to the `A` field on a particular lattice site, site "`i`" on this node, you say

```
    lattice[i].A
```

In addition to the fields in the `t_site` structure, there is the set of vectors whose elements correspond to lattice sites. This is the six vectors of `integer`'s:

```
  static t_dirs* neighbor
```

where `t_dirs` is the array of six `integers`.

```
  neighbor[XDOWN][i]
```

is the index of the site in the `XDOWN` direction from the `i`'th site on the node, if that site is on the same node. If the neighboring site is on another node, this pointer will be `NOWHERE (= -1)`.

Often we use the name of a field as an argument to a routine. These fields are elements of the structure `t_site`, and such variables can not be used directly as arguments in C. Instead, we use a macro to convert the name of a field into an integer, and another one to convert this integer back into an address at a given site. A type `field_offset`, which is secretly an integer, is defined to help make the programs clearer.

`F_OFFSET(fieldname)` gives the offset in the site structure of the named field. `F_PT(*site, field_offset)` gives the address of the field whose offset is `field_offset` at the site `*t_site`.

The algorithm was implemented both as a stand-alone program and as a module of the multipurpose scientific package ESPResSo [122]. This is a newly written

program package, that was designed to perform numerical MD/MC simulations for a broad class of soft matter systems in a parallel computing environment. For the short–range interactions the link–cell method is used. The particles are sorted into cells which are about as large as the largest range of a short–ranged interaction. Then short–ranged interactions only occur between particles in adjacent cells. For systems of homogeneous density the number of particles in these cells is constant, therefore reducing the computational order to $\mathcal{O}(N)$. Distributing the particles according to their spatial position, known as domain decomposition, is also a standard method for parallelization in multiprocessor environments.

The input/output of data is done on script language level. The whole system setup is contained within a Tcl [123] script. Inside a simulation script, one can handle the entire simulation process from the specification of a system, the actual simulation, its analysis and the graphical output of the results.

3.8.3. Validity check of the algorithm

As a validity check of the algorithm we have simulated two unlike charges in the box. The electrostatic potential for such a system is given by the approximate expression [113]:

$$V = -\frac{q^2}{4\pi\epsilon_0 r} - \frac{q^2 r^2}{6\epsilon_0 L^3} \tag{3.183}$$

where L is the dimension of the simulation box. We have used the value of $L = 8.0$ and the Bjerrum length $l_b = 1.0$. Figure 3.14 shows a good agreement with the experimental data.

3.9. Numerical results

As a simple test system, we have studied N charged particles in a cubic box with periodic boundary conditions. They interact via a purely repulsive Lennard–Jones (LJ) potential

$$U_{LJ} = \begin{cases} 4\epsilon \left[\left(\frac{\sigma}{r}\right)^{12} - \left(\frac{\sigma}{r}\right)^6 + \frac{1}{4} \right] & r \le 2^{1/6}\sigma \\ 0 & r \ge 2^{1/6}\sigma \end{cases}. \tag{3.184}$$

We choose a unit system where the potential parameters σ and ϵ, as well as the particle mass m, are set to unity. Time is thus measured in units of $\tau_{LJ} = \sqrt{m\sigma^2/\epsilon}$. We study systems at temperature $k_B T = 1$ and particle number density $\rho = 0.07$. The equations of motion were integrated by the algorithm outlined in Sec. 3.8 (no Yukawa subtraction), using a time step $h = 0.01$. The friction constant for the Langevin thermostat was set to $\gamma = 1$.
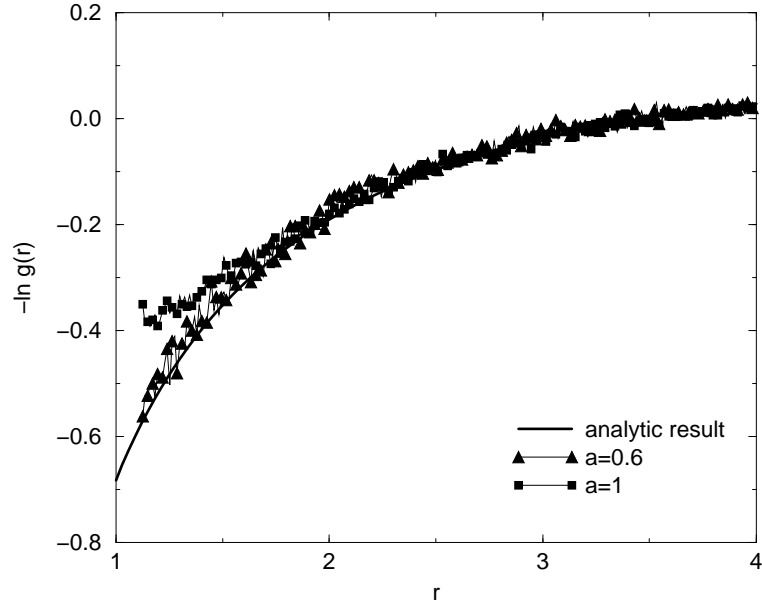
Figure 3.14.: Pair potential from the pair correlation function of two charges for $L = 8$, comparing to the analytical curve. Two different lattice spacings are used.

Each particle is assigned a charge $\pm q$. The strength of the electrostatic interaction is given in terms of the Bjerrum length

$$l_B = \frac{e^2}{4\pi\epsilon_0 k_B T}, \qquad (3.185)$$

for which we used the value $l_B = 20$ (rather strong electrostatic coupling). We chose this system because it had been studied previously by P^{3}M [122]. However, meanwhile it has turned out that this is probably not the best state point for a benchmark, since the coupling is so strong that it actually induces phase separation (gas–liquid transition). This is in accord with the phase diagram presented in Ref. [124]; the system studied there is not too different from ours.

The simulation was carried out in the NVT-ensemble. After warm-up and equilibration period we have measured the CPU time. The runs were performed on an IBM Regatta H Server (eServer 690 Modell 681 with 32 Power4 Processors at 1.3 GHz each).

The previous P^{3}M studies [122] have used system sizes between $N = 2000$ and $N = 64000$. For each system size the P^{3}M parameters were optimized separately; for $N = 2000$ they were: Mesh size 32^3; 5th order charge assignment; real–space cutoff 8.2; $\alpha = 0.36$ (this parameter controls the split–up of the computational load between real and Fourier space). This results in an estimated relative error of the force per particle of roughly 10^{-3}. For further details, see Refs. [125, 126].

The pair correlation functions of this system are shown in Figs. 3.15 and 3.16. The run was long enough to equilibrate the system reasonably well on the local
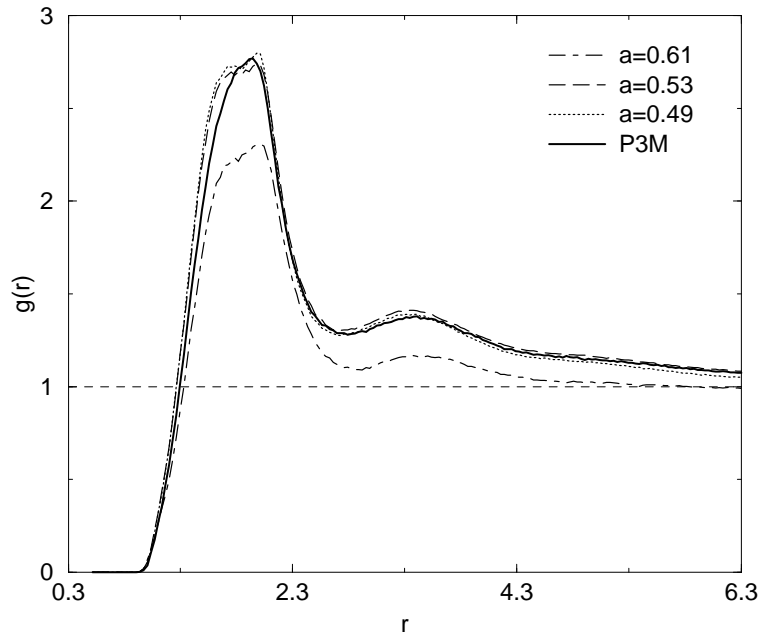
Figure 3.15.: Pair correlation function of like charges at density $\rho = 0.07$, comparing data obtained with P^{3}M with those from MEMD for different lattice spacings.
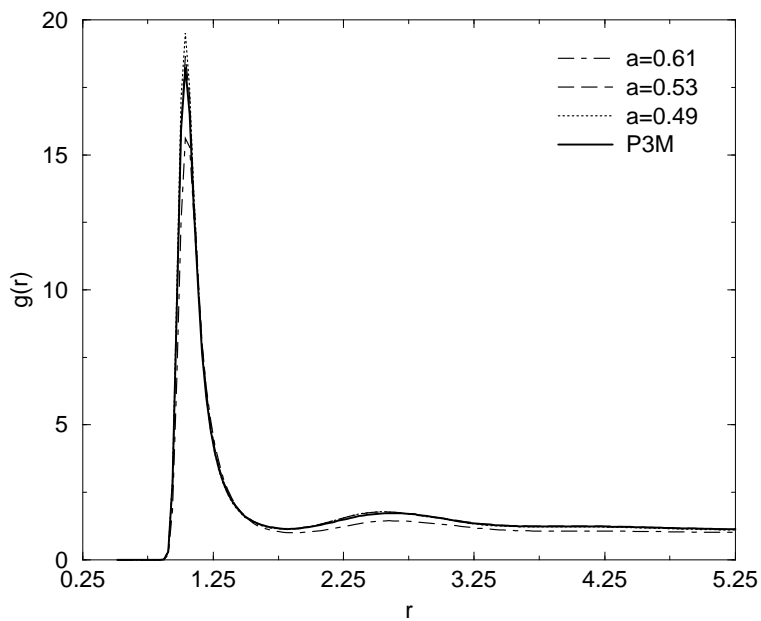

Figure 3.16.: Pair correlation function of unlike charges at density $\rho = 0.07$, again comparing P^{3}M with MEMD.

scale. As a control, we also ran a more accurate P^{3}M simulation and found no visible difference. We then estimated the performance of the P^{3}M program by measuring the CPU time needed until the single–particle mean square displacement reaches the value $\langle \Delta \vec{r}^2 \rangle = 20$. For the $N = 2000$ system, this is 230 seconds on a single processor of an IBM Regatta H server. Further increase of the particle number and processor number (always keeping $N = 2000$ particles on each processor on average) results in considerable loss of performance due to parallelization overhead; for a large system on 32 processors the program runs at roughly half the single–processor speed, while for 16 processors the performance was roughly 75%. We believe that a great deal of these losses can be explained by load–balancing problems due to a substantially inhomogeneous density.

We now turn to the simulation of the same system by MEMD. Firstly, we varied the lattice spacing a and measured the pair correlation functions, as shown in Figs. 3.15 and 3.16. For large lattice spacings, there are systematic deviations, while the correlation function converges to the P^{3}M result with decreasing a. We found a value of $a = 0.53$ acceptable, corresponding to a 58^3 lattice for the $N = 2000$ system. For such a fine lattice, there is practically never more than one particle per cube.

We then varied the speed of light c. The single–particle mean square displacement as a function of time (measured in Lennard–Jones units) is shown in Fig. 3.17. Since the CPU time per step does not depend on c, we see that the fastest dynamics (i. e. fastest decorrelation) occurs for the largest values of c. The optimum choice is therefore mainly dictated by stability considerations. For $c = 20$, we find that 170 seconds CPU time (again one processor IBM Regatta H) are needed for the $N = 2000$ system until the single–particle mean square displacement reaches the value 20. This means that MEMD for that system is slightly faster than P^{3}M. However, the P^{3}M simulation probably provides somewhat more accurate results. Nevertheless, this result is encouraging enough to pursue the MEMD approach further in the future.

Furthermore, we studied the scalability of our parallel program, systematically increasing the particle number and the number of processors such that each processor keeps $N = 2000$ particles on average. Figure 3.18 presents the scalabity factors as a function of the number of processors. The decrease is rather similar to what was found with P^{3}M, and this further supports our speculation that the losses are mainly a result of an inhomogeneous density. The snapshot of the system configuration provides clear evidence, that there is indeed a phase–separating region (Figure 3.19).

We have therefore seen that MEMD with our current implementation is quite competitive for sufficiently dense systems. However, in electrostatic problems one often goes to much smaller densities. If we would apply the present MEMD method to such a dilute system, the number of grid points would become overwhelmingly large. P^{3}M does not have this problem; due to the split–up of the work between real space and Fourier space it is possible to keep the number of grid points reasonably small. It is therefore clear that MEMD for such systems can only be competitive
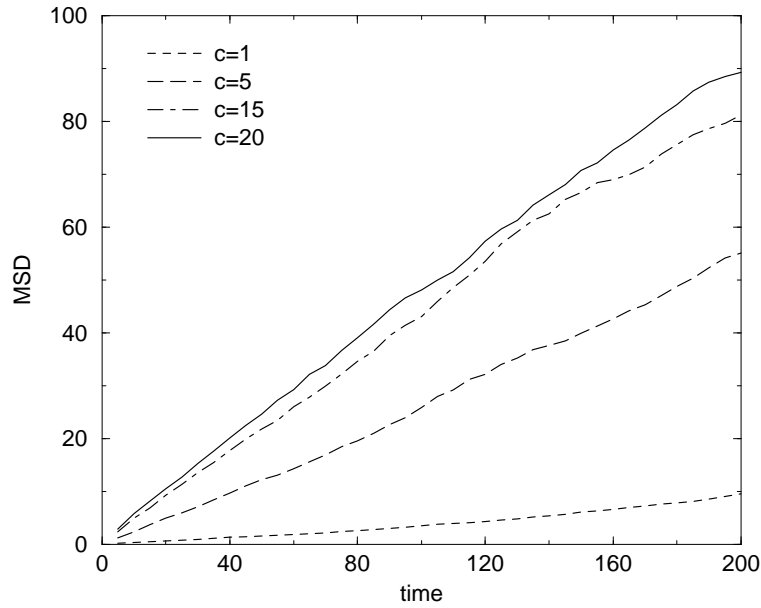
Figure 3.17.: Single–particle mean square displacement as a function of time, for different speeds of light, for the $N = 2000$ system at density $\rho = 0.07$.
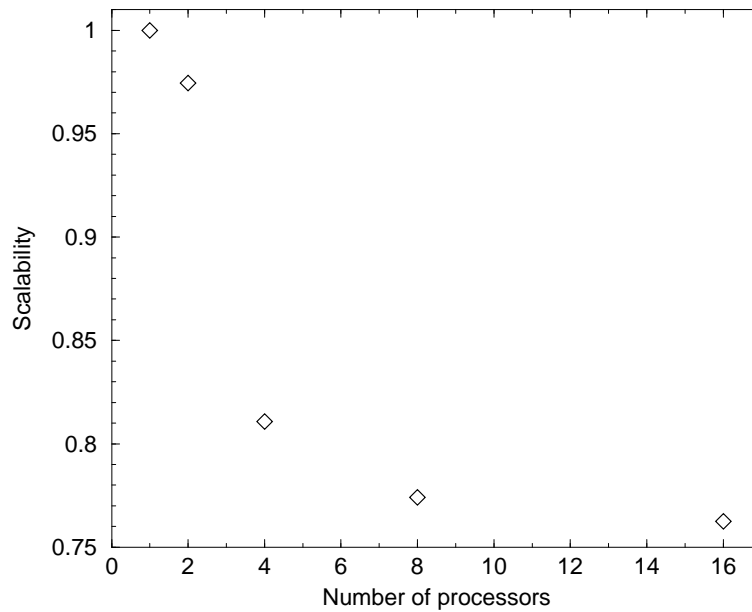

Figure 3.18.: Scalability factor (i. e. performance of the parallel program, divided by the ideal value that would occur if there were no parallelization overhead) of MEMD of the $\rho = 0.07$ system, as a function of processor number. Each processor contains $N = 2000$ particles on average.
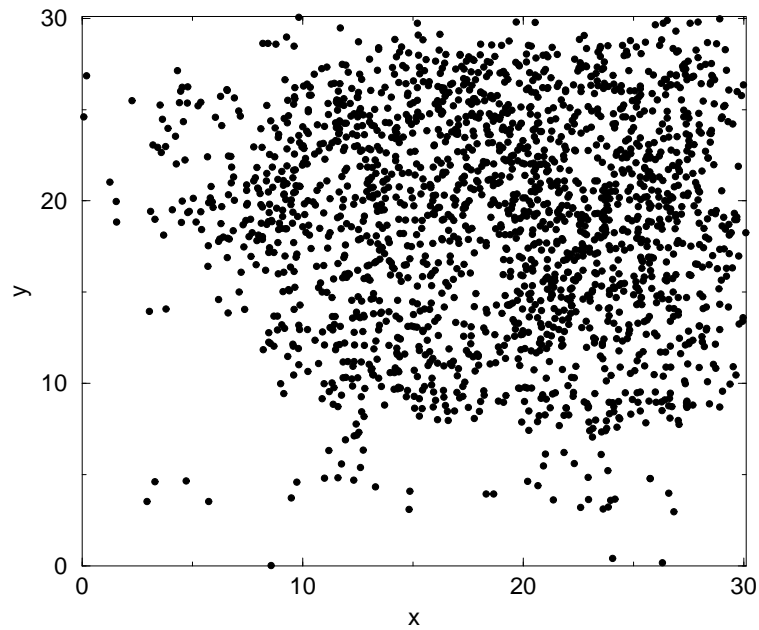
Figure 3.19.: System configuration snapshot for the parameters used in the bench-
marking simulations. On the figure the xy-projection of the particles'
coordinates is presented.

if it is also possible to use a reasonably coarse grid. We believe that this might be
possible by introducing Yukawa subtraction combined with our Green's function
subtraction for both the unscreened and the screened interaction. Such further
refinements are left for future work.

Conclusion

Part 1 is devoted to the study of dense systems of Brownian particles in solution. The solvent is modeled explicitly via the hybrid scheme of particle–Lattice Boltzmann fluid. The D3Q19 velocity version of Lattice Boltzmann method was implemented and tested. A modification of the coupling presented in [8] was proposed and its equivalence with the original one is proved. The validity of the D3Q19 model in the almost incompressible regime was investigated.

Part 2 of the present work describes the new method of simulating Coulomb interactions as the potential of mean force between charges which are dynamically coupled to a local electromagnetic field. The study of large ionic systems is always limited by the computationally demanding treatment of long-range interactions. The MEMD ("Maxwell equations Molecular Dynamics") discussed and used in this work offer an elegant solution to this problem due to its local character. The efficiency of the method and the gain of CPU power during the last years gives the possibility to study more complex system of charged particles.

The numerical results, though being far from conclusive yet, seem to indicate that the algorithm is a competitive alternative to existing schemes, at least for dense systems. The effect of self-interaction of the charges due to the lattice discretization artefacts has been controlled by introducing an effective counter–interaction between interpolated charges. It is hoped that a combination of the Yukawa subtraction scheme by Maggs *et al.* with our lattice Green's function method will allow us to use coarser discretization lattices, and thus better numerical performance.

On the other hand, it is necessary to investigate the accuracy of momentum conservation, and how this depends on the lattice spacing and the speed of light. This latter question is particularly important when considering applications which aim at dynamic properties, like, e. g. the dynamic behavior of charged colloidal suspensions. Much remains to be done, but the existing results are reasonably encouraging.

Bibliography

[1] B. Dünweg and K. Kremer. Molecular-Dynamics Simulation of a Polymer-Chain in Solution. *Journal of Chemical Physics*, 99:6983, 1993.

[2] P. Ahlrichs. *Computersimulationen zur Dynamik von verdünnten und halbverdünnten Polymerlösungen*. PhD thesis, Universität Mainz, 1999.

[3] A.J.C. Ladd. Short-time motion of colloidal particles: Numerical simulation via a fluctuating lattice-Boltzmann equation. *Phys. Rev. Lett.*, 70:1339, 1993.

[4] A.J.C. Ladd. Numerical simulations of particulate suspensions via a discretized Boltzmann equation Part I. Theoretical foundation. *J. Fluid Mech.*, 271:285, 1994a.

[5] P. Ahlrichs, R. Everaers, and B. Dünweg. *Phys. Rev. E*, 64:040501(R), 2001.

[6] R. Groot and P. Warren. Dissipative particle dynamics: Bridging the gap between atomistic and mesoscopic simulation. *Journal of Chemical Physics*, 107:4423–4435, 1997.

[7] A. Malevanets and R. Kapral. Mesoscopic model for solvent dynamics. *Journal of Chemical Physics*, 110:8605–8613, 1999.

[8] P. Ahlrichs and B. Dünweg. Simulation of a single polymer chain in solution by combining lattice Boltzmann and Molecular Dynamics. *Journal of Chemical Physics*, 1999.

[9] E. Pitard and H. Orland. Dynamics of the swelling or collapse of a homopolymer. *Europhysics Letters*, 41:467, 1999.

[10] A. Halperin and P.M. Goldbart. Early stages of homopolymer collapse. *Physical Review E*, 61:565–573, 2000.

[11] A. Milchev, W. Paul, and K. Binder. Off-Lattice Monte-Carlo Simulation of Dilute and Concentrated Polymer Solutions under Theta Conditions. *Journal of Chemical Physics*, 99:4786, 1993.

[12] H. Noguchi and K. Yoshikawa. Folding path in a semiflexible homopolymer chain: A Brownian dynamics simulation. *Journal of Chemical Physics*, 113:854–862, 2000.

[13] Y. Kong, C.W. Manke, W.G. Madden, and A.G. Schlijper. Effect of solvent quality on the conformation and relaxation of polymers via dissipative particle dynamics. *Journal of Chemical Physics*, 107:592–602, 1997.

[14] R.W. Chang and A. Yethiraj. Solvent effects on the collapse dynamics of polymers. *Journal of Chemical Physics*, 114:7688–7699, 2001.

[15] N. Kikuchi, A. Gent, and J.M. Yeomans. Polymer collapse in the presence of hydrodynamic interactions. *European Physical Journal E*, 9:63–66, 2002.

[16] C.F. Abrams, N.K. Lee, and S.P. Obukhov. Collapse dynamics of a polymer chain: Theory and simulation. *Europhysics Letters*, 59:391–397, 2002.

[17] G.R McNamara and G. Zanetti. Use of the Boltzmann equation to simulate lattice-gas automata. *Phys. Rev. Lett.*, 61:2332, 1988.

[18] F. Higuera, S. Succi, and R. Benzi. Lattice gas dynamics with enhanced collisions. *Europhys. Lett.*, 9:345, 1989.

[19] B. Dubrulle, U. Frisch, M. Hénon, and J.-P. Rivet. Low viscosity lattice gases. *Physica D*, 47:27–29, 1991.

[20] U. Frisch, B. Hasslacher, and Y. Pomeau. Lattice gas automata for the Navier-Stokes equation. *Phys. Rev. Lett.*, 56:1505, 1986.

[21] S. Chen, Z. Wang, X. Shan, and G.D. Doolen. Lattice Boltzmann computational fluid dynamics in three dimensions. *J. Stat. Phys*, 68:379, 1992.

[22] G.R. McNamara and B.J. Alder. Analysis of the lattice Boltzmann treatment of hydrodynamics. *Physica A*, 194:218, 1993.

[23] Y.H. Qian, D. d'Humiéres, and P. Lallemand. Lattice BGK models for the Navier-Stokes equation. *Europhysics Lett.*, 17:479–484, 1992.

[24] S. Chen and G.D. Doolen. Lattice Boltzmann method for fluid flows. In J.L. Lumley, M.V. Duke, and H.L. Reed, editors, *Annual Review of Fluid Mechanics*, pages 329–364. Palo Alto, California, 1998.

[25] U. Frisch, D. d'Humiéries, B. Hasslacher, P. Lallemand, Y. Pomeau, and J.-P. Rivet. Lattice gas hydrodynamics in two and three dimensions. *Complex systems*, 1:649, 1987.

[26] D.L. Ermak and J.A. McCammon. Brownian dynamics with hydrodynamic interactions. *J. Chem. Phys.*, 69:1352, 1978.

[27] G. Bossis and J.F. Brady. Self-diffusion of Brownian particles in concentrated suspensions under shear. *J. Chem. Phys.*, 87:5437, 1987.

[28] A. Koponen. *Simulations of Fluid Flow in Porous Media by Lattice-Gas and Lattice-Boltzmann Methods.* PhD thesis, University of Jyvakyla, Finland, 1998.

[29] H. Chen, S. Chen, and W.H. Matthaeus. Recovery of the Navier-Stokes equations using a lattice-gas Boltzmann method. *Phys. Rev.*, A 45:R5339–5342, 1992.

[30] N.S. Martys, X. Shan, and H. Chen. Evaluation of the external force term in the discrete Boltzmann equation. *Phys. Rev. E*, 58:6855, 1998.

[31] L.D. Landau and E.M. Lifshitz. *Fluid Mechanics.* Addison-Wesley, London, 1959.

[32] J.P. Hansen and I.R. McDonald. *Theory of simple liquids.* Academic Press, 1986.

[33] F. Müller-Plathe. A simple nonequilibrium molecular dynamics method for calculating the thermal conductivity. *J. Chem. Phys.*, 106(14):6082–6085, 1997.

[34] F.H. Harlow. Hydrodynamic Problems Involving Large Fluid Distortion. *J. Assoc. Comp. Mach.*, 4:137, 1957.

[35] E.I. Cussler. *Diffusion: Mass Transfer in Fluid Systems.* Cambridge University Press, Cambridge, UK, 2 edition, 1998.

[36] L.D. Landau and E.M. Lifshitz. *Statistical Physics.* Addison-Wesley, Reading, Massachusetts, 1969.

[37] H. Risken. *The Fokker-Planck equation.* Springer-Verlag, 1989.

[38] M.P. Allen and D.J. Tildesley. *Computer simulation of liquids.* Clarendon, Oxford, 1987.

[39] D. Frenkel and B. Smith. *Understanding molecular simulation.* Academic Press, San Diego, 1996.

[40] B. Dünweg, G.S. Grest, and K. Kremer. Molecular dynamics simulations of polymer systems. In S.G. Whittington, editor, *IMA volumes in mathematics and its applications*, volume 102, page 159. Springer, 1998.

[41] E.J. Hinch. Application of the Langevin equation to fluid suspensions. *J. Fluid. Mech.*, 72:499, 1975.

[42] B.J. Alder and T.E. Wainwright. Decay of the velocity autocorrelation function. *Phys. Rev.*, 1:18, 1970.

[43] R.W. Hockney and J.W. Eastwood. *Computer simulation using particles.* IOP Publishing Ltd, Londom, 1994.

[44] L. Greengard and V. Rokhlin. A fast algorithm for particle simulations. *J. Comput. Phys.*, 73:325, 1987.

[45] M. Doi and S. F. Edwards. *The Theory of Polymer Dynamics.* Clarendon Press, Oxford, 1986.

[46] A. J. C. Ladd. *Phys. Rev. Lett.*, 76:1392, 1996.

[47] R. Car and M. Parrinello. Unified Approach for Molecular Dynamics and Density-Functional Theory. *Phys. Rev. Lett*, 55:2471, 1985.

[48] H. Löwen, J. P. Hansen, and P. A. Madden. *J. Chem. Phys.*, 98:3275, 1993.

[49] A.C. Maggs and V. Rossetto. Local Simulation Algorithms for Coulomb Interactions. *Phys. Rev. Lett.*, 88:196402, 2002.

[50] A.C. Maggs. Dynamics of a Local Algorithm for Simulating Coulomb Interactions. *Journal of Chemical Physics*, 117:1975–1981, 2003.

[51] J. Rottler and A.C. Maggs. Local Molecular Dynamics with Coulombic Interaction. cond-mat/0312438.

[52] I. Pasichnyk and B. Dünweg. Coulomb Interactions via Local Dynamics: A Molecular-Dynamics Algorithm. *Journal of Physics: Condensed Matter*, 2004. submitted.

[53] W. Kohn and P. Vashishta. *Theory of the Inhomogeneous Electron Gas.* Plenum Press, New York, 1983.

[54] P. Hohenberg and W. Kohn. Inhomogeneous Electron Gas. *Phys. Rev.*, 136:B864–B871, 1964.

[55] W. Kohn and L. Sham. Self-Consistent Equations Including Exchange and Correlation Effects. *Phys. Rev.*, 140:A1133–A1138, 1965.

[56] W.E. Pickett. Pseudopotential Methods in Condensed Matter Applications. *Comp. Phys. Reports*, 9:115, 1989.

[57] R. Car and P. Parrinello. Simple Molecular Systems at Very High Density. page 455. Plenum Press, New York, 1988.

[58] V.I. Arnold. *Mathematical methods of classical mechanics.* Springer, New York, second edition, 1989.

[59] G. Ciccotti and W. Hoover, editors. *Molecular Dynamics Simulations of Statistical Mechanical Systems.* Plenum Press, New York, 1986.

[60] S. Kirkpatrick, Gelatt, C.D. Jr., and M.P. Vecchi. Optimization by Simulated Annealing. *Science*, 220:671, 1983.

[61] T. Schlick, R.D. Skeel, A.T. Brunger, L.V. Kalé, J.A. Board, J. Hermans, and K. Schulten. Algorithmic Challenges in Computational Molecular Biophysics. *J. Comput. Phys.*, 151:9–48, 1999.

[62] D.M. York, T.A. Darden, and L.G. Pedersen. The effect of long-ranged electrostatic interactions in simulations of macromolecular crystals: A comparison of Ewald and truncated list methods. *J. Chem. Phys.*, 99:8345, 1994.

[63] T. Ito, T. Ebisuzaki, J. Makino, and D. Sugimoto. A special-purpose computer for gravitational many-body systems: GRAPE-2. *Publ. Astron. Soc. Jpn.*, 43:547, 1991.

[64] P.P. Ewald. Die Berechnung optischer und elektrostatischer Gitterpotentiale. *Ann. Phys.*, 64:253, 1921.

[65] E.T. Whittaker and G.N. Watson. *A course of modern analysis : an introduction to the general theory of infinite processes and of analytical functions.* Cambridge University Press, Cambridge, 1992.

[66] J.W. Perram, H.G. Petersen, and S.W. de Leeuw. An algorithm for the simulation of condenced matter which grows as the 3/2 power of the number of particles. *Molecluar Physics*, 65:875–893, 1988.

[67] A.W. Appel. An efficient program for many-body simulation. *SIAM J. Sci. Stat. Comput.*, 6:85, 1985.

[68] J. Barnes and P. Hut. A hierarchical $\mathcal{O}(N \ln N)$ force calculation algorithm. *Nature*, 324:446, 1986.

[69] W.H. Press, S.A. Teukolsky, W.T. Vetterling, and B.P. Flannery. *Numerical Recipes in C.* Cambridge University Press, Cambridge, second edition, 1992.

[70] T.A. Darden, D.M. York, and L.G. Pedersen. Particlemesh Ewald: An $Nlog(N)$ method for Ewald sums in large systems. *J. Chem. Phys.*, 98(12):10089, 1993.

[71] U. Essmann, L. Perera, M.L. Berkowitz, T. Darden, H. Lee, and L.G. Pedersen. A smooth particle mesh Ewald method. *J. Chem. Phys*, 103(19):8577, 1995.

[72] H. Weyl. Eine neue Erweiterung der Relativitätstheorie. *Ann. der Phys.*, 59(10):101–133, 1919.

[73] F. Wegner. Duality in Generalized Ising Models and Phase Transitions without Local Order Parameter. *J. Math. Phys.*, 12:2259, 1971.

[74] K.G. Wilson. Confinement of quarks. *Phys. Rev. D*, 14:2455, 1974.

[75] A.M. Polyakov. Compact gauge fields and the infrared catastrophe. *Phys. Lett. B*, 59:82, 1975.

[76] J. Kogut and L. Susskind. Hamiltonian formulation of Wilson's lattice gauge theories. *Phys. Rev. D*, 11(2):395, 1975.

[77] H. Weyl. Elektron und Gravitation. *Zeitschrift für Physik*, 56:330, 1929.

[78] W. Heisenberg and W. Pauli. Zur Quantentheorie der Wellenfelder. II. *Zeitschrift für Physik*, 59:168, 1930.

[79] J. Schwinger. Field theory commutators. *Phys. Rev. Lett.*, 3(6):296, 1959.

[80] K. Binder, editor. *Monte Carlo Methods in Statistical Physics*. Springer Verlag, Berlin, 1979.

[81] M. Wilson and P.A. Madden. Polarization effects in ionic systems from first principles. *J. Phys.: Condens. Matter*, 5:2687, 1993.

[82] M. Sprik and M.L. Klein. A polarizable model for water using distributed charge sites. *J. Chem. Phys.*, 89(12):7556, 1988.

[83] M. Deserno. *Counterion condensation for rigid linear polyelectrolytes*. PhD thesis, Universität Mainz, 2000.

[84] K.E. Brenan, S.L. Campbell, and L.R. Petzold. *Numerical Solution of Initial Value Problems in Differential-Algebraic Equations*. North-Holland, 1989.

[85] L. Verlet. Computer "Experiments" on Classical Fluids. I. Thermodynamical Properties of Lennard-Jones Molecules. *Phys. Rev.*, 159:98–103, 1967.

[86] D.I. Okunbor and R.D. Skeel. Canonical numerical methods for Molecular-Dynamics simulations. *J. Comp. Chem.*, 15:72, 1994.

[87] J.P. Ryckaert, G. Ciccotti, and H.J.C. Berendsen. Numerical-integration of cartesian equations of motion of a system with constraints - molecular-dynamics of n-alkanes. *J. Comp. Phys.*, 23:327–341, 1977.

[88] H.C. Andersen. RATTLE - a velocity version of the SHAKE algorithm for molecular-dynamics calculations. *J. Comp. Phys.*, 52:24–34, 1983.

[89] B.J. Leimkuhler and R.D. Skeel. Symplectic Numerical Integrators in Constrained Hamiltonian Systems. *J. Comp. Phys.*, 112:117–125, 1994.

[90] J.M. SanzSerna. Symplectic integrators for Hamiltonian problems: an overview. *Acta Numerica*, 1:243–286, 1992.

[91] B. Leimkuhler and S. Reich. Symplectic integration of constrained Hamiltonian systems. *Math. Comput.*, 63:589, 1994.

[92] S. Reich. Symplectic Integration of Constrained Hamiltonian Systems by Composition Methods. *SIAM J. Numer. Anal.*, 33:475–491, 1996.

[93] M.Q. Zhang and R.D. Skeel. Symplectic integrators and the conservation of angular momentum. *J. Comput. Chem.*, 16:365–369, 1995.

[94] E. Barth, K. Kuczera, B. Leimkuhler, and R.D. Skeel. Algorithms for constrained molecular dynamics. Technical report, Kansas Institute for Theoretical and Computational Science, University of Kansas, 1994.

[95] J.M. Ortega and W.C. Rheinboldt. *Iterative Solution of Nonlinear Equations in Several Variables.* Academic Press, 1970.

[96] G. Arfken. *Mathematical Methods for Physicists.* Academic Press, Orlando, FL, 3rd edition, 1985.

[97] B.J. Hunt. *The Maxwellians.* Cornell University Press, 1991.

[98] M. Thies. QCD in the axial gauge. hep-ph/9511450, 1995.

[99] J. D. Jackson. *Classical electrodynamics.* Wiley, New York, 1999.

[100] V.I. Arnold, V.V. Kozlov, and A.I. Neistadt. *Mathematical aspects of classical and celestial mechanics.* Springer, Berlin, 1987.

[101] C.K. Birdsall and A.B. Langdon. *Plasma Physics via Computer Simulation.* Adam-Hilger, Bristol, 1991.

[102] A.D. Lewis and R.M. Murray. Variational Principles for Constrained Systems: Theory and Experiment. *International Journal of Non-Linear Mechanics*, 30(6):793–815, 1995.

[103] E.T. Whittaker. *A Treatise on the Analytical Dynamics of Particles and Rigid Bodies.* Cambridge University Press, Cambridge, 4th edition, 1988.

[104] C. Lanczos. *The Variational Principles of Mechanics.* University of Toronto Press, Toronto, 4th edition, 1970.

[105] E. Tonti. Finite Fromulation of the Electromagnetic Field. In Teixeira, F.L., editor, *Progress in Electromagnetics Research, PIER*, volume 32, pages 1–44. EMW, Cambridge, MA, 2001.

[106] A. Bossavit. 'Generalized Finite Differences' in Computational Electromagnetics. In F.L. Teixeira, editor, *Progress in Electromagnetics Research, PIER*, volume 32, pages 45–64. EMW, Cambridge, MA, 2001.

[107] A. Bossavit. A Rationale for 'Edge-Elements' in 3-D Fields Computations. *IEEE Transactions on Magnetics*, 24:74–79, 1988.

[108] H.S.M. Coxeter. *Introduction to Geometry*. Wiley, New York, 2nd edition, 1969.

[109] F.L. Teixeira and W.C. Chew. Lattice electromagnetic theory from a topological viewpoint. *Journal of Mathematical Physics*, 40(1):169–187, 1999.

[110] R. Schuhmann and T. Weiland. Conservation of Discrete Energy and Related Laws in the Finite Integration technique. In F.L. Teixeira, editor, *Progress in Electromagnetics Research, PIER*, volume 32, pages 301–316. EMW, Cambridge, MA, 2001.

[111] J. Villasenor and O. Buneman. Rigorous charge conservation for local electromagnetic field solvers. *Comp. Phys. Comm.*, 69:306–316, 1992.

[112] C. Sagui and T. Darden. Multigrid methods for classical molecular dynamics simulations of biomolecules. *Journal of Chemical Physics*, 114:6578–6591, 2001.

[113] J. Rottler and A.C. Maggs. A Continuum, $\mathcal{O}(\mathcal{N})$ Monte-Carlo algorithm for charged particles. cond-mat/0308441.

[114] P.M. Chaikin and T.C. Lubensky. *Principles of Condensed Matter Physics*. Cambridge University Press, Cambridge, England, 1995.

[115] J.M. Ziman. *Principles of the Theory of Solids*. Cambridge University Press, Cambridge, England, 1972.

[116] C. Kittel. *Introduction to Solid State Physics*. John Wiley and Sons, New York, 1986.

[117] M.L. Glasser and J. Boersma. Exact values for the cubic lattice Green functions. *Journal of Physics A-Mathematical and general*, 33:5017–5023, 2000.

[118] T. Horiguchi and T. Morita. Note on the lattice Green's function for the simple cubic lattice. *Journal of Physics A- Solid State Physics*, 8:L232–L235, 1975.

[119] R.J. Duffin and E.P. Shelly. Difference equations of polyharmonic type. *Duke mathematical journal*, 25(2):209–238, 1958.

[120] Message-Passing Interface Forum. MPI: A message-passing interface standard. http://www.mpi-forum.org, 1995.

[121] Message-Passing Interface Forum. MPI-2: Extensions to the message-passing interface. http://www.mpi-forum.org, 1997.

[122] A. Arnold, B.A. Mann, H.J. Limbach, and C. Holm. ESPResSo - An Extensible Simulation Package for Research on Soft Matter Systems. http://www.espresso.mpg.de, 2003.

[123] Tcl/Tk. Homepage, 2003. http://tcl.activestate.com/.

[124] Q. Yan and J. J. de Pablo. *Phys. Rev. Lett.*, 86:2054, 2001.

[125] M. Deserno and C. Holm. *J. Chem. Phys.*, 109:7678, 1998.

[126] M. Deserno and C. Holm. *J. Chem. Phys.*, 109:7694, 1998.

Curriculum vitae

Personal data

Igor Pasichnyk
Am Eselsweg 56B
55128 Mainz, Germany

born on 08. October 1972 in Maksimowka/Ukraine
married, daughter Nastasia born in November 2001

Professional Experience

09/1997–09/1998	Engineer of Physics at the Institute of Physics and Technology in Kharkiw (Ukraine)
10/1998–10/2000	Software developer, private company, Ukraine

Education and University Studies

09/1988–06/1989	Physics and Mathematics School by the Novosibirsk State University (Russia)
09/1989–05/1992	Study of Physics at the Physics and Technics Department, St-Petersburg State Technical University (Russia)
09/1992–03/1996	Study of Physics at the Physics and Technics Department, University of Kharkiw (Ukraine)
07/1995–03/1996	Diploma thesis (grade: 1) in Nuclear and Plasma Physics, Prof. A. Bakai, University of Kharkiw (Ukraine)
03/1996	Physics Diploma (with Honor), University of Kharkiw (Ukraine)
since 02/2001	PhD-Student, Theory Group, B. Dünweg Max Planck Institute for Polymer Research, Mainz